



A centrifuge and analytical study of stabilising base retaining walls

**Prepared for Quality Services, Civil Engineering,
Highways Agency**

M Daly and W Powrie (University of Southampton)

First Published 1999
ISSN 0968-4107
Copyright Transport Research Laboratory 1999.

This report has been produced by the Transport Research Laboratory, under/as part of a Contract placed by the Highways Agency. Any views expressed are not necessarily those of the Agency.

TRL is committed to optimising energy efficiency, reducing waste and promoting recycling and re-use. In support of these environmental goals, this report has been printed on recycled paper, comprising 100% post-consumer waste, manufactured using a TCF (totally chlorine free) process.

Transport Research Foundation Group of Companies

Transport Research Foundation (a company limited by guarantee) trading as Transport Research Laboratory. Registered in England, Number 3011746.

TRL Limited. Registered in England, Number 3142272.

Registered Offices: Old Wokingham Road, Crowthorne, Berkshire, RG45 6AU.

CONTENTS

	Page
Executive Summary	1
1 Introduction	3
2 Centrifuge model tests	3
2.1 Model geometry	3
2.2 Sample preparation	3
2.2.1 <i>Speswhite kaolin clay</i>	3
2.2.2 <i>52/100 Leighton Buzzard Sand</i>	5
2.3 Model instrumentation	5
2.4 Centrifuge testing sequence	5
2.5 Boundary stresses imposed on the model during the reconsolidation phase in the centrifuge	8
2.6 The stiffness of speswhite kaolin clay	8
2.7 Centrifuge model test results	8
2.7.1 <i>Speswhite kaolin clay tests (Tests TRL 1 & TRL 4)</i>	8
2.7.2 <i>52/100 Leighton Buzzard Sand tests (Tests TRL 2 and TRL 3)</i>	20
3 Limit-equilibrium analyses	26
3.1 Bearing capacity of a stabilising base	26
3.2 Conditions investigated in the limit-equilibrium analyses	27
3.3 Possible collapse limit states for a stabilising base retaining wall.	27
3.3.1 <i>Failure mechanisms and stress distributions based on Schemes 1 and 2</i>	27
3.3.2 <i>Failure mechanisms and stress distributions based on Scheme 3</i>	29
3.3.3 <i>Failure mechanisms and stress distributions based on Scheme 4</i>	29
3.4 The results of limit-equilibrium analyses of stabilising base retaining walls based on Scheme 3.	29
3.4.1 <i>Walls retaining speswhite kaolin clay</i>	30
3.4.2 <i>Walls retaining Leighton Buzzard Sand</i>	31
3.5 The results of limit-equilibrium analyses of stabilising base retaining walls based on Scheme 4.	31
3.5.1 <i>Stabilising base walls retaining speswhite kaolin clay</i>	32
3.5.2 <i>Stabilising base walls retaining Leighton Buzzard Sand</i>	33
3.6 The results of limit-equilibrium analyses of free cantilever walls	33
3.7 A summary of the results of the limit-equilibrium analyses	34

	Page
4 Finite element analyses	34
4.1 Scope and description	34
4.2 Soil parameters	34
4.3 In situ stress state and soil stiffness profile	36
4.4 Construction sequence	36
4.5 Results of finite element analyses	38
4.5.1 <i>Test TRL 1 (8m embedment wall in speswhite kaolin clay)</i>	38
4.5.2 <i>Test TRL 4 (4m embedment wall in speswhite kaolin clay)</i>	43
4.5.3 <i>Test TRL 2 (8m embedment wall in 52/100 Leighton Buzzard Sand)</i>	51
4.5.4 <i>Test TRL 3 (4m embedment wall in 52/100 Leighton Buzzard Sand)</i>	55
4.6 A summary of the results of the finite element analyses	59
5 Summary and implications for design	59
6 Acknowledgements	64
7 References	64
Appendix A	67
Abstract	72
Related publications	72

Executive Summary

For roads located below existing ground level increasing use is being made of retaining walls with a stabilising base (ie. a stub prop at formation level that extends only a short distance from the wall). This form of construction is generally more economical than either an unpropped wall of deeper embedment or, in the case of a wide road cutting, the installation of a continuous prop at formation level between the opposing walls. Minimal design guidance is available for this particular class of wall and centrifuge model tests and complementary finite element analyses have therefore been carried out to provide further information.

Centrifuge tests were carried out using a retained height of 8m, a stabilising base projection of 4m, and both 4m and 8m embedments at prototype scale. Tests were carried out in kaolin clay and in sand. In kaolin clay, both embedments were of sufficient depth to prevent a short term undrained collapse. However in the long term the 4m embedment wall was in a state of collapse whereas the 8m embedment wall apparently stabilised. With the tests in sand, wall movements were much smaller because of the greater soil stiffness. Different modes of movement also occurred: the 4m embedment wall suffered forwards translation together with backwards rotation whereas the 8m embedment wall translated forwards without significant rotation.

Generally, reasonable agreement was obtained between the centrifuge model tests and the finite element analyses with the same broad trends being apparent in each. The applicability of various possible limit equilibrium calculations has also been assessed. The findings of this study will be of value in updating BD42 (Design of embedded retaining walls and bridge abutments) to include advice on stabilising base retaining walls.

1 Introduction

Highway improvement schemes in urban areas are increasingly being constructed within a retained cutting or a shallow tunnel, thereby minimising their environmental impact. The side walls of these excavations are often constructed in situ using diaphragm or bored pile walling. In the permanent condition, stability and serviceability criteria are usually satisfied by the provision of carriageway slabs, cut-and-cover tunnel roofs, structural floors, or ground anchors at one or more levels. In certain circumstances, however, these traditional forms of permanent support may be impracticable or uneconomic e.g. where the excavation is very wide, where there is no opposite retaining wall, where there are concerns about the durability and maintenance of ground anchors and/or where ground anchors would be close to existing structures. In situations such as these, stabilising base retaining walls can provide an economic and effective means of enhancing the long term stability of an embedded wall.

Stabilising base retaining walls are not new, having been used since the 1970s in grade separation schemes such as on the A406 at Waterworks Corner and Harrow Road, and the A40 at West End Road, Perivale Lane, Swakeleys Road and Long Lane. The stabilising base principle relies on the bearing pressure on the underside of a slab attached rigidly to the front of the wall at formation level imparting a restoring moment to the retaining wall and increasing passive resistance.

There is no guidance on the effectiveness of stabilising base retaining walls in current design methods such as CIRIA Report 104 (Padfield & Mair, 1984) and BS 8002 (BSI, 1994). Field investigations and finite element back-analyses, however, have been carried out to assess the long term performance of this method of construction (Carder et al, 1999; Powrie & Chandler, 1998).

In the research described in this report, the effectiveness of stabilising base retaining walls has been investigated by means of a series of parametric centrifuge model tests and complementary finite element analyses. The applicability of various possible limit-equilibrium calculations has also been assessed.

2 Centrifuge model tests

2.1 Model geometry

The 1:94 scale models used to investigate the effectiveness of stabilising base retaining walls were made from blocks of soil of dimensions 20cm x 55cm on plan x 28.5cm deep (Figure 2.1).

Common retained heights of 8.5cm and stabilising base projections from the wall of 4.25cm, corresponding to 8m and 4m respectively at prototype scale, were adopted in all of the tests. This gave a ratio of stabilising base projection to retained height of 0.5 which is consistent with the recommended optimum value suggested by Powrie & Chandler (1998). The right hand side of the model represented the centreline of a wide excavation and therefore a line of symmetry, at a distance of 28.7m at

prototype scale from the centreline of the wall. The length of the model perpendicular to the plane of cross section was 20cm, corresponding to 18.8m at prototype scale.

Each model wall and stabilising base assembly was cast in one piece in aluminium alloy LM25 TF by Wessex Casting Techniques Limited. Casting tolerances of $\pm 0.5\text{mm}$ required that the material was then machined to the desired uniform thickness of 7.3mm throughout. Each side of the wall and stabilising base was coated with a machined-uniform layer of epoxy resin (Araldite 2003), giving overall wall and slab thicknesses of 10mm. The epoxy resin provided protection to the strain gauges and the associated wiring. The composite flexural rigidity (EI) of both the wall and the slab corresponded to $1.95 \times 10^6 \text{ kNm}^2/\text{m}$ at prototype scale, based on $E_{\text{aluminium}} = 72 \text{ kN/mm}^2$ and $E_{\text{araldite}} = 2 \text{ kN/mm}^2$.

Four parametric centrifuge model tests were carried out, in which the soil type and the depth of wall embedment were varied. Depths of wall embedment of 4.25cm and 8.5cm, corresponding to 4m and 8m respectively at prototype scale, were investigated in both 52/100 Leighton Buzzard Sand and overconsolidated speswhite kaolin clay. A summary of each test is given in Table 2.1.

Table 2.1 Details of centrifuge tests undertaken

<i>Test reference</i>	<i>Description</i>
TRL 1	Overconsolidated speswhite kaolin clay; 8m wall embedment; Excavation time = 3.7 days.
TRL 2	Normally consolidated 52/100 Leighton Buzzard Sand; 8m wall embedment; Excavation time = 3.2 days.
TRL 3	Normally consolidated 52/100 Leighton Buzzard Sand; 4m wall embedment; Excavation time = 4.4 days.
TRL 4	Overconsolidated speswhite kaolin clay; 4m wall embedment; Excavation time = 2.9 days.

Conditions of plane strain were assumed throughout. Excavation in the model was simulated with the stabilising base already in place, and no attempt was made to support the model wall by berms or temporary props during this process. In addition, simulation of the construction of a carriageway at formation level, which would result in a surcharge being applied to the soil in front of a wall, was beyond the scope of the project. Although these limitations mean that movements during excavation may not correspond quantitatively to those that would be observed in the field, it is considered that the effect on the overall mechanism of displacement and/or failure in the long term would be minimal.

2.2 Sample preparation

2.2.1 Speswhite kaolin clay

The overconsolidated kaolin samples were prepared by one-dimensional consolidation in a press from a slurry of water content 100% to a maximum vertical effective stress

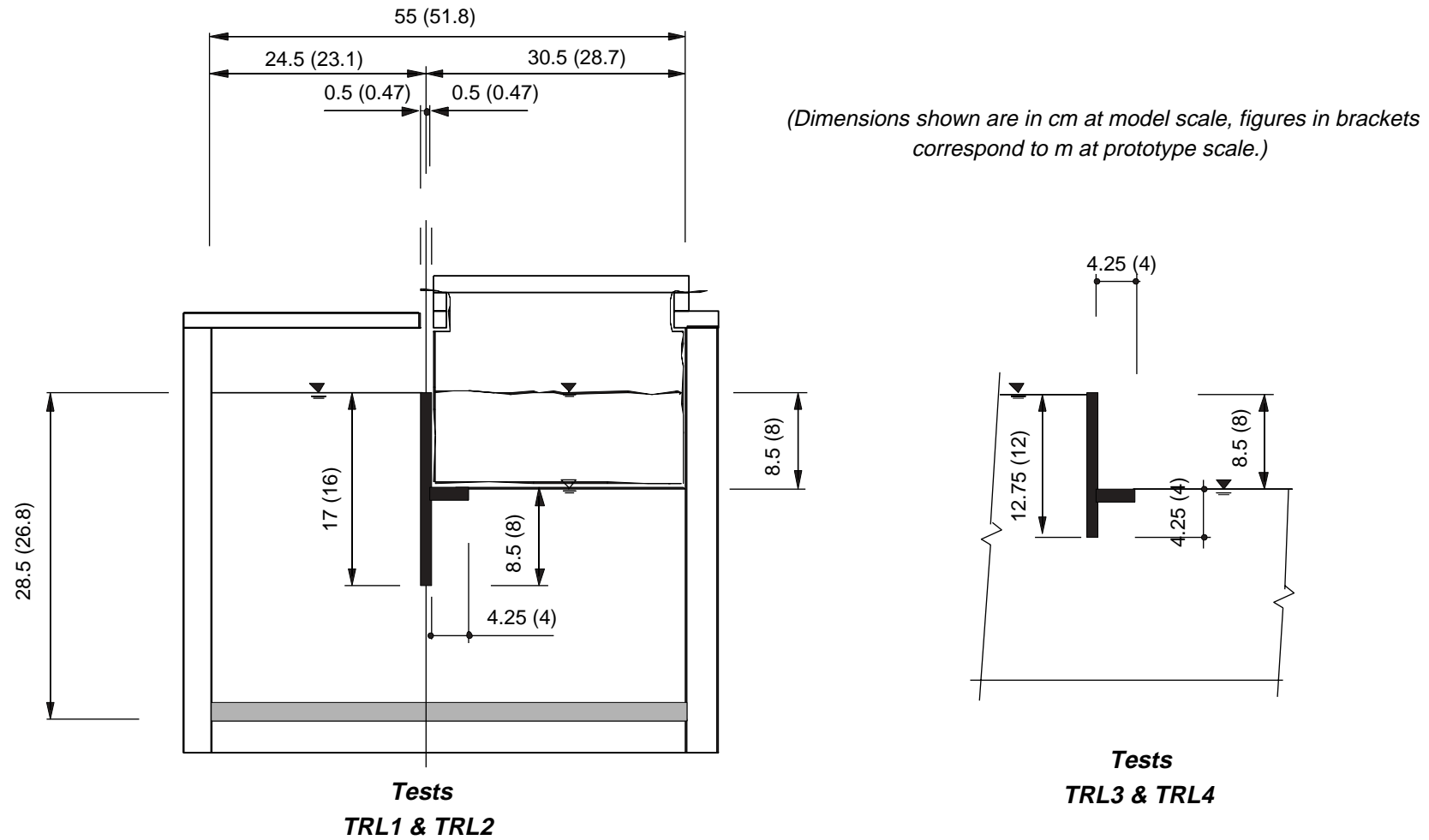


Figure 2.1 Schematic cross section of centrifuge model showing wall and stabilising base geometry

of 1250kPa, followed by swelling back to a vertical effective stress of 80kPa.

On removal from the press, the clay was cut to the required wall/stabilising base/excavation profile with the aid of templates. The aluminium alloy model wall and integral stabilising base was then inserted, and the clay removed from the excavation replaced by a flexible PVC bag containing zinc chloride solution mixed to the same mass density as the clay. Average moisture contents following sample preparation in centrifuge tests TRL1 and TRL4 were 38.7% and 38.8% respectively, giving a mass density (assuming full saturation) of approximately 1800kg/m³.

2.2.2 52/100 Leighton Buzzard Sand

Preparation of the fine sand samples involved raining sand from a hopper into the strongbox. During this procedure the strongbox was placed on its back with the model wall and integral stabilising slab bolted to the backplate in the correct locations. Average dry densities of 1626kg/m³ and 1635kg/m³ were obtained in Tests TRL2 and TRL3 respectively.

After placement of the sand, the strongbox was rotated back to its correct orientation. The required excavation profile was then achieved by attaching a specially developed component to a vacuum cleaner and suspending it from the top of the strongbox. This ensured minimal sample disturbance. The model wall and integral stabilising slab was then unbolted from the backplate and the excavated sand replaced by a flexible PVC bag containing zinc chloride solution mixed to the same mass density as the saturated sand (2012kg/m³).

2.3 Model instrumentation

Following sample preparation, the centrifuge model was instrumented to measure sub-surface soil deformations, soil surface settlements on the retained side, lateral displacements at the wall crest, pore water pressures in the soil and bending moments in the wall and integral stabilising slab. Model instrumentation and calibration techniques and procedures developed by Daly (1998) for centrifuge model tests investigating the effectiveness of earth berms as temporary supports for embedded retaining walls were adopted. A brief description is given here.

Sub-surface soil deformations were measured using an image processing system developed at City University. Images captured during a test by a CCTV camera located within a windshield encompassing the swinging platform of the centrifuge were stored on computer and later compared so that soil strains and overall patterns of soil deformation could be determined. Further details of the image processing system are given by Chen et al (1996). Image processing was not used in the tests conducted in sand because of the poor contrast between the reference targets and the sand.

Soil surface settlements on the retained side and lateral displacements at the crest of the wall were monitored using linear variable displacement transducers (lvdt's) having a linear range of ± 15 mm. A schematic layout of the lvdt's is given in Figure 2.2.

Pore water pressures were measured using miniature

pore water pressure transducers: a schematic layout is given in Figure 2.3. Pore water pressure transducers (with the porous stones removed) were also used to monitor the level of zinc chloride solution in the flexible PVC bag and the level of free water in the main excavation.

Each of the two model walls was instrumented with up to seven sets of four fully active temperature compensated strain gauges. Each integral stabilising base was instrumented with two sets of four strain gauges of the same type as used on the wall. The procedures adopted for fixing, wiring and protecting the strain gauges were similar to those described by Daly (1999).

Photographs of a typical fully assembled centrifuge model are shown in Figures 2.4 and 2.5.

2.4 Centrifuge testing sequence

During an initial period of reconsolidation in the centrifuge at 94g, water was fed via a standpipe to the retained surface, the excavated surface and a drainage layer at the base of the model. Details of the drainage arrangement are shown schematically in Figure 2.6. The base drainage layer was used to reduce the consolidation time for the clay samples (compared with one way drainage to the surface) by a factor of four. Reconsolidation was considered complete in the clay tests when pore water pressures corresponding to hydrostatic conditions had been achieved and vertical settlements measured by the lvdt's had stabilised. In general this took approximately six hours.

In the sand tests, the drainage arrangement was changed slightly with a second water feed being introduced to supply water directly to the base of the model. The sand samples achieved equilibrium with pore water pressures corresponding to hydrostatic conditions soon after the centrifuge had reached 94g. A period of one hour, however, was allowed to elapse before starting excavation to ensure that there were no problems with the model.

Prior to excavation, a pneumatic pilot valve (Valve 1 in Figure 2.6) was actuated, isolating the excavation surface and the base drain. Excavation was simulated by actuating both Valve 2 and Valve 3, draining the free water from the excavation and the zinc chloride solution from the flexible PVC bag. The zinc chloride solution was collected in a series of brass catchtanks mounted on a plate positioned at the base of the strongbox. This base plate also incorporated the groundwater level control standpipe and all pneumatic and solenoid valves.

Daly (1999) found that the rate of simulated excavation in the centrifuge had a significant effect on soil and wall movements in tests using kaolin clay. Excavation was therefore simulated as rapidly as possible to ensure undrained conditions, at rates corresponding to between 2.9 and 4.4 days at prototype scale (Table 2.1).

Following excavation, each test was continued for a number of hours to observe wall and soil movements, pore water pressures and bending moments as long term equilibrium conditions were reached.

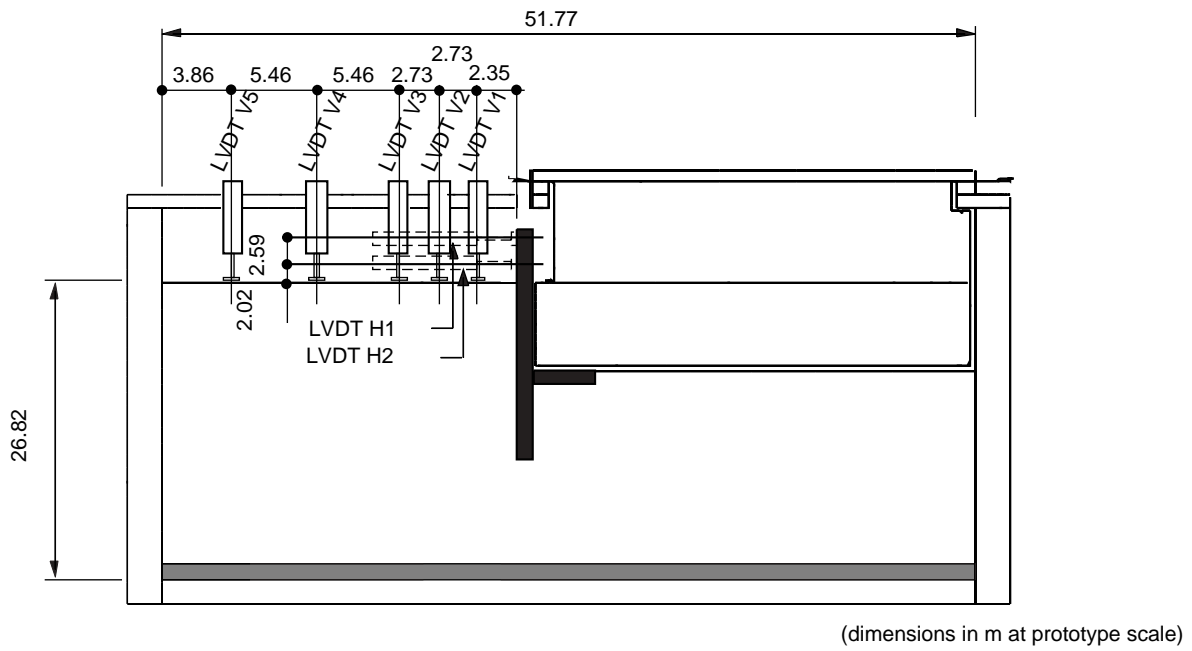


Figure 2.2 Locations of linear variable displacement transducers (lvdt's)

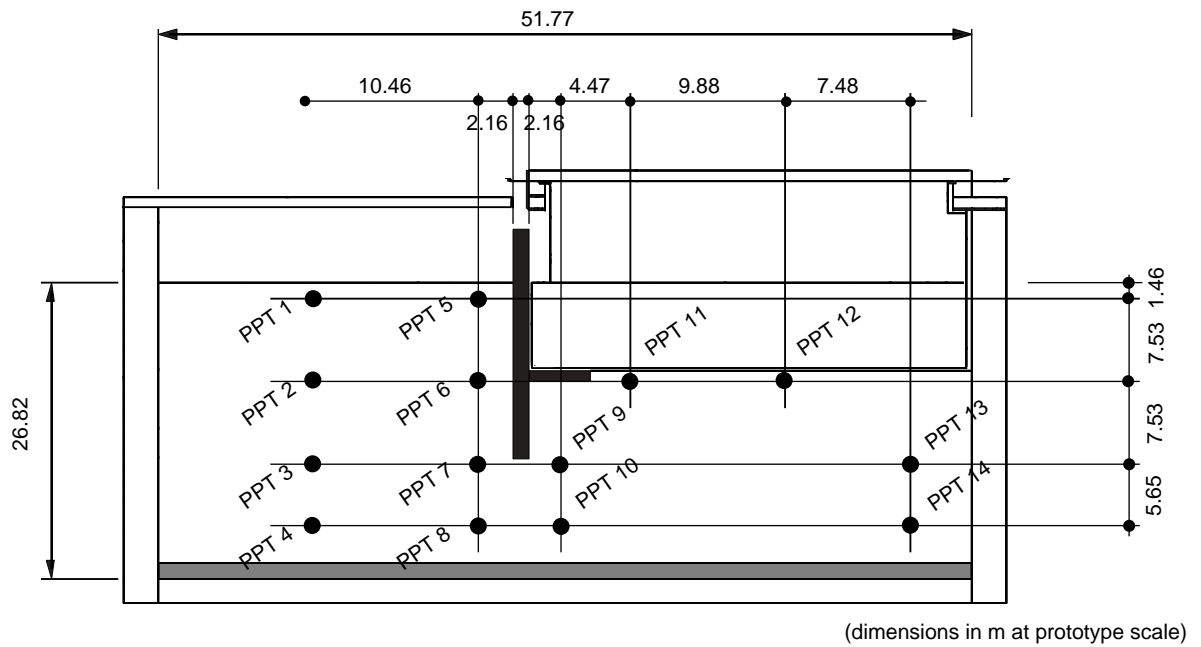


Figure 2.3 Locations of pore water pressure transducers (ppt's)

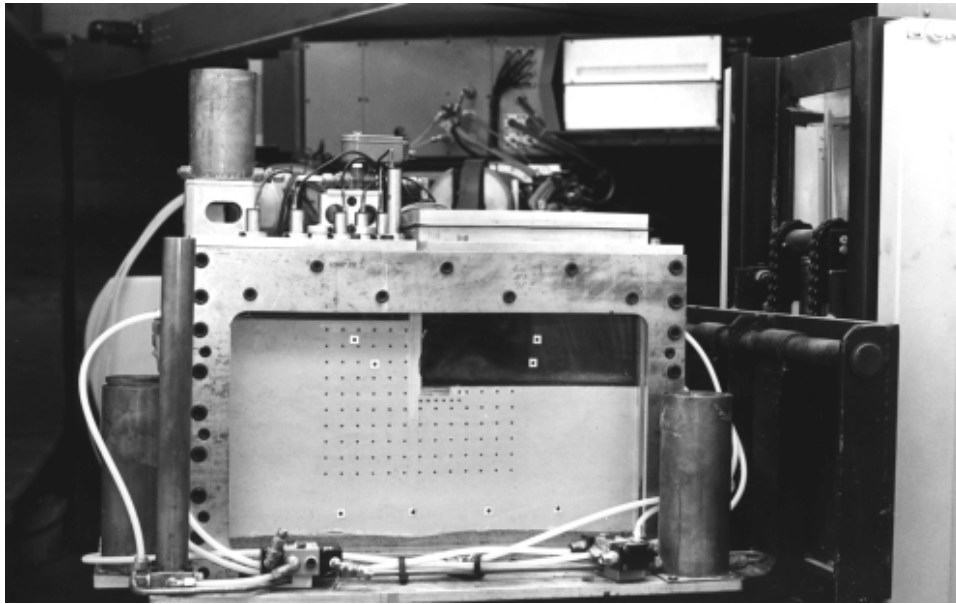


Figure 2.4 Typical fully assembled centrifuge model

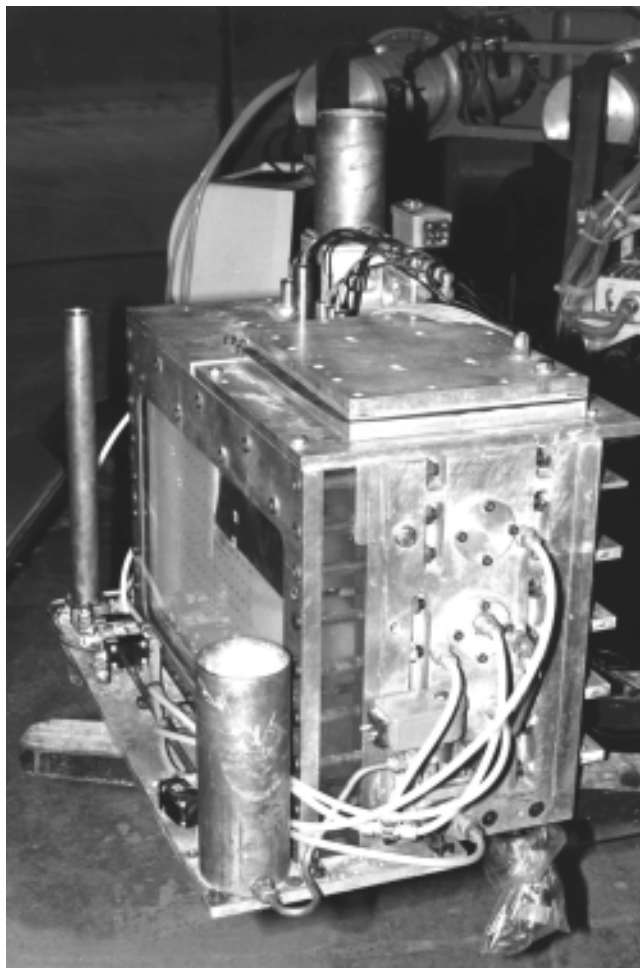


Figure 2.5 Typical fully assembled centrifuge model

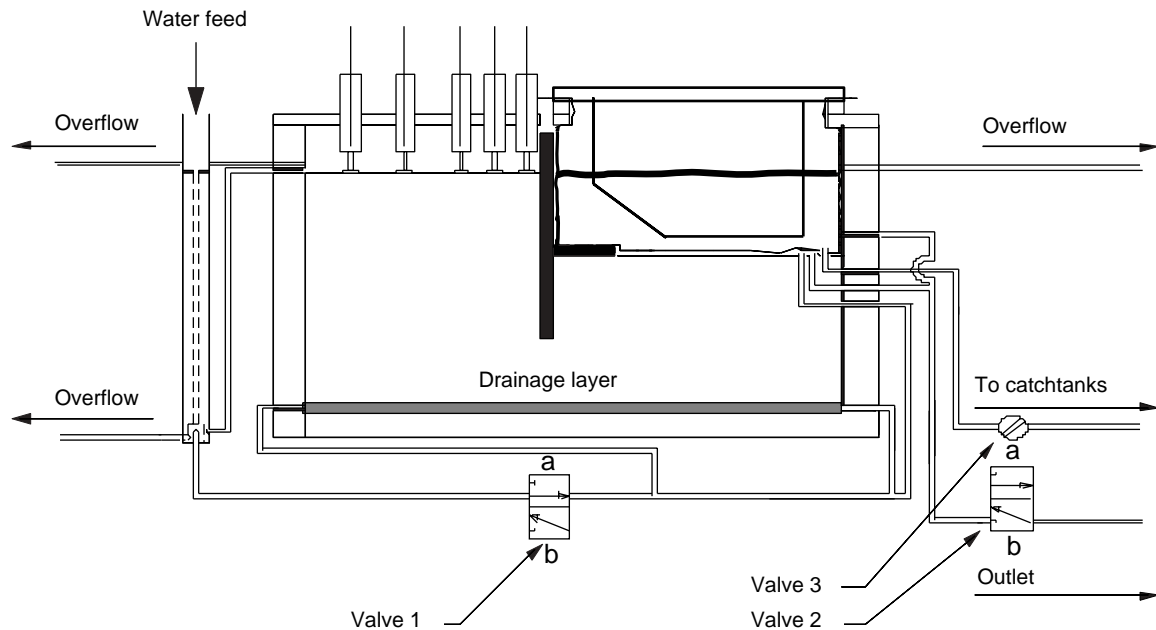


Figure 2.6 Drainage arrangement for a typical centrifuge model test

2.5 Boundary stresses imposed on the model during the reconsolidation phase in the centrifuge

Research into the effects of in situ retaining wall installation in overconsolidated clay has shown that the coefficient of lateral earth pressure is reduced from the in situ value during diaphragm wall installation (Tedd et al, 1984; Powrie, 1985; Symons & Carder, 1993; Page, 1996; Powrie & Kantartzi, 1996). It is also reduced, but to a lesser extent, during the installation of bored piled walls (Symons & Carder, 1993). No attempt was made to model the installation of the wall in the centrifuge as this was not economically viable and was beyond the scope of this project. Instead, the centrifuge tests started with the wall already in place. This meant that the effects of wall installation had to be simulated in some other way.

The boundary stresses imposed by the zinc chloride solution in the centrifuge model at the end of the reconsolidation stage of a typical test are shown in Figure 2.7. As the zinc chloride solution is liquid, the stress at any point in the rubber bag is isotropic. As the density of the zinc chloride solution is the same as that of the soil and the flexible PVC bag is filled to the same level as the retained soil surface, it follows that the lateral stresses imposed on the front of the wall are consistent with a pre-excavation lateral earth pressure coefficient of unity above formation level.

In the case of the tests on walls in sand, the imposition of $K = 1$ implies a probable increase in the lateral earth pressure coefficient from an in situ value K_o of perhaps 0.4 to 0.5 (e.g. $K_o = 0.43$ assuming $K_{onc} = 1 - \sin \phi'_{crit}$ and $\phi'_{crit} = 35^\circ$). Although some increase in lateral earth pressure coefficient will occur during diaphragm and bored pile wall installation in sands owing to the increase in lateral stress during concreting (Batten, 1998), it is likely to be less than this.

2.6 The stiffness of speswhite kaolin clay

Speswhite kaolin clay has been used extensively in centrifuge model tests. It is commercially available and has

a relatively high permeability for a clay. Moreover, its stress-strain and strength characteristics have been the subject of detailed investigation (Al-Tabaa, 1987). However, it possesses stiffnesses and undrained shear strengths that are significantly lower than naturally occurring clays such as London Clay. This is highlighted in Figure 2.8, in which the stiffness variation with depth for the speswhite kaolin clay samples described in this report is compared with the stiffness profile for London Clay that is often assumed in design.

It is therefore reasonable to assume that the magnitudes of soil and wall movements in the centrifuge model tests described in this report are significantly larger than would occur in a field construction of the same geometry in London Clay.

2.7 Centrifuge model test results

Throughout this report, test data are given at prototype scale in accordance with the appropriate scaling laws (Schofield, 1980). For example, measurements of length and elapsed time have been multiplied by a factor of 94 ($= n$) and $94^2 (= n^2)$ respectively.

2.7.1 Speswhite kaolin clay tests (Tests TRL 1 & TRL 4)

The behaviour of two stabilising base walls retaining 8m of speswhite kaolin clay with a nominally full height groundwater level behind the wall and embedment depths of 4m (Test TRL 4) and 8m (Test TRL 1) was investigated.

Wall and soil movements

The movement of the crest of the wall into the excavation is shown as a function of time in Figure 2.9. Both walls were of sufficient depth to prevent a short-term undrained collapse. In the long term, however, there were two distinct modes of behaviour.

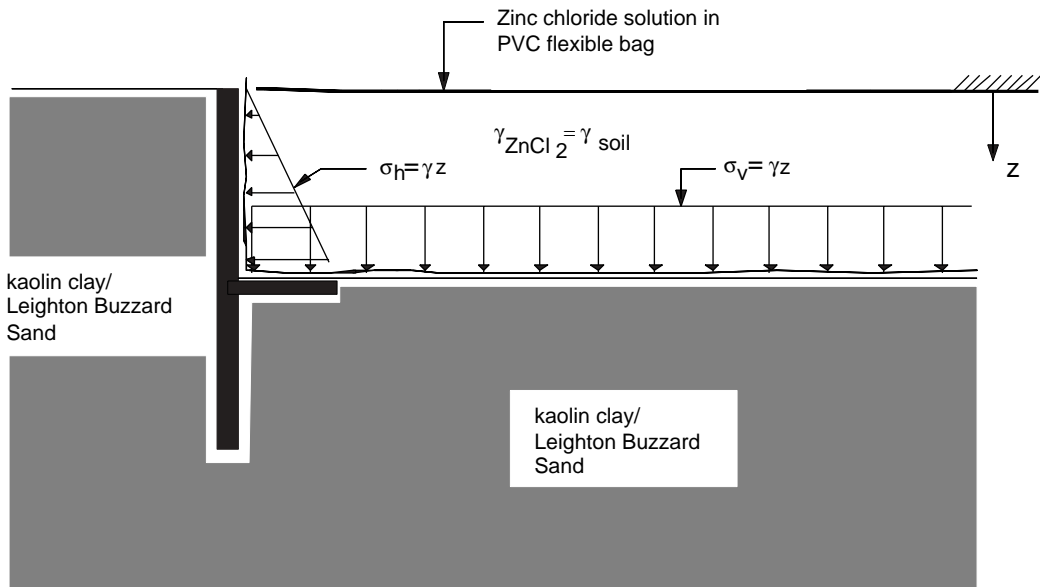


Figure 2.7 Boundary stress distributions at the end of reconsolidation in the centrifuge

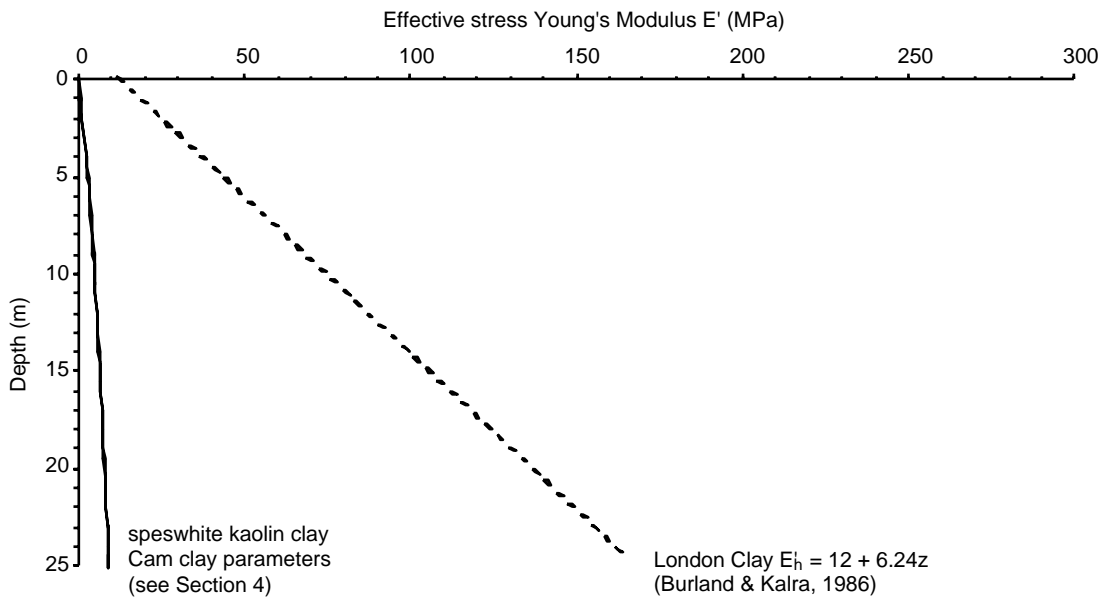


Figure 2.8 Stiffness variation with depth for speswhite kaolin clay and London Clay

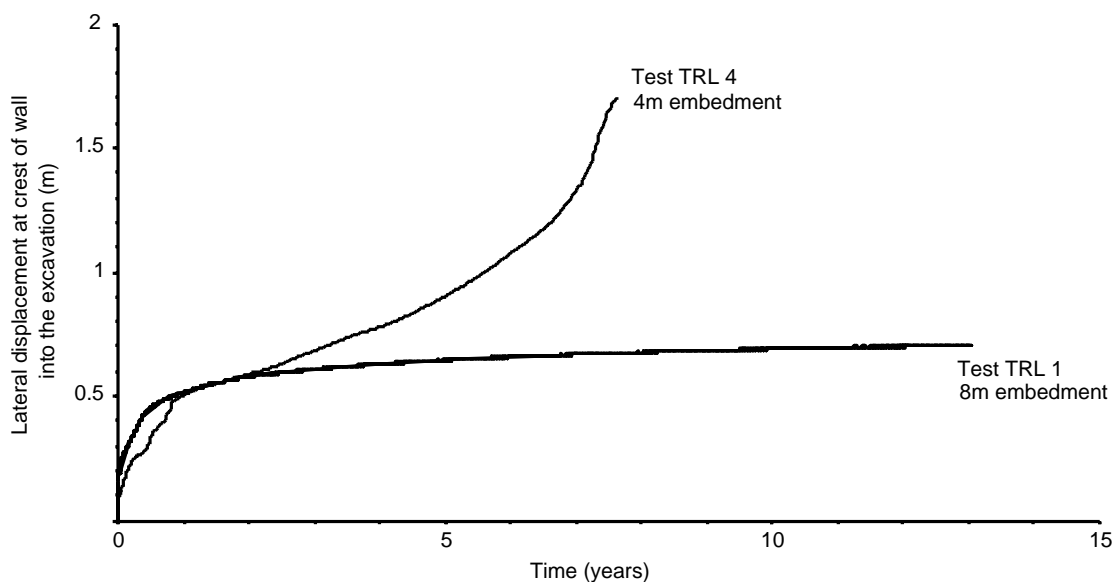


Figure 2.9 Crest movements into the excavation vs time for Test TRL 1 and TRL 4

The wall of shallower embedment (Test TRL 4) suffered relatively large movements on excavation. Wall and soil movements continued after excavation with no sign of abatement. Soil settlement profiles behind the wall at various stages of the test are shown in Figure 2.10. The deformations were so large that the test eventually had to be stopped (after approximately 7 years) when the lvdt's measuring lateral displacements at the crest of the wall reached the end of their ranges and started to restrain the top of the wall.

The soil and wall movements in Test TRL 4 were influenced by the development of a series of slip surfaces behind the wall some time after excavation. The most significant slip surface developed approximately 6.5m behind the wall and extended to the toe of the wall. This can clearly be seen in the final pattern of rupture lines illustrated in the post-flight photograph in Figure 2.11.

The wall of 8m embedment (Test TRL 1) also suffered relatively large movements on excavation. Figure 2.9 shows that initial wall movements were greater than that of the wall of 4m embedment (Test TRL 4), as does a comparison of the soil settlements behind the wall at the end of excavation (Figure 2.12). This was due to a difference between the levels of zinc chloride solution in the flexible PVC bag in the two tests, and is discussed later.

Soil settlement profiles behind the wall at various stages of Test TRL 1 (8m embedment) are shown in Figure 2.13. Figures 2.9 and 2.13 both indicate that the rates of wall and soil movement reduced dramatically in the long term. At the end of the test, corresponding to approximately 13 years at prototype scale, the rate of increase of crest movement into the excavation was approximately 4.5mm/year.

A comparison of the soil settlement profiles behind the wall measured in the two tests after approximately 7 years (Figure 2.14), i.e. corresponding to the end of Test TRL 4, shows that the wall of deeper embedment (Test TRL 1) also suffered severe differential settlements immediately behind

the wall. Post-test examinations of this wall, however, showed no evidence of the development of rupture surfaces. Remote from the wall, the settlement profiles in the two tests were identical reflecting the effects of consolidation following the change in the groundwater regime.

Cumulative soil deformation patterns at various stages of Tests TRL 1 and TRL 4, measured using the in-flight image processing technique described in Section 2.4, are given in Figures 2.15 and 2.16 respectively. Although the extent of the data is limited, the soil deformation pattern during excavation in both tests (Figures 2.15a and 2.16a) appears to be compatible with that of a rigid wall, in that the boundaries of significant soil movement on excavation are well defined with little or no movement outside lines drawn at 45° from the toe of the wall. Wall movement data in both tests using the in-flight image processing technique were consistent with the lvdt data presented in Figure 2.9. The soil deformation patterns during Test TRL 4 (Figure 2.16) confirm the settlement data in Figure 2.10 indicating that the large wall and soil movements following excavation were predominantly due to the sliding of a triangular block of soil along a slip surface approximately 6.5 m behind the wall. The soil deformation patterns during Test TRL 1 (Figure 2.15) are also in close agreement with the settlement profiles measured using lvdt's shown in Figure 2.13.

If - as is sometimes assumed in design (BS 8002 Clause 3.2.5 {BSI, 1994}) - a serviceability criterion corresponding to a limit on wall movement of 0.5% of the retained height (40mm in this case) is adopted, both walls would have been judged to have suffered a serviceability failure immediately following excavation. This is not surprising because of the low stiffness of the kaolin clay (Section 2.6). In the long term, the wall/stabilising base arrangement of Test TRL 4 was probably in a state of collapse.

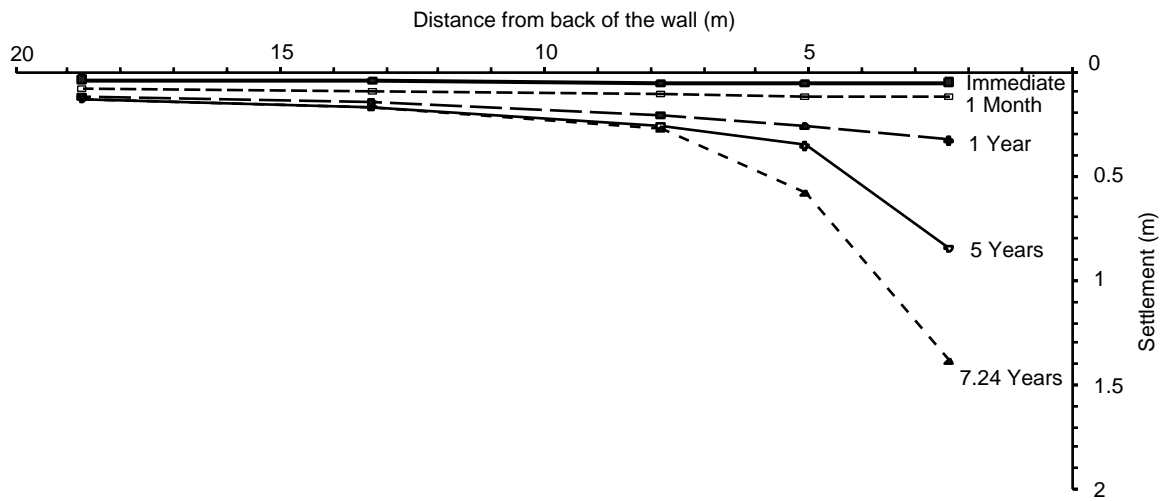


Figure 2.10 Soil settlement profiles behind the wall, Test TRL 4

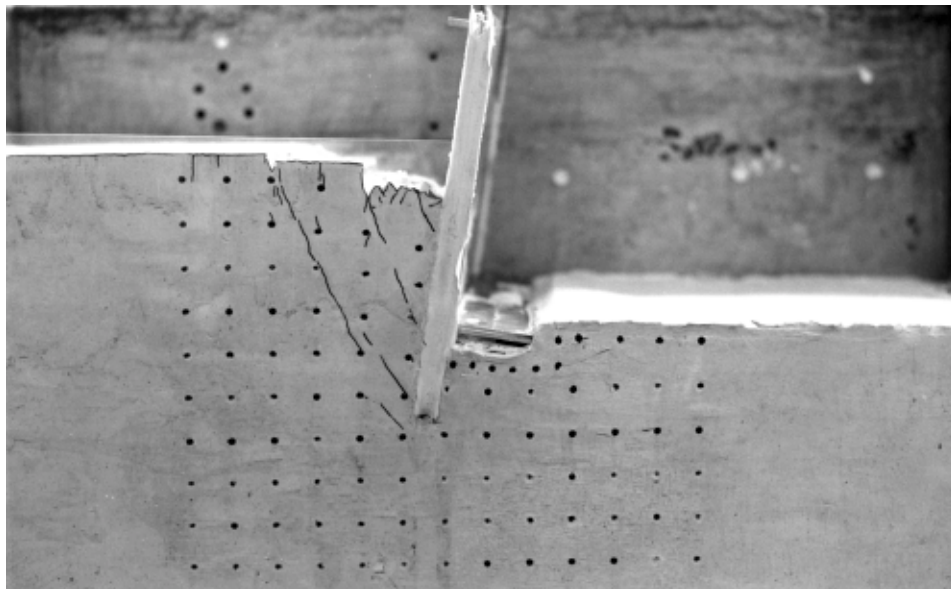


Figure 2.11 Post-flight view of Test TRL 4 showing slip surfaces

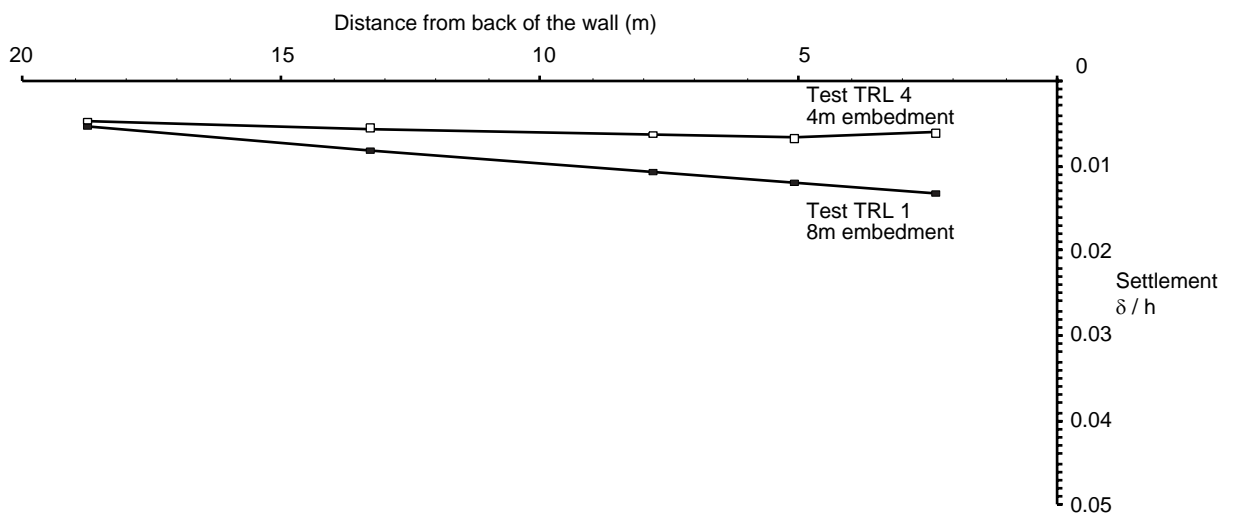


Figure 2.12 Normalised soil settlement profiles behind the wall immediately after excavation, Tests TRL 1 and TRL 4

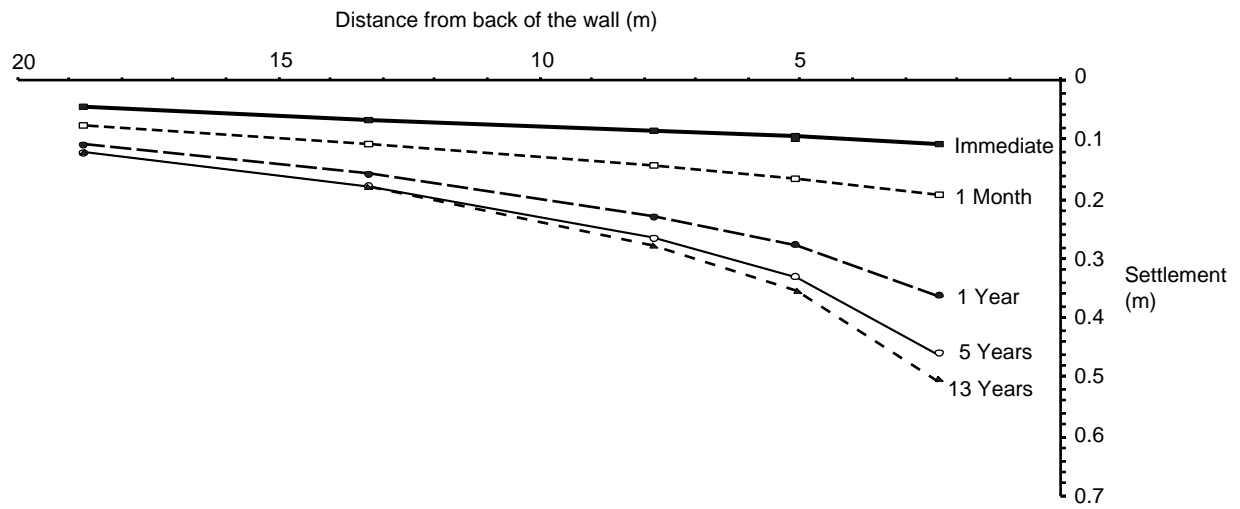


Figure 2.13 Soil settlement profiles behind the wall, Test TRL 1

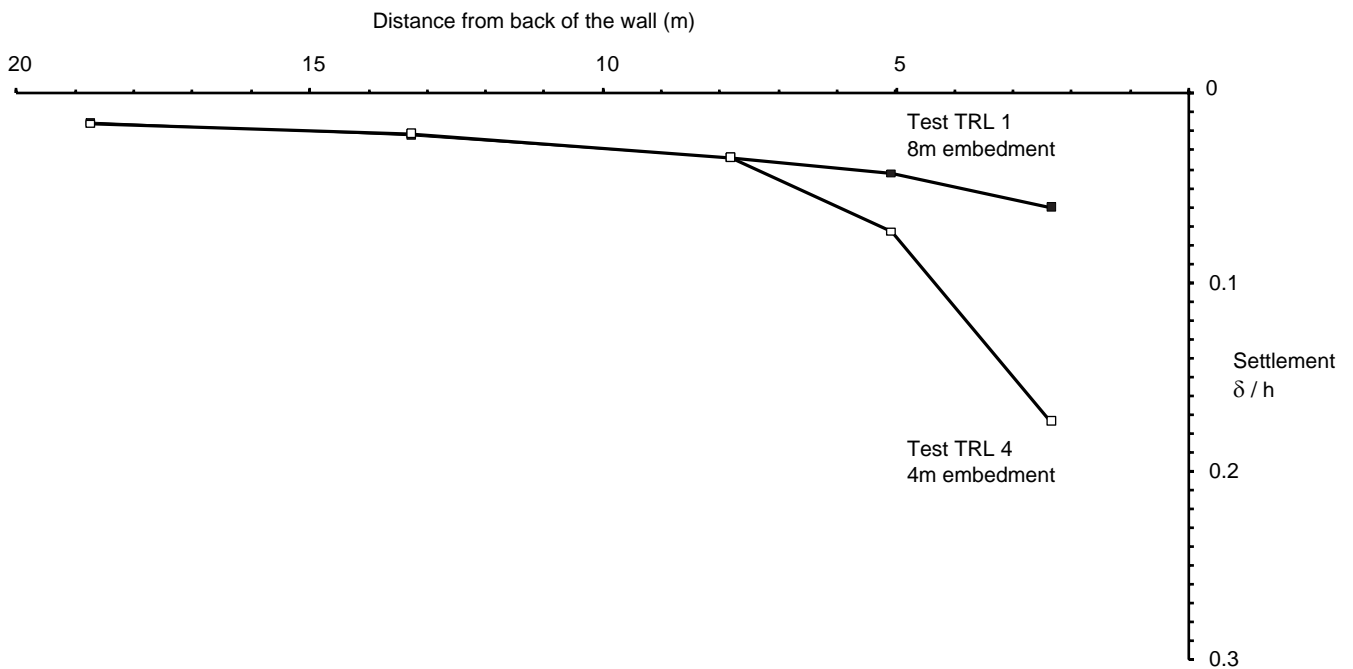
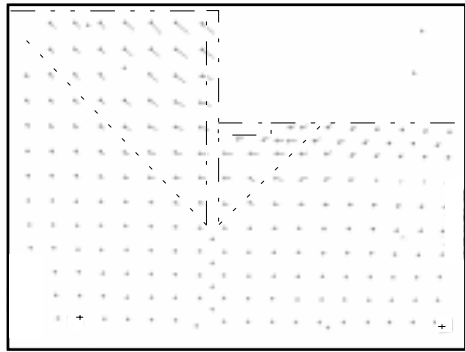
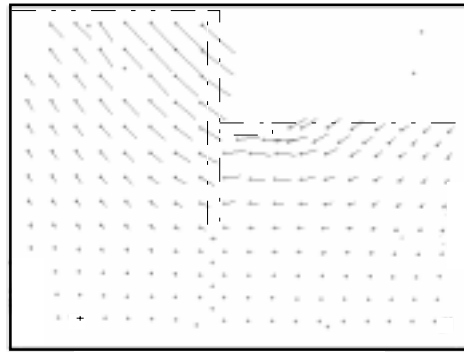


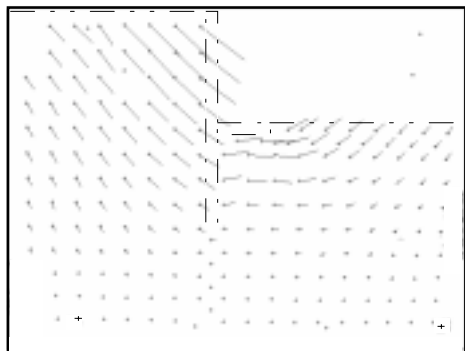
Figure 2.14 Normalised soil settlement profiles behind the wall after 7.24 years, Tests TRL 1 and TRL 4



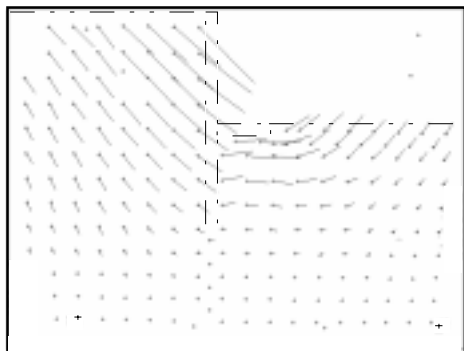
(a) Immediate (3.7 days)



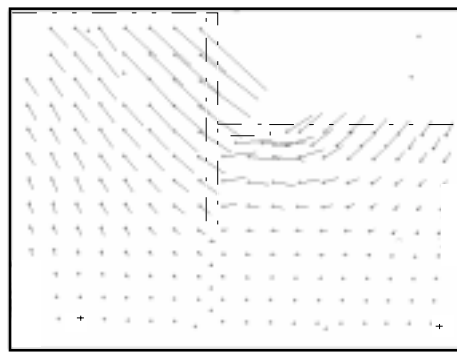
(b) 6 months post-excavation



(c) 1 year post-excavation



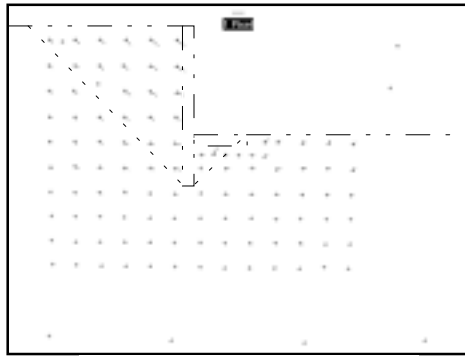
(d) 5 year post-excavation



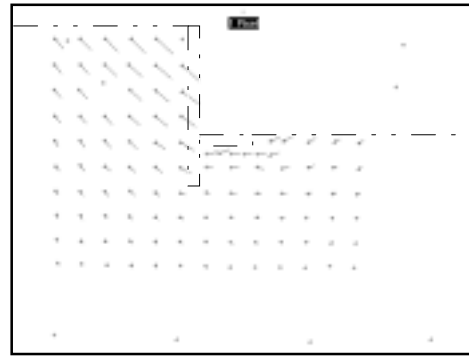
(e) End of test

Space scale 0 4 cm
 Displacement scale 0 4 pixels

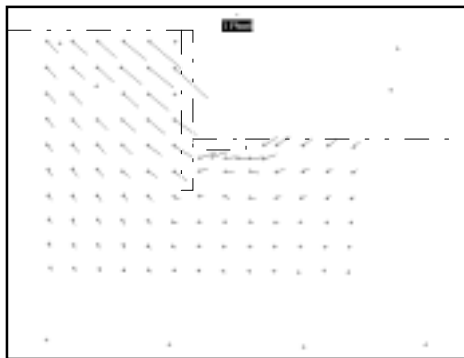
Figure 2.15 Soil deformation patterns at various stages in Test TRL 1



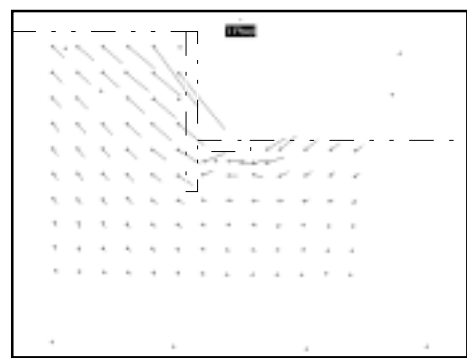
(a) Immediately after excavation



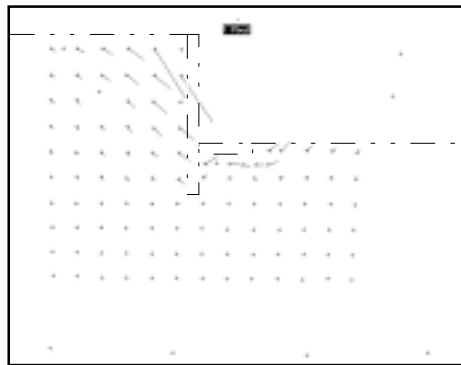
(b) 6 months post-excavation



(c) 5 years post-excavation



(d) End of test (7.24 years)



(e) Soil movements between 6 months and 7.24 years

Space scale 0 4 cm

Figure 2.16 Soil deformation patterns at various stages in Test TRL 4

Pore water pressures

Pore water pressure distributions at various stages of Tests TRL 1 and TRL 4 are presented in Figures 2.17 and 2.18 respectively. Unfortunately, a few of the pore water pressure transducers malfunctioned during spin-up or reconsolidation in each test: data from these transducers are not presented. The measurements of pore water pressure at the end of reconsolidation in each test (Figures 2.17a and 2.18a) show that the clay was in a state of hydrostatic equilibrium at this stage.

During excavation (Figures 2.17b and 2.18b), the pore water pressures in the soil in front of the wall beyond the stabilising base (i.e. 6.4m and 24m in front of the wall) fell considerably due to the removal of the overburden and then rose in the ensuing period as long term equilibrium conditions were approached (Figures 2.17c and 2.18c). The responses of these transducers during excavation were expected to be similar in each test. However, the response appears to have been more pronounced in Test TRL 1 (Figure 2.17b). Figure 2.19 suggests that before excavation commenced there was a difference in the pressure, and therefore the level, of zinc chloride solution in the bag. The target pressure was approximately 141kPa (i.e. $8\text{m} \times 17.66\text{kN/m}^3$). The pressure measured by the bag transducer in Test TRL 4 was 142kPa whereas in Test TRL 1 it was 170kPa. It is therefore not surprising that the response of the transducers to overburden removal was more significant, and that the soil and wall movements were greater, in Test TRL 1.

Pore water pressure measurements immediately (2.16m) in front of the wall on excavation in the two tests (Figures 2.17b and 2.18b) suggest that the effect of overburden removal beneath the stabilising base was less than it was beyond the base. Excavation in the model was simulated with the stabilising base already in place. Rotation of the wall into the excavation probably resulted in the development of significant bearing pressures beneath the base during excavation, partly compensating for the effects of vertical unloading beneath the stabilising base.

In the long term, the pore water pressures beneath the stabilising base continued to fall until they reached their equilibrium values (Figures 2.17c and 2.18c). Linear regression lines through the data points in Figures 2.17c and 2.18c give pore water pressure gradients of 11.71kPa/m depth in Test TRL 1 and 11.83kPa/m depth in Test TRL 4.

Behind the wall, pore water pressures fell in all cases on excavation (Figures 2.17b and 2.18b), with the lateral unloading effect most pronounced closest to the wall. In the ensuing period, the pore water pressures furthest away from the wall (i.e. 12.8m behind) continued to fall until they reached their long term equilibrium values. Following excavation, the pore water pressures immediately behind and within the depth of the wall tended to rise to their long term equilibrium values as the clay in this region swelled and softened (Figures 2.17c and 2.18c). Linear regression lines through the data points in Figures 2.17c and 2.18c give pore water pressure gradients of 7.08kPa/m depth in Test TRL 1 and 6.31kPa/m depth in Test TRL 4.

Bending moments in the wall and stabilising base

Bending moments measured in the walls in the two tests immediately after excavation and after 7.24 years are compared in Figures 2.20 and 2.21 respectively. With the stabilising base already in place, the restoring moment imparted by the base as the wall rotates into the excavation is evident in both tests. Unfortunately, measurement of the full magnitude of the stabilising moment was not possible because strain gauges - which were attached to both sides of the wall - could not be located on the wall exactly at the level of the stabilising base. The bending moments in the wall on either side of the stabilising base have been joined by a straight dotted line.

Figure 2.20 shows that immediately after excavation, the maximum measured bending moment in Test TRL 1 was a factor of approximately 2.75 greater than that in Test TRL 4. Bending moments in the wall tended to increase (i.e. become more negative) in the long term in both tests as the pore water pressures immediately behind the wall increased. Figure 2.21 suggests that after 7.24 years, the maximum measured bending moment in Test TRL 1 was approximately 2.1 times greater than that in Test TRL 4.

The maximum bending moment measured in the wall at the end of Test TRL 1, corresponding to approximately 18 years at prototype scale, was -1390kNm/m at a depth of 6.75m (tension on the excavated face of the wall is taken as positive) and the pore water pressure gradient behind the wall was approximately 7.1kPa/m depth. The implied horizontal effective stresses behind the wall corresponded to an earth pressure coefficient $K = 1.9$ (assuming $\gamma = 17.66\text{kN/m}^3$) - an increase from the pre-excavation value of approximately unity that was not consistent with the sense of rotation of the wall. Implausibly high bending moments were also found in Test TRL 2 in which the same wall was used (Section 2.7.2).

At the end of Test TRL 4, corresponding to 7.24 years at prototype scale, a maximum bending moment in the wall of -650kNm/m was measured at a depth of 6.75m (Figure 2.21). At the same instant, the pore water pressure gradient behind the wall was approximately 6.3kPa/m depth. The horizontal effective stresses behind the wall corresponded to a lateral earth pressure coefficient $K = 0.56$ (assuming $\gamma = 17.66\text{kN/m}^3$). Assuming full wall friction, $K = 0.56$ equates to a mobilised soil strength $\phi' = 13^\circ$ based on the tables of active earth pressure coefficients given in Caquot and Kerisel (1948). As mentioned previously, the wall/stabilising base arrangement of Test TRL 4 was at or close to a state of collapse at the end of the test, and would therefore have been expected to be mobilising a significant proportion of its shear strength, i.e. $\phi' \Rightarrow 22^\circ$. Although the calculated earth pressure coefficient was consistent with the sense of rotation of the wall, the measured bending moments in the wall were, once again, greater than expected. However, the change in the measured bending moment in the wall at formation level (i.e. at a depth of 8m) was consistent with that in the stabilising base (compare Figures 2.21 and 2.22).

Initially, the greater than expected wall bending moments measured in the two tests were thought to have been due to incorrect calibration of the walls. Successive calibrations of the 8m embedment wall, however, gave average and

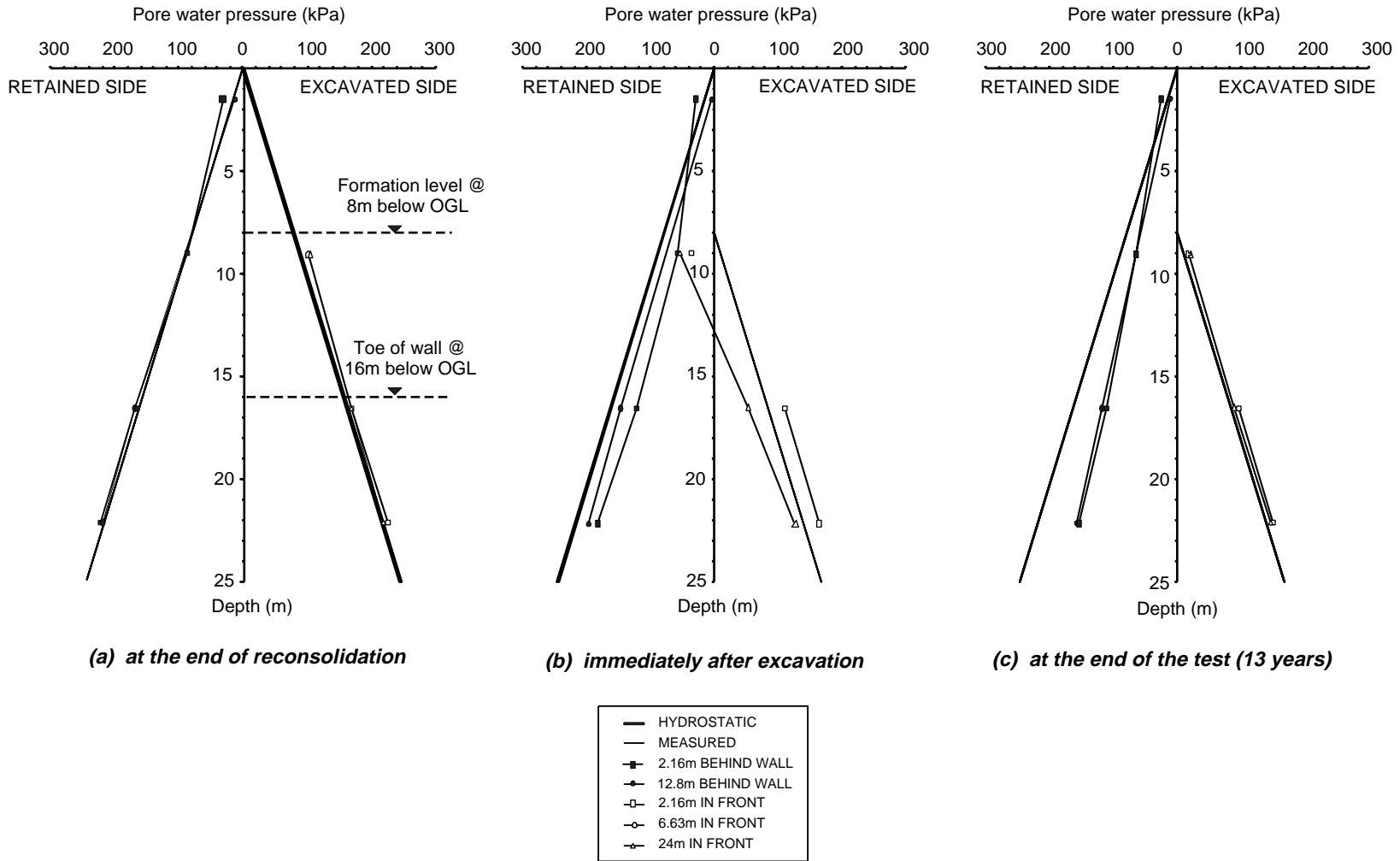


Figure 2.17 Pore water pressure profiles at various stages of Test TRL 1

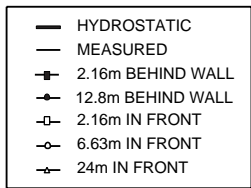
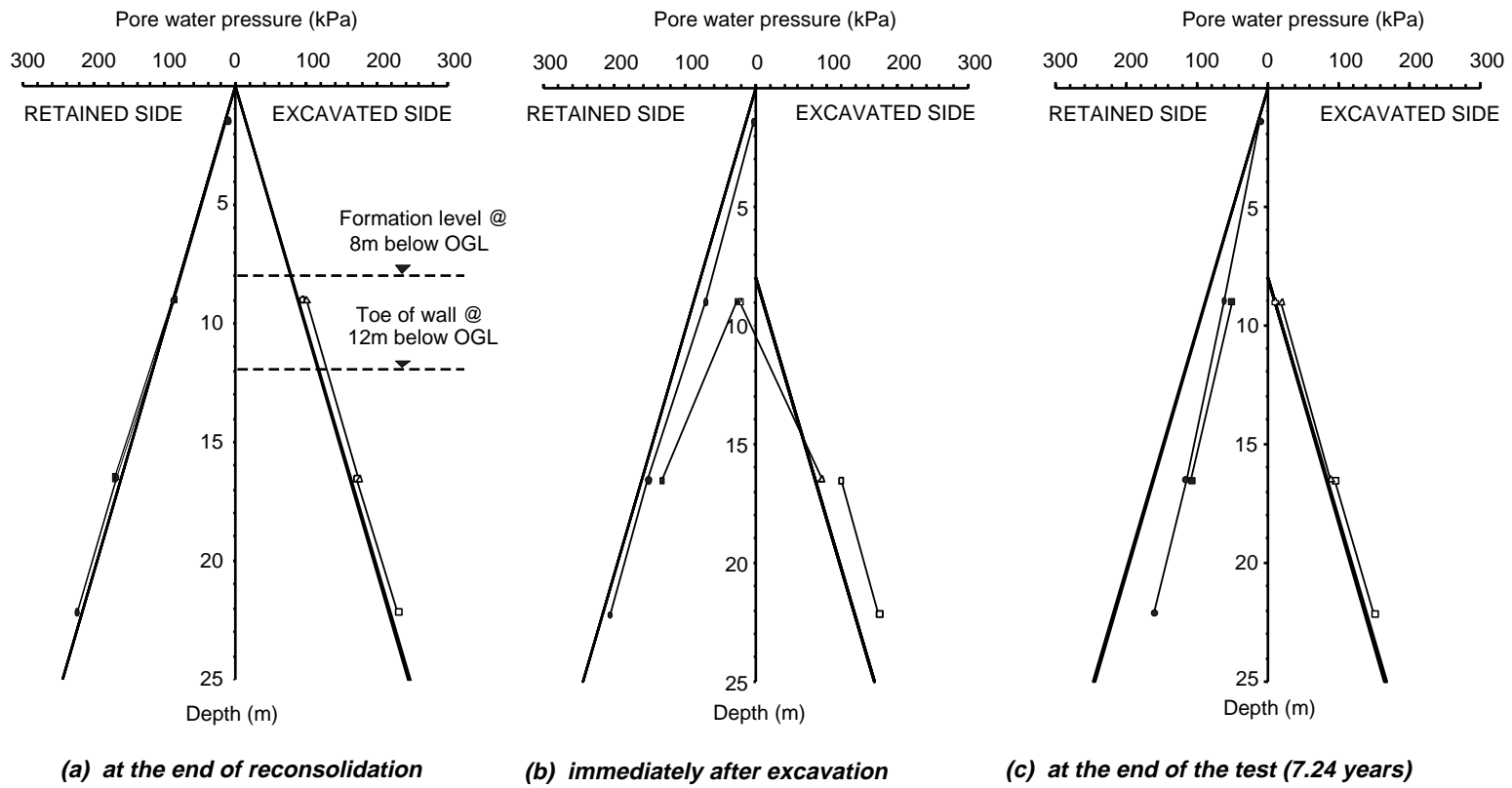


Figure 2.18 Pore water pressure profiles at various stages of Test TRL 4

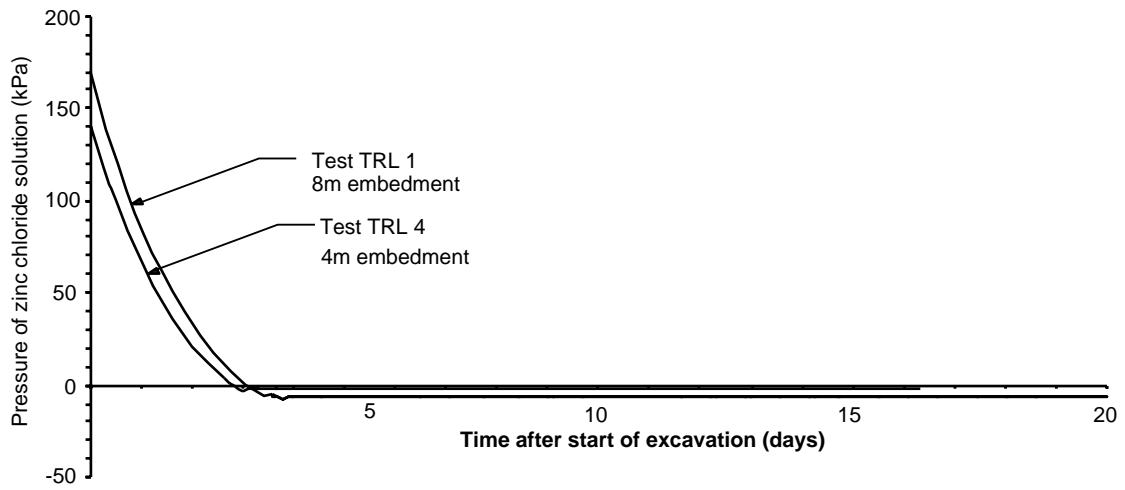


Figure 2.19 Responses of the bag transducers in Tests TRL 1 and TRL 4

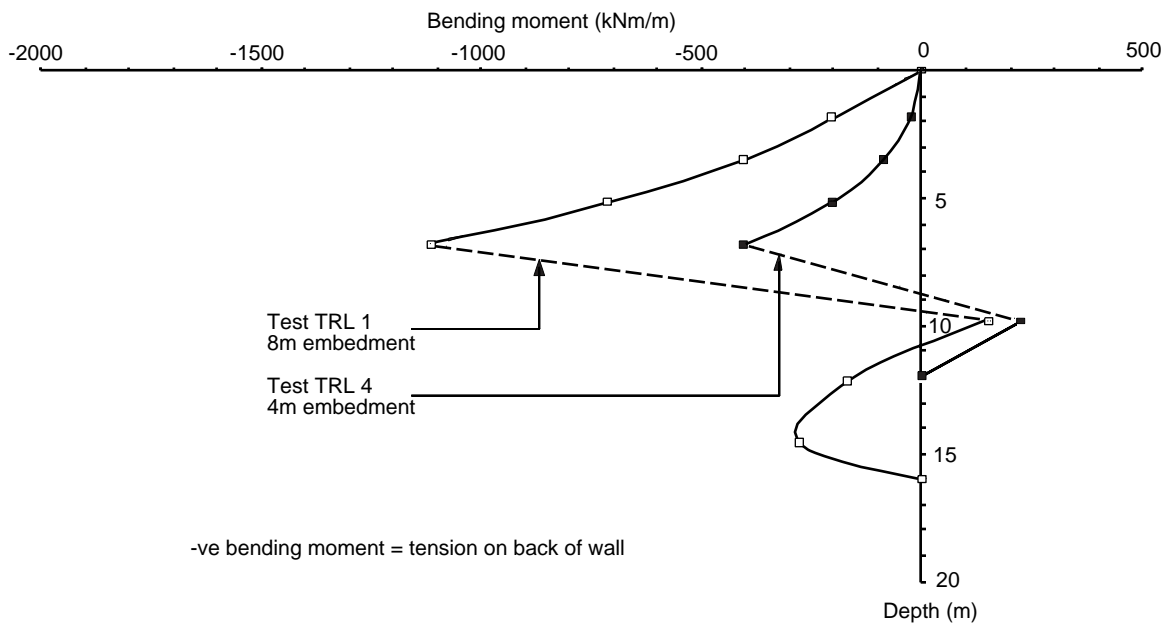


Figure 2.20 Bending moment profiles in the wall immediately after excavation, Tests TRL 1 and TRL 4

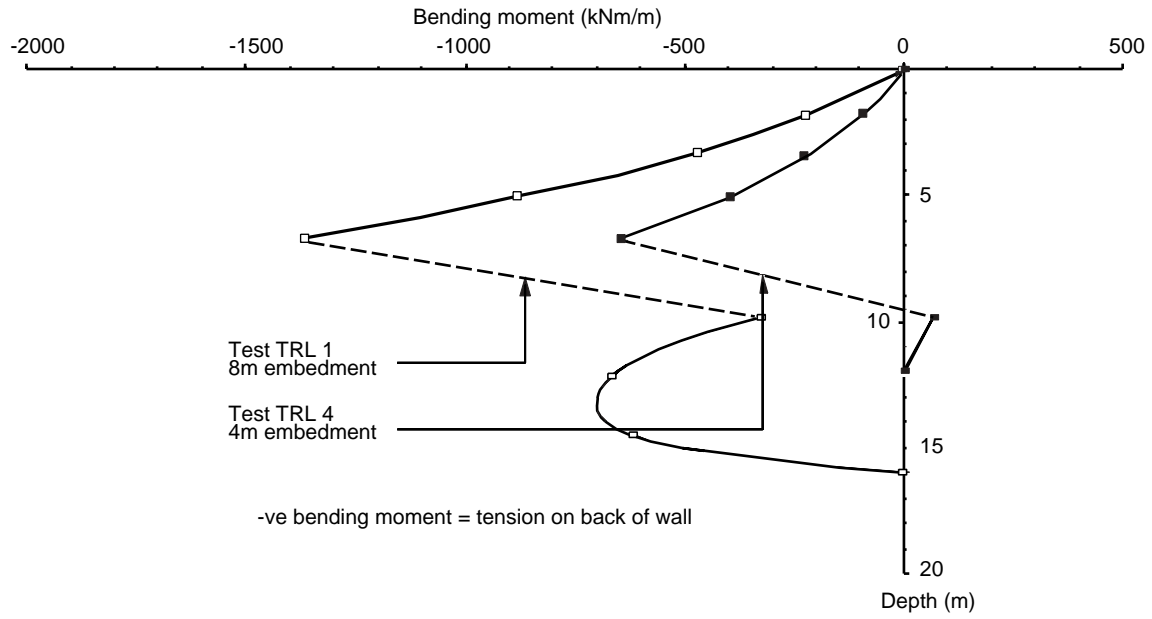


Figure 2.21 Bending moment profiles in the wall after 7.24 years, Tests TRL 1 and TRL 4

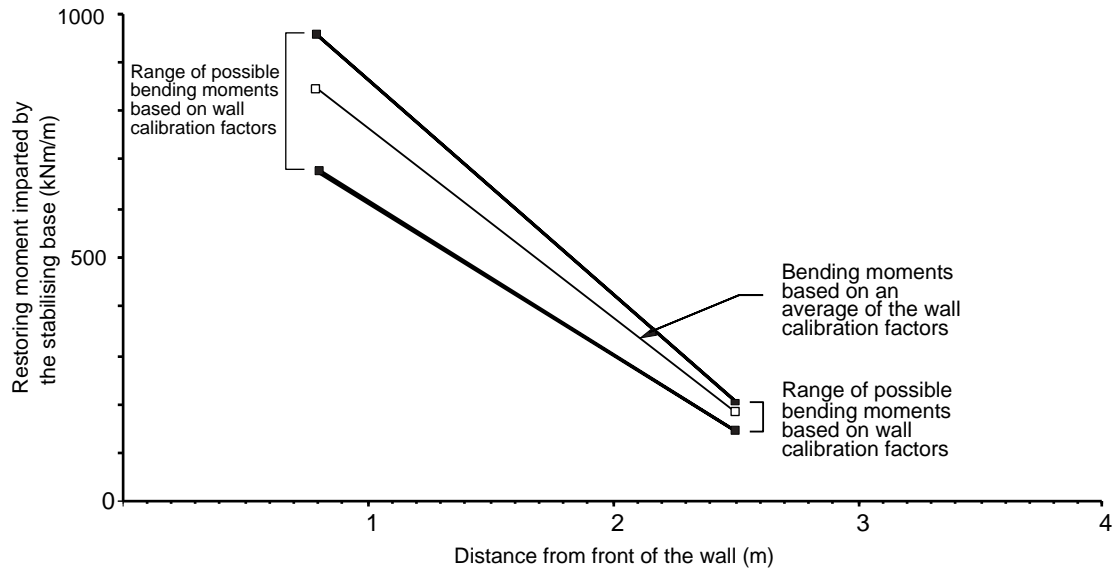


Figure 2.22 Bending moments measured in the stabilising base at the end of the test, Test TRL 4 (7.24 years)

maximum discrepancies of $\pm 2.9\%$ and -7.2% respectively in the calibration factor. Similarly, successive calibrations of the 4m embedment wall gave an average error of $\pm 2.5\%$ with a maximum error of $+4.4\%$. An alternative cause of the discrepancy was that the actual pore water pressures immediately behind the wall were significantly greater than those measured 2.16m away. Whilst the shape of the bending moment profiles in Figure 2.21 appears logical, it was concluded that not too much reliance should be placed on their magnitudes.

Calibration of the bending moment gauges on the wall involved supporting the wall on knife edge supports and hanging a series of known loads at designated points along the wall (Daly, 1999). This technique was not suitable for the bending moment gauges on the stabilising base because of the small size of the model base. The range and average of possible bending moments in the stabilising base is therefore presented in Figure 2.22, based on the largest, smallest and average calibration factors found during wall calibration. Bending moments between the two gauge positions in Figure 2.22 have been connected by a straight line, but it is recognised that the bending moment profile would probably be more parabolic than linear.

The estimated bearing pressures acting on the underside of the stabilising base (assuming a rectangular stress distribution) for the range of measured bending moments given in Figure 2.22 are shown in Table 2.2.

Table 2.2 Estimated bearing pressures on the underside of the stabilising base at the end of the test, Test TRL 4

Distance of gauge from face of wall	Bearing pressures on u/s of base (kPa)		
	Upper limit	Lower limit	Average
0.8m	187	132	166
2.5m	182	130	163

The estimated bearing pressures at the two gauge locations in Table 2.2 suggest that the assumption of a rectangular stress distribution appears to be reasonable in this case. On the basis of Equation 3.1, with $\sigma'_o = 5.83\text{kPa}$ (i.e. $\sigma'_v = 17.66\text{kN/m}^3 \times 1\text{m}$; $u = 11.83\text{kPa}$ as measured) and

$$(\gamma = 17.66\text{kN/m}^3; b = 4\text{m and } \Delta u = 23.66\text{kPa}),$$

the bearing pressures (σ'_v) given in Table 2.2 suggest a range of mobilised soil strengths of $24.4^\circ \leq \phi' \leq 27^\circ$ assuming zero friction on the underside of the base. In theory, there should have been a bearing capacity failure (i.e. $\phi' > \phi'_{crit} \{22^\circ\}$) but post-test inspections of the model showed no evidence of this.

Unfortunately, no data were forthcoming from the bending moment gauges in the stabilising base in Test TRL 1.

2.7.2 52/100 Leighton Buzzard Sand tests (Tests TRL 2 and TRL 3)

The behaviour of two stabilising base walls retaining 8m of Leighton Buzzard Sand with embedment depths of 4m (Test TRL 3) and 8m (Test TRL 2) was investigated.

The crest movement of each wall into the excavation is shown as a function of time in Figure 2.23. Magnitudes of wall movement of less than 25mm in both tests reflect the significantly greater stiffness and possibly strength of the sand compared with the speswhite kaolin clay. However, there were problems with the post-excavation groundwater boundary conditions in the sand tests which probably resulted in a stiffer response than would otherwise have been the case. These will now be discussed.

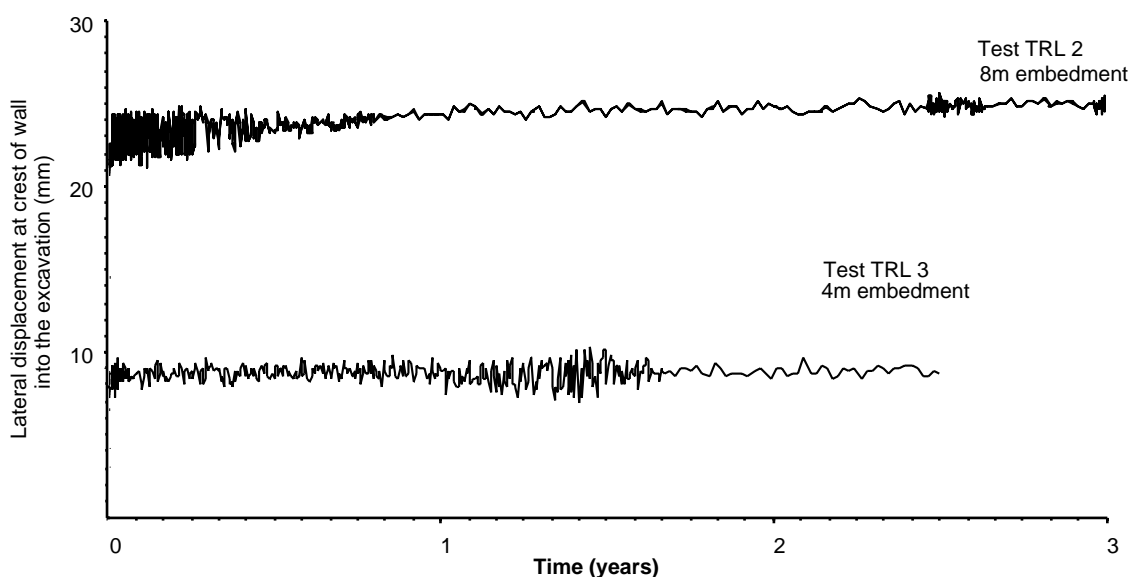


Figure 2.23 Crest movements into the excavation vs time, Tests TRL 2 and TRL 3

Pore water pressures

Pore water pressure distributions at various stages of Tests TRL 2 and TRL 3 are shown in Figures 2.24 and 2.25 respectively. The pore water pressures at the end of the 'bedding in' period in Test TRL 3 (Figure 2.25a) suggest that the water supply, drainage arrangement and transducers were all functioning satisfactorily. In Test TRL 2, however, the measured pore water pressures appear to suggest that the model was not in a state of hydrostatic equilibrium at the end of 'bedding in' (Figure 2.24a). In some cases the difference between the measured and theoretical pore water pressure was in excess of 30kPa. Post-test investigations showed that the snap-fit replacement ceramic stones in the transducers had in most cases become dislodged. This probably happened during installation of the transducers and a different installation procedure was therefore adopted in Test TRL 3. Without the porous stone, the sand was in direct contact with the transducer diaphragm resulting in an incorrect reading. The indicated changes in pore water pressures following excavation were, however, consistent with those measured by the other transducers. Sensible measurements were therefore obtained throughout the test when a correction was applied so that at the start of excavation the measurements corresponded to hydrostatic conditions.

During excavation in each test, the phreatic surface behind the wall fell towards the same level (i.e. formation level) as that on the excavated side. This was because the rate of water feed provided by the hydraulic slip rings to the retained surface was insufficient for the high permeability of the sand. Although there were minor fluctuations in the pore water pressures, each test generally reached a state of equilibrium shortly after excavation. The pore water pressure distributions at the end of each test (Figures 2.24b and 2.25b) show that the phreatic surface was in effect at formation level.

Wall and soil movements

Figure 2.23 shows that wall movements were at all times larger for the wall of 8m embedment (Test TRL 2) than for the 4m embedment wall (Test TRL 3). This is confirmed by the normalised soil settlements behind the wall after 2.54 years (Figure 2.26). In Test TRL 2, the rates of excavation (3.2 days) in front of the wall and fall in phreatic surface behind the wall were similar. In Test TRL 3, however, the rate of excavation (4.4 days) was slightly slower than the rate at which the phreatic surface behind the wall fell (3.2 days), leading to smaller soil and wall movements than in Test TRL 2.

Wall and soil movements in both tests stabilised shortly after excavation as the groundwater regime reached its equilibrium state. Maximum measured soil settlements immediately behind the wall at the end of each test of approximately 10mm in Test TRL 3 and 24mm in Test TRL 2 are similar to the measured crest movements into the excavation of 9.2mm and 24.9mm respectively. If a limitation on wall movement of 0.5% of the retained height (40mm in this case) is again adopted as a serviceability criterion, the wall/stabilising base arrangements in both tests were sufficient to prevent a serviceability failure.

Bending moments in the wall and stabilising base

The bending moments measured in the wall in the two tests after 2.54 years (i.e. corresponding to the end of Test TRL 3) are compared in Figure 2.27. The restoring moment imparted by the stabilising base is again evident in both cases. The maximum bending moment in Test TRL 2 (8m embedment) was a factor of approximately 1.6 greater than that in Test TRL 3 (4m embedment).

The maximum bending moment measured in the wall in Test TRL 2 was -807kNm/m (at a depth of 6.75m). Assuming zero pore water pressures above formation level and that the density of the soil remained unchanged (i.e. $\gamma = 19.7\text{kN/m}^3$), the lateral stresses acting on the back of the wall correspond to an earth pressure coefficient $K = 0.8$. The maximum bending moment measured in the wall in Test TRL 3 was -504kNm/m. Making similar assumptions, this gives an earth pressure coefficient $K = 0.5$. Tables of active earth pressure coefficients given by Caquot and Kerisel (1948) suggest a mobilised soil friction angle in Test TRL 3 of $\phi' = 19^\circ$ assuming zero wall friction and $\phi' = 16^\circ$ assuming full wall friction. In Test TRL 2 an earth pressure coefficient $K = 0.8$ corresponds to a mobilised soil friction angle of $\phi' = 6.5^\circ$ assuming zero wall friction.

The bending moment data of Test TRL3 are plausible bearing in mind the relatively small wall movements. The bending moment data of Test TRL 2 (8m embedment), however, are not consistent with those of Test TRL 3 (4m embedment) because the wall movements were significantly greater in this test and the soil would therefore be expected to have mobilised more of its shear strength. Whilst the validity of the maximum measured bending moment in the 8m embedment wall (Test TRL 1) is open to question, the change in measured bending moment in the wall at formation level and the measured bending moment in the stabilising base were once again broadly consistent (compare Figures 2.27 and 2.28).

The bending moments measured in the stabilising base at the end of Tests TRL 2 and TRL 3 are shown in Figures 2.28 and 2.29 respectively. A range of possible bending moments is given, as described in Section 2.7.1. The estimated bearing pressures on the underside of the stabilising base (assuming a rectangular stress distribution) for the range of bending moments given in Figures 2.28 (Test TRL 2) and 2.29 (Test TRL 3) are shown in Tables 2.3 and 2.4 respectively.

The results presented in Tables 2.3 and 2.4 suggest that the assumption of a rectangular stress distribution is again not unreasonable. On the basis of Equation 3.1, with $\sigma'_o = 9.89\text{kPa}$ (i.e. $\sigma'_v = 19.7\text{kN/m}^3 \times 1\text{m}$; $u = 9.81\text{kPa}$ as measured) and

($\gamma = 19.7\text{kN/m}^3$; $b = 4\text{m}$ and $\Delta u = 19.62\text{kPa}$), the bearing pressures (σ'_r) given in Table 2.3 suggest a range of mobilised soil strengths in Test TRL 2 (8m embedment) of $23.3^\circ \leq \phi' \leq 29.7^\circ$ assuming zero friction on the underside of the base. It is unlikely, however, that the upper limit represents a realistic estimate because it is based on the

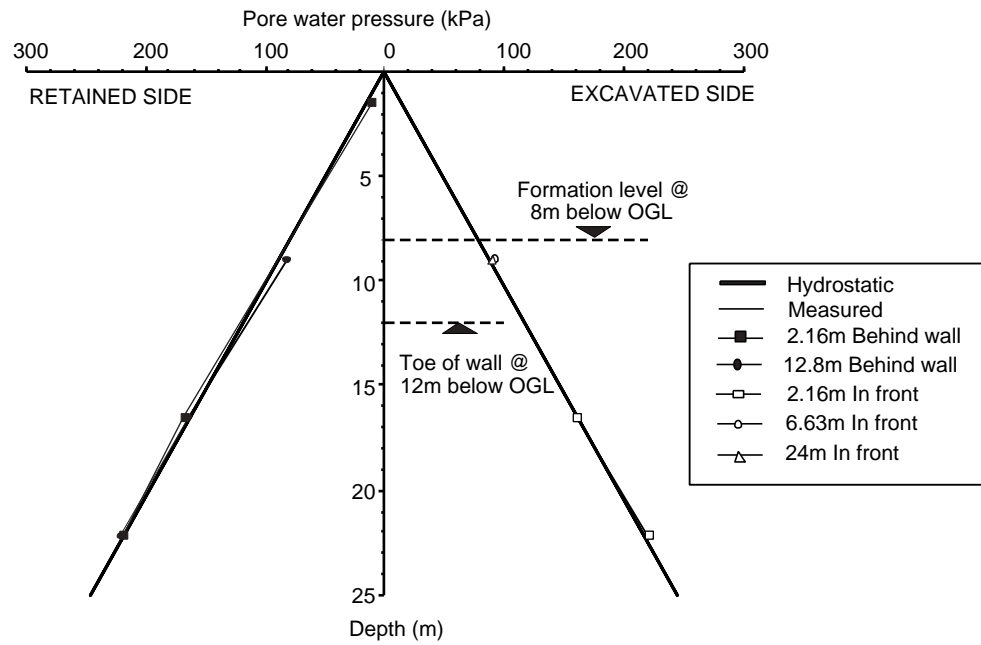


Figure 2.24a Pore water pressure profiles at the end of the *bedding in* period, Test TRL3

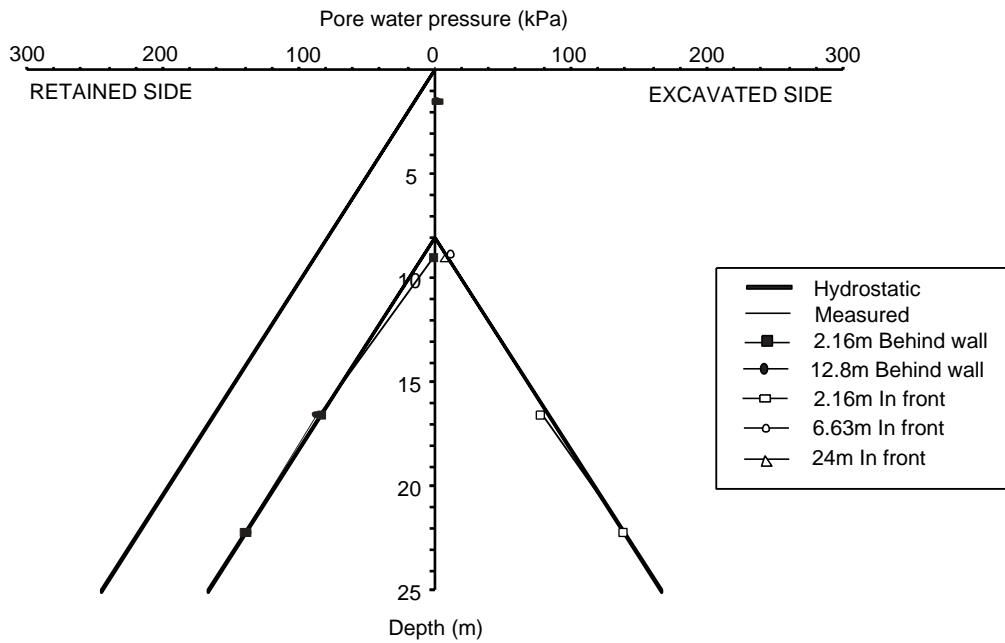


Figure 2.24b Pore water pressure profiles at the end of Test TRL 3 (2.54 years)

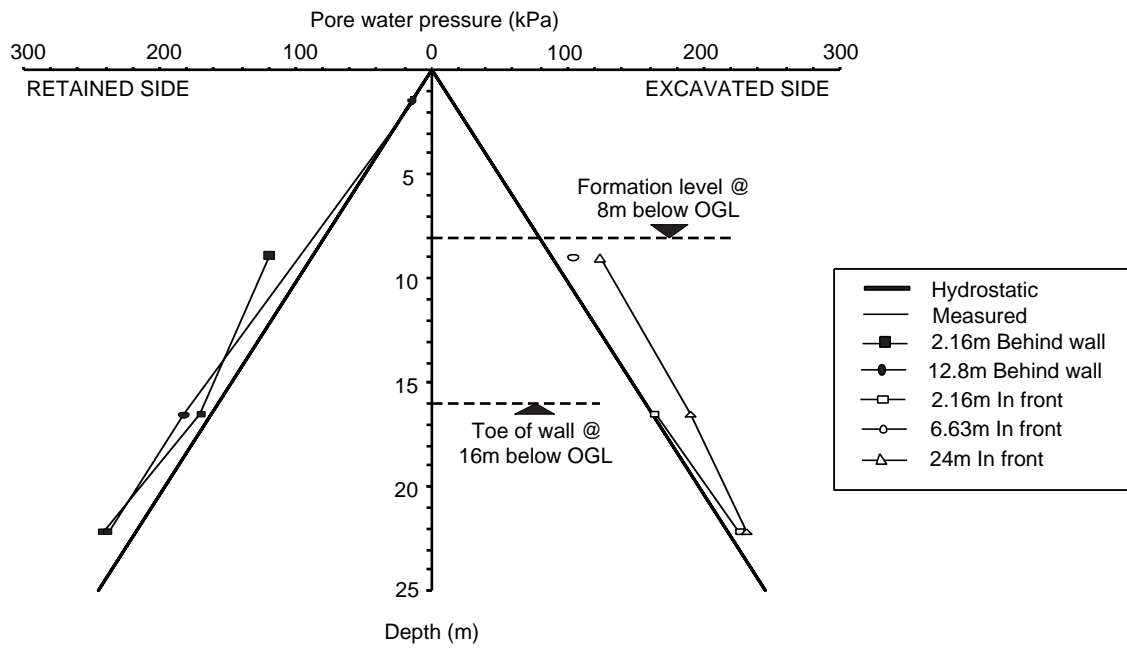


Figure 2.25a Uncorrected pore water pressure profiles at the end of the *bedding* in period, Test TRL 2

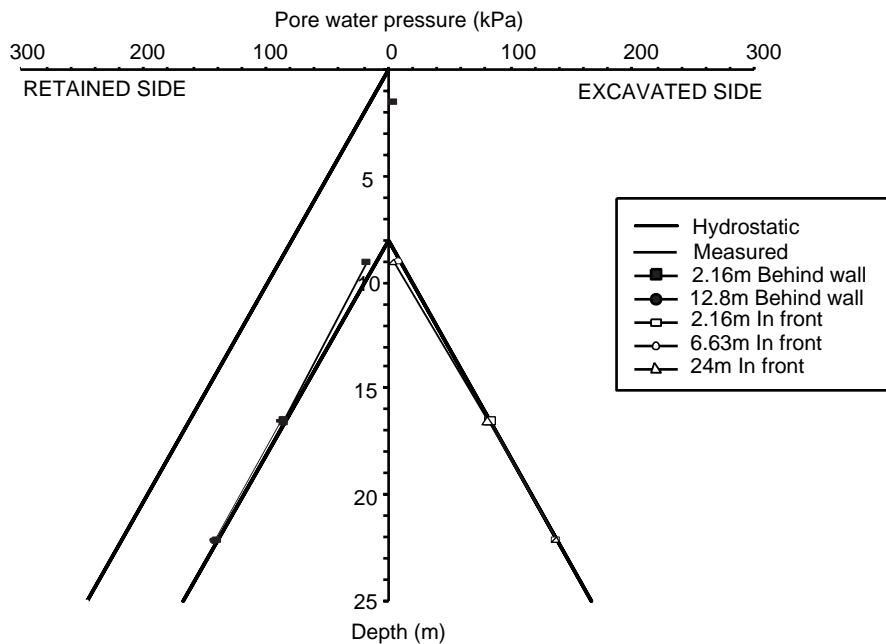


Figure 2.25b Corrected pore water pressure profiles at the end of Test TRL 2 (2.93 years)

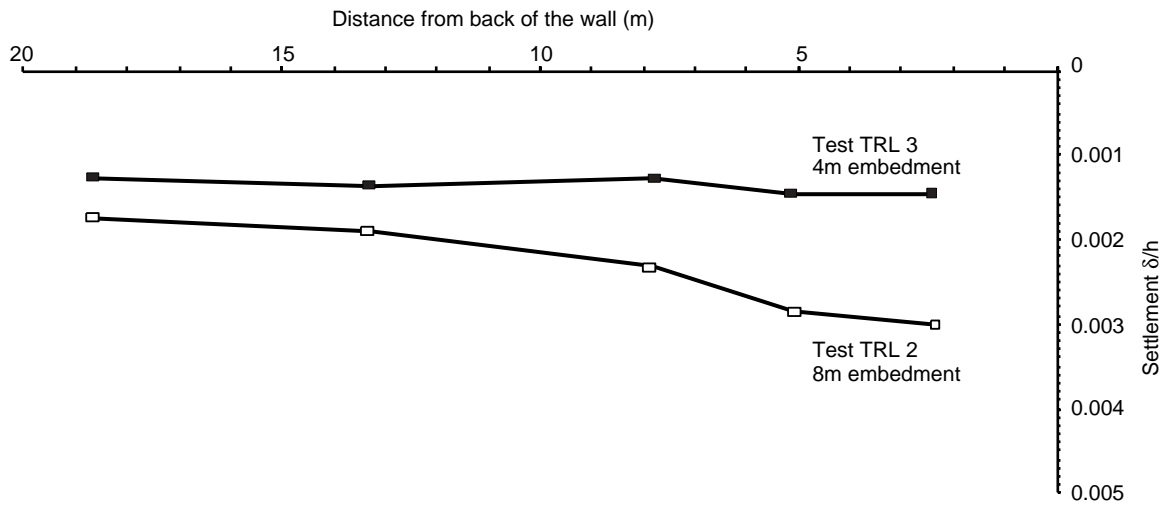


Figure 2.26 Normalised soil settlement profiles behind the wall after 2.54 years, Tests TRL 2 and TRL 3

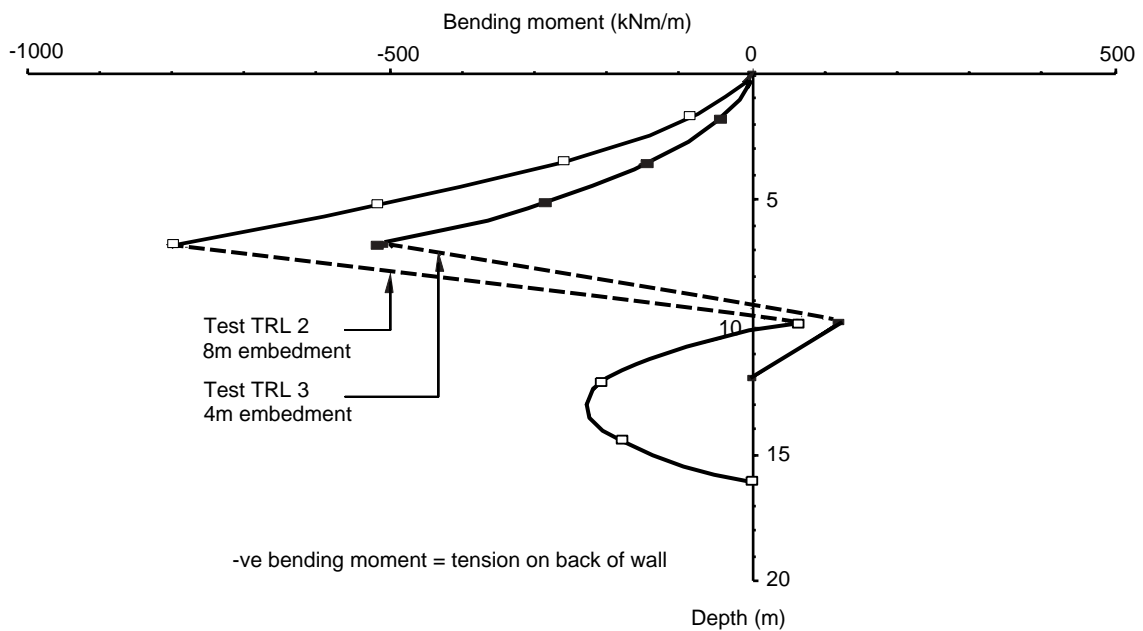


Figure 2.27 Bending moment profiles in the wall after 2.54 years, Tests TRL 2 and TRL 3

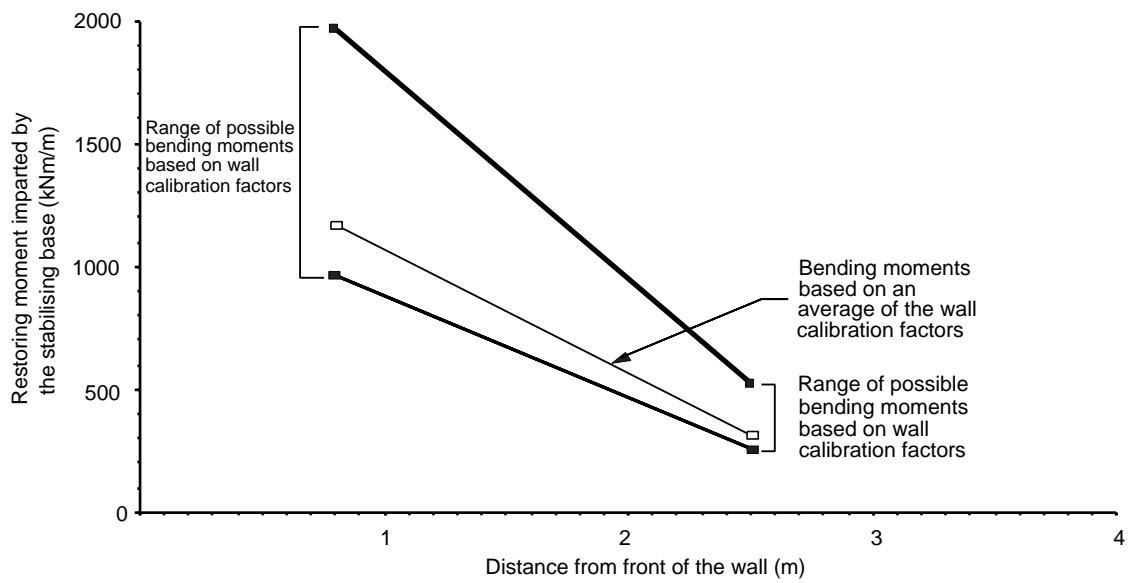


Figure 2.28 Bending moments measured in the stabilising base at the end of Test TRL 2 (2.93 years)

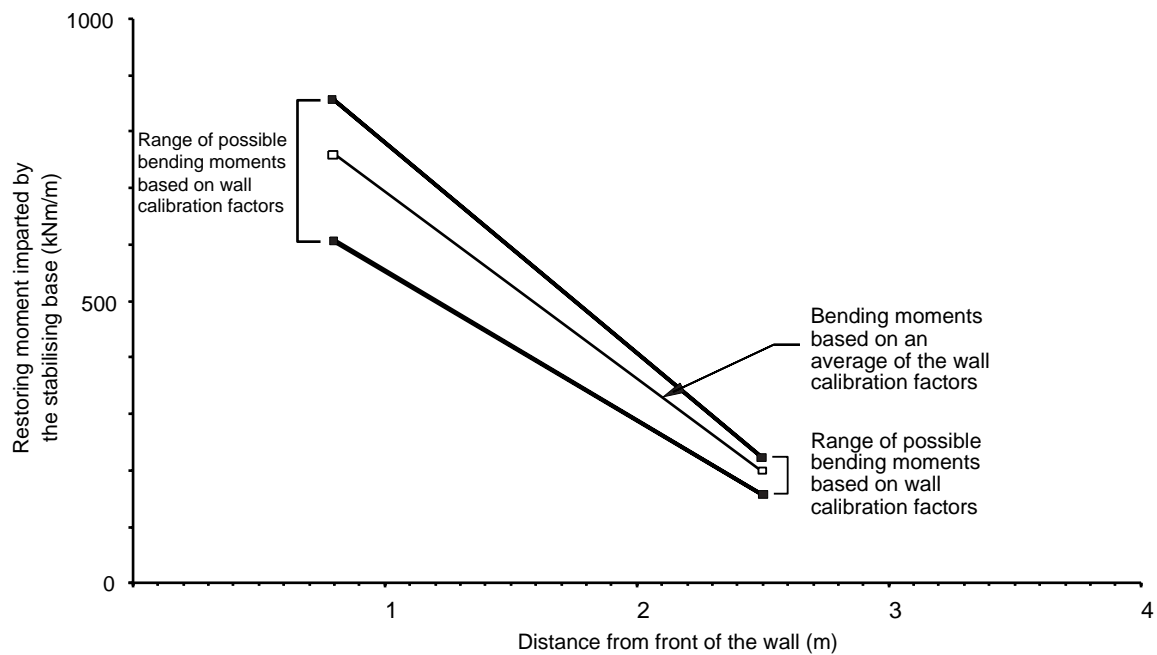


Figure 2.29 Bending moments measured in the stabilising base at the end of Test TRL 3 (2.54 years)

Table 2.3 Estimated bearing pressures on the underside of the stabilising base at the end of Test TRL 2 (8m embedment)

Distance of gauge from face of wall	Bearing pressures on u/s of base (kPa)		
	Upper limit	Lower limit	Average
0.8m	385	188	228
2.5m	466	228	276

Table 2.4 Estimated bearing pressures on the underside of the stabilising base at the end of Test TRL 3 (4m embedment)

Distance of gauge from face of wall	Bearing pressures on u/s of base (kPa)		
	Upper limit	Lower limit	Average
0.8m	167	119	148
2.5m	197	140	175

calibration characteristics of a single strain gauge which were significantly greater than the average. The lower limit probably represents a better estimate.

Adopting a similar approach, the estimated bearing pressures in Table 2.4 suggest a range of mobilised soil strengths in Test TRL 3 (4m embedment) of $20^\circ \leq \phi' \leq 23.6^\circ$ again assuming there is zero friction on the underside of the base.

The results suggest that a bearing capacity failure would not have been expected in either of the tests (i.e. $\phi' < \phi'_{crit} \{35^\circ\}$). Post-test inspections of the model confirmed that this was indeed the case.

3 Limit-equilibrium analyses

3.1 Bearing capacity of a stabilising base

The stabilising base principle relies on the bearing pressure (σ'_f) on the underside of a slab attached rigidly to the front of the wall imparting a restoring moment to the retaining wall. In addition, shear stresses (τ) may act at the soil/base interface. The combined effect of the two stresses will give a resultant stress at an angle δ_b to the vertical (where $0 \leq \delta_b \leq \phi'$). The stresses acting on the underside of a stabilising base are shown in Figure 3.1.

The bearing capacity (σ'_f) of a foundation founded in a purely frictional soil obeying the failure criterion $(\tau/\sigma')_{max} = \tan \phi'$ is often estimated using Equation 3.1 (e.g. Powrie, 1997)

$$(3.1)$$

where σ'_o is the vertical effective stress in the adjacent soil at the underside of the founding plane, b is the width of the foundation and Δu is the difference in the pore water pressure between the founding plane and a depth 0.5b below it. The enhancement factors s_q and d_q are applied to

the bearing capacity factor N_q to account for the shape and depth of the foundation. The bearing capacity factor N_q for inclined loads on shallow foundations can be calculated, for example, from the following expression (Powrie, 1997).

$$(3.2)$$

where

The relationship between bearing capacity factor, N_q , and soil friction angle, ϕ' , for various angles of load inclination δ_b , is shown graphically in Figure A1 in Appendix A. Numerical values for $\phi' = 22^\circ$ and $\phi' = 35^\circ$ are given in Table 3.1.

Table 3.1 Bearing capacity factors N_q for inclined loads of $\delta_b/\phi' = 1.0$ and $\delta_b/\phi' = 0$ according to Equation 3.2

Soil friction ϕ' (degrees)	Bearing capacity factor, N_q	
	Base friction $\delta_b/\phi' = 1.0$	Base friction $\delta_b/\phi' = 0$
22	2.22	7.82
35	3.08	33.30

The bearing capacity is further enhanced by the second term on the right hand side of Equation 3.1, which takes account of the increase in vertical effective stress with depth below the founding plane. This is discussed in more detail by Powrie (1997). Numerical values of s_q , d_q , N_γ , s_γ and d_γ are given by Meyerhof (1963) and Brinch Hansen (1970). In this report, the enhancement factors suggested by Meyerhof (1963) have been adopted (Table 3.2).

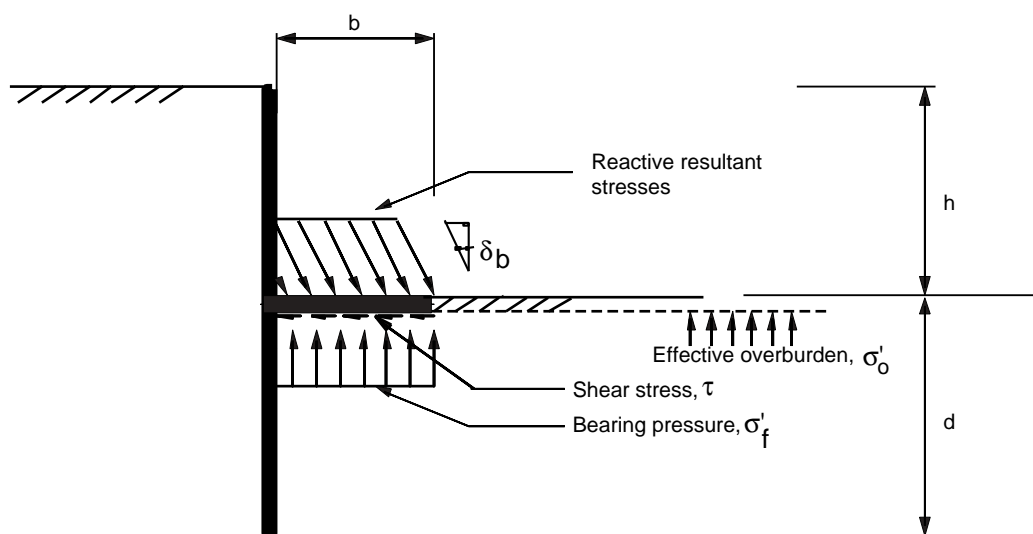


Figure 3.1 Stresses acting on the underside of a stabilising base

Table 3.2 Bearing capacity enhancement factors after Meyerhof (1963)

Parameter	Value
Shape factor, s_q	$1 + 0.1 K_p (b/L)$
Depth factor, d_q	$1 + 0.1 (d/b) (K_p)^{0.5}$
N_γ	$(N_q - 1) \tan (1.4\phi')$
Shape factor, s_γ (for N_γ)	$= s_q$
Depth factor, d_γ (for N_γ)	$= d_q$
r_γ for $b \geq 2m$ (Bowles, 1988)	$1 - 0.25 \log_{10} (b/2)$

Expressions apply for $\phi' > 10^\circ$; $K_p = (1 + \sin \phi') / (1 - \sin \phi')$;
Foundation breadth b , length L and depth d .

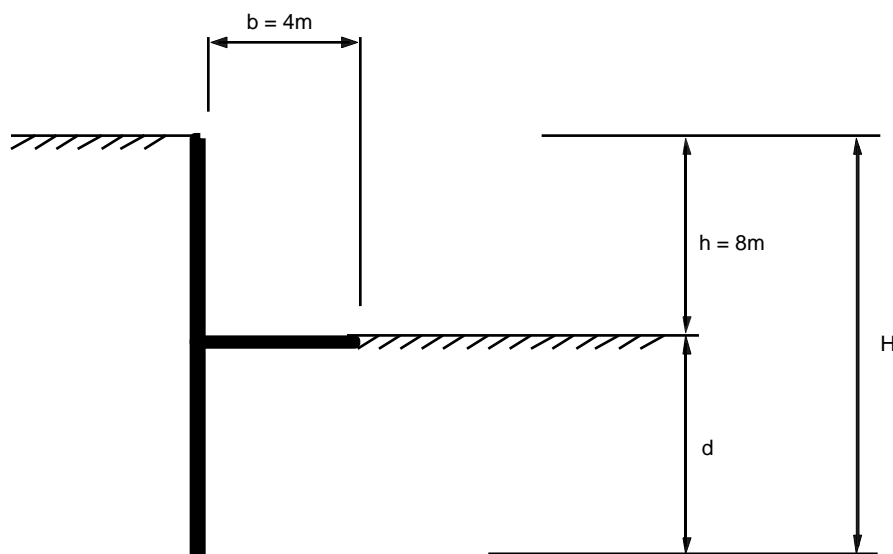
On the basis of Equations 3.1 and 3.2, the range of bearing capacities σ'_f (normal component) for $0 \leq \delta_b \leq \phi'$ for an infinitely long foundation of 1m depth and 4m breadth in a soil of unit weight 17.5 kN/m^3 and friction angle $\phi' = 22^\circ$, would be between 278.4kPa and 64.7kPa assuming that the groundwater level is coincident with the underside of the foundation (i.e. at a depth of 1m below the soil surface). This difference between $\delta_b = 0$ and $\delta_b = \phi'$ becomes even more pronounced at higher values of ϕ' . A groundwater level at the excavated soil surface significantly reduces the range of bearing capacities to between 122.4kPa and 28.4kPa (assuming hydrostatic conditions).

Shear stresses on the underside of a stabilising base, the groundwater conditions and the increase in vertical effective stress below the founding plane may all have a significant influence in the design of a stabilising base retaining wall.

3.2 Conditions investigated in the limit-equilibrium analyses

The conditions investigated in the analyses are indicated in Figure 3.2.

The analyses involved the determination of the depth of embedment at limiting equilibrium based on the actual



Estimated actual condition

Figure 3.2 Conditions examined in limit-equilibrium analyses

retained height with no allowance being made for overexcavation in front of the wall, surcharge loading behind the wall or reduced soil-wall friction.

3.3 Possible collapse limit states for a stabilising base retaining wall.

Four possible collapse limit states for a stabilising base retaining wall are illustrated in Figure 3.3. The limiting stress distributions consistent with each mode of collapse are also shown.

3.3.1 Failure mechanisms and stress distributions based on Schemes 1 and 2

The collapse mechanisms for Schemes 1 and 2 are analogous to those for a wall with a rigid prop at formation level. The limiting equilibrium of embedded retaining walls rigidly propped at formation level (without stabilising bases) has been investigated previously by Powrie and Li (1991).

The Scheme 1 approach assumes rigid body rotation about the prop, with the wall above the prop moving into the excavation. Behind the wall, active conditions are assumed above formation level. At formation level there is a transition from active to passive conditions, with passive conditions then being taken to apply down to the toe of the wall. In front of the wall active conditions are assumed below formation level. Powrie and Li (1991), however, question the applicability of stress distributions based purely on rotational deformations since excavation in front of an in situ embedded retaining wall in overconsolidated clay is likely to bring the soil remaining below formation level towards passive failure. Also, it is likely that there will be a degree of forward movement at the position of the prop, particularly in the case of a stabilising base wall, as discussed later.

The Scheme 2 approach again assumes rigid body rotation about the prop but with the wall above the prop

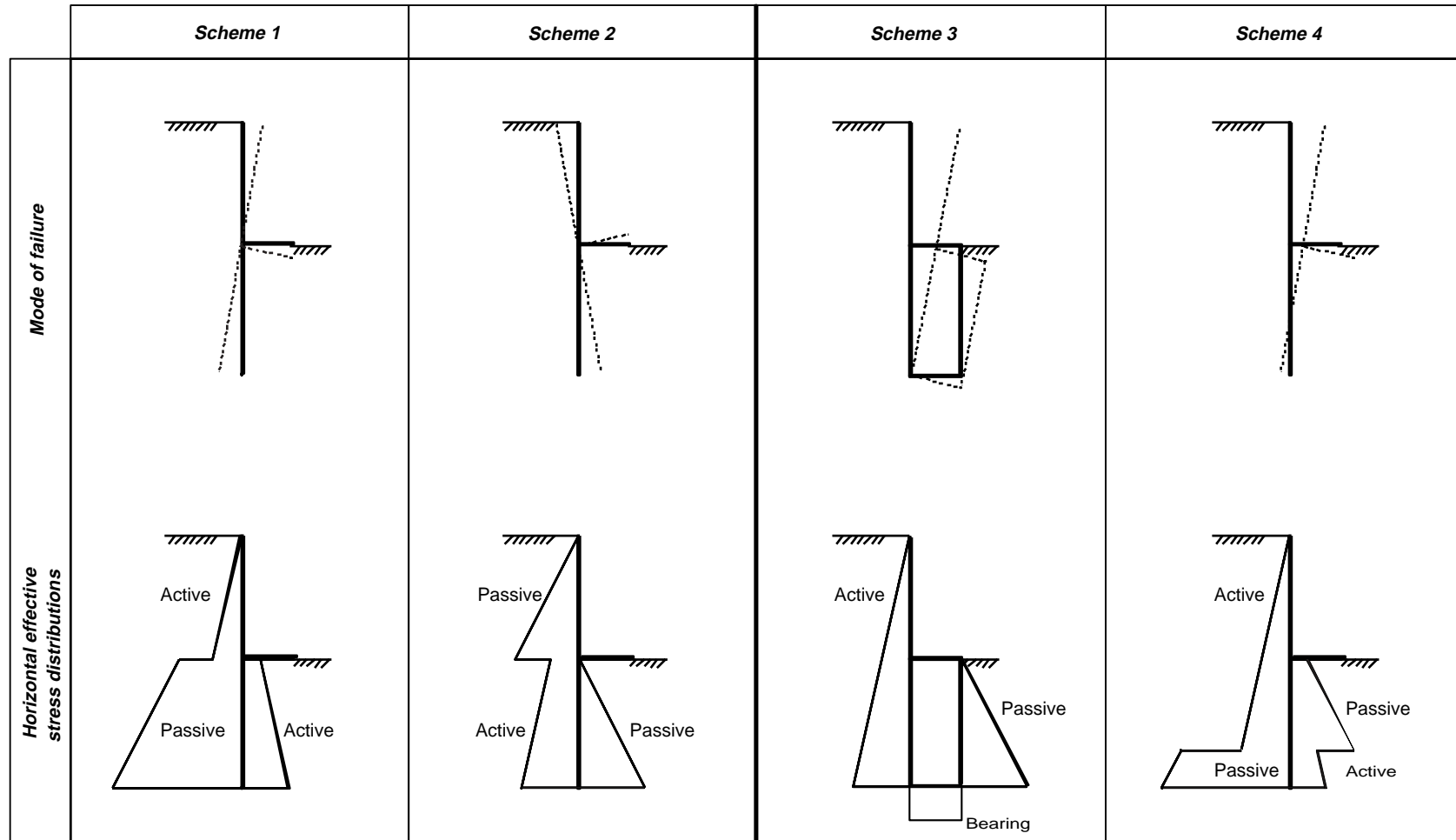


Figure 3.3 Possible modes of failure of a stabilising base retaining wall

moving backwards into the retained soil. Behind the wall, passive conditions are assumed above formation level with a transition at formation level to active conditions, which are then assumed to apply down to the toe of the wall. In front of the wall, passive conditions are assumed below formation level.

The solution in both of these cases involves first determining the depth of embedment required to maintain moment equilibrium about the (assumed rigid) prop. The prop force can then be calculated from the condition of horizontal force equilibrium.

The analyses carried out by Powrie and Li (1991) assumed a retained height of 10m and a soil of unit weight $\gamma/\gamma_w = 1.7$. The results of similar analyses assuming a smooth wall retaining 8m of soil of unit weight 17.5kN/m³ and a full height groundwater level behind the wall with steady state seepage pore water pressures modelled as suggested by Symons (1983) are presented in Figure A2 in Appendix A. The results suggest that for $\phi' = \phi'_{crit} = 22^\circ$, a depth of embedment of 2.38m is required to prevent failure of the wall by forward rotation with a coefficient of lateral earth pressure $K = K_a$ in front of the wall below formation level. The prop force in this case is 1017kN/m. Further analyses were then carried out in which the effect of an increased coefficient of lateral earth pressure in front of the wall was investigated. These suggested that a slightly increased depth of embedment of 2.4m and a reduced prop force of 1014kN/m would be required to prevent failure of the wall by forward rotation with $K = K_p$ in front of the wall due to the unloading effect of excavation.

In the case of a stabilising base retaining wall, the large prop forces calculated from horizontal force equilibrium when failure is assumed to occur by rotation about the prop cannot be provided by the shear at the underside of the base and the end bearing of the base against the soil. Schemes 1 and 2 are therefore unlikely to represent realistic failure mechanisms and any design based on these approaches could be unsafe, particularly if horizontal force equilibrium is not checked.

3.3.2 Failure mechanisms and stress distributions based on Scheme 3

The collapse mechanism for Scheme 3 is analogous to that for a mass gravity wall or a cantilever L-wall. The wall and the soil below the stabilising base and above the toe of the wall are assumed to act as a rigid block. Collapse will occur when there is limiting equilibrium with active conditions behind the block, passive conditions in front of the block and such bearing pressures as are required to maintain equilibrium on the underside of the block. The proportions of the block must be arranged such that, for a given mobilised or ultimate angle of shearing resistance ϕ' , there is global equilibrium of the forces acting on the block.

3.3.3 Failure mechanisms and stress distributions based on Scheme 4

The collapse mechanism for Scheme 4 is analogous to that for an unpropped cantilever wall. Rigid body rotational failure is assumed to occur about an axis lying in the plane of the wall at some point between formation level and the

toe. The bearing pressure on the underside of the stabilising base imparts a restoring moment to the retaining wall and also acts as a surcharge on the soil in front of the wall. Shear stresses on the underside of the stabilising base may also provide some degree of horizontal resistance. If ϕ' and the soil/structure friction angles are known, the coefficients of lateral earth pressure (after Caquot & Kerisel, 1948), the bearing capacity factor (after Equation 3.2) and stabilising base shear stress can be determined. The unknown quantities are the depth of embedment d and the distance below formation level to the point of rotation Z_p . These can be determined from the conditions of horizontal force and moment equilibrium.

3.4 The results of limit-equilibrium analyses of stabilising base retaining walls based on Scheme 3.

The stresses acting on a stabilising base wall treated as a soil/wall block (Scheme 3) are shown in Figure 3.4. In the analyses presented in this section, a rectangular base bearing pressure distribution (consistent with a plastic collapse analysis) has been assumed. A typical analysis involved the following steps:

a Input data:

- Mobilised angle of shearing resistance ϕ'
- Wall friction on the vertical sides of the wall/soil block δ
- Earth pressure coefficients K_a and K_p from Caquot and Kerisel (1948)
- Base friction on the underside of the wall/soil block δ_b
- Retained height h
- Wall and stabilising base thicknesses t_1 and t_2 respectively
- Unit weights of soil γ and wall/stabilising base γ_{conc}
- Pore water pressure regime, i.e. steady state linear seepage
- Surcharge on retained side (if any)

b Unknowns:

- Vertical effective force on the underside of the wall/soil block N'_b
- Shear force on the underside of the wall/soil block T_b
- Depth of embedment d
- Width of the stabilising base b

c The following quantities were written in terms of b and d (see Figure 3.4):

- Horizontal effective force on the back of the wall/soil block $R'_{w h active}$
- Vertical effective force on the back of the wall/soil block $R'_{w v active}$
- Horizontal effective force on the front of the wall/soil block $R'_{w h passive}$
- Vertical effective force on the front of the wall/soil block $R'_{w v passive}$

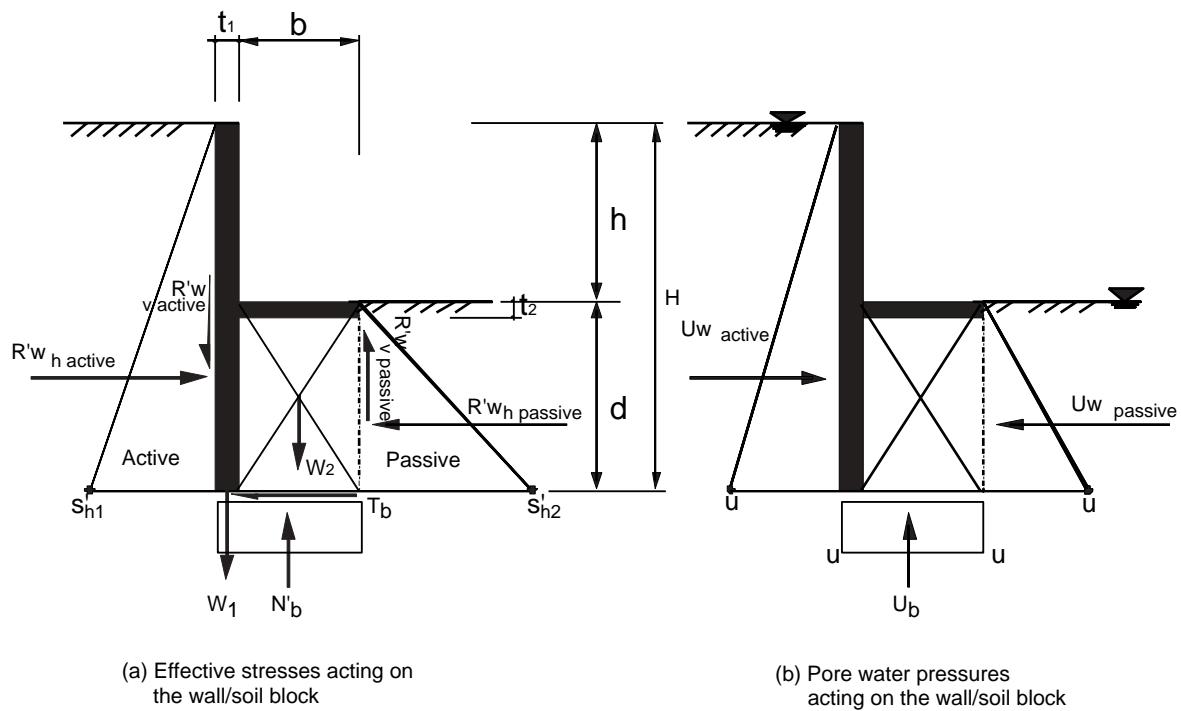


Figure 3.4 Forces acting on a stabilising base wall/soil block after Scheme 3

Pore water force on the back of the wall/soil block $U_{w \text{ active}}$

Pore water force on the front of the wall/soil block $U_{w \text{ passive}}$

Pore water force on the underside of the wall/soil block U_b

Self weight of the wall W_1

Combined weight of the stabilising base and soil block below the stabilising base W_2

d Check for global equilibrium of the structure:

Using the condition of vertical force equilibrium, calculate the vertical effective force on the underside of the wall/soil block N'_b

Using the condition of horizontal force equilibrium, calculate the shear force on the underside of the wall/soil block T_b i.e. $T_b = N'_b \tan \delta_b$

Check for moment equilibrium about the toe of the wall/soil block

Adjust b and d as necessary until there is global equilibrium of the forces acting on the structure

Finally, check that the bearing pressures on the underside of the wall/soil block do not exceed the bearing capacity given by Equation 3.1

A spreadsheet version of the calculation was developed in order to reduce the time taken to carry out the analyses.

3.4.1 Walls retaining speswhite kaolin clay

Two series of analyses based on the estimated actual conditions were undertaken. These assumed a prototype

wall retaining 8m of saturated kaolin of unit weight 17.5kN/m^3 , a full height groundwater level behind the wall and steady state linear seepage conditions. The wall and stabilising base thicknesses were taken as 1m and their density as 22kN/m^3 . The first series of analyses investigated the depth of embedment and stabilising base projection from the wall required to prevent collapse assuming full friction on both vertical sides of the wall/soil block and zero base friction on the underside of the wall/soil block. The second series of analyses followed a similar approach but full friction on the base of the wall/soil block was assumed. The results of the analyses for different mobilised angles of soil friction f' are presented in Figures A3 ($\delta_b/\phi' = 0$) and A4 ($\delta_b/\phi' = 1$) in Appendix A. The results of the analyses for $\phi' = \phi'_{\text{crit}} = 22^\circ$ are summarised in Table 3.3.

Table 3.3 Results of limit-equilibrium analyses using Scheme 3 assuming 'estimated actual conditions' with $\phi' = 22^\circ$

	Zero base friction $\delta_b/\phi' = 0$		Full base friction $\delta_b/\phi' = 1^{(a)}$	
	Depth of embedment, d (m)	Width of stabilising base, b (m)	Depth of embedment, d (m)	Width of stabilising base, b (m)
kaolin clay $\gamma = 17.5\text{kN/m}^3$ (21.07 ^b)	13.07	10.68	9.79	14.53
			(17.79 ^b)	

(a) In this case δ_b/ϕ' was restricted to 0.977 to ensure that the bearing capacity of the soil was not exceeded;

(b) Figures in brackets represent the overall wall height (H) in metres; (Retained height = 8.0m; Full height groundwater level; Steady state linear seepage conditions)

While carrying out the analyses with $\delta_b/\phi' = 1$ (Figure A4), it became apparent that global equilibrium of the forces acting on the wall/soil block could not be satisfied in every case. The wall/soil base friction angle δ_b had to be restricted in some instances so that the bearing pressure on the underside of the wall/soil block did not exceed the bearing capacity of the soil: For example, for the case assuming estimated actual conditions with $\phi' = 22^\circ$ presented in Table 3.3, δ_b had to be reduced to 21.5° .

The results of the analyses tend to suggest that the wall/stabilising base arrangements of centrifuge tests TRL 1 (8m embedment) and TRL 4 (4m embedment) should have collapsed. For an embedment of 8m, a base width of 7.58m would be required and the soil would have to mobilise $\phi' = 30^\circ$ (Figure A3 in Appendix A) for global equilibrium. Although the analyses are all based on calculated and not measured pore water pressures, it is unlikely that this would make a very significant difference to the results.

The results of the analyses using the Scheme 3 approach are not consistent with the findings of the centrifuge model tests carried out in kaolin clay. In this case, a design based on the Scheme 3 analysis would probably be overconservative and therefore uneconomic.

3.4.2 Walls retaining Leighton Buzzard Sand

For completeness, curves are presented for a series of analyses based on the estimated actual conditions for a wall/soil block retaining 8m of saturated Leighton Buzzard Sand of unit weight 20 kN/m^3 . Analyses assumed a full height groundwater level behind the wall and steady state linear seepage conditions. The results of the analyses for different mobilised angles of soil friction ϕ' are presented in Figure A5 ($\delta_b/\phi' = 0$) and Figure A6 ($\delta_b/\phi' = 1$). A summary of the results for $\phi' = \phi'_{\text{crit}} = 35^\circ$ is given in Table 3.4.

Table 3.4 Results of limit-equilibrium analyses using Scheme 3 assuming 'estimated actual conditions' with $\phi' = 35^\circ$

	Zero base friction $\delta_b/\phi' = 0$		Full base friction $\delta_b/\phi' = 1^{(a)}$	
	Depth of embedment, d (m)	Width of stabilising base, b (m)	Depth of embedment, d (m)	Width of stabilising base, b (m)
L.B. Sand $\gamma = 20 \text{ kN/m}^3$	4.69 (12.69*)	4.25	2.97 (10.97*)	5.9

* Figures in brackets represent the overall wall height (H) in metres. (Retained height = 8.0m; Full height groundwater level; Steady state linear seepage conditions)

The analyses suggest that at limiting equilibrium with $\phi'_{\text{crit}} = 35^\circ$, the stabilising base projection from the wall of 4m in Tests TRL 2 (8m embedment wall) and TRL 3 (4m embedment wall) would be insufficient to prevent collapse. However, an assessment of the stability of the stabilising base walls in centrifuge tests TRL 2 and TRL 4 based on a full height groundwater level behind the wall is conservative because the actual groundwater conditions in the centrifuge tests corresponded to a phreatic surface at formation level.

The Scheme 3 approach of designing for a stabilising base retaining wall also restricts the freedom of the designer in that it gives a paired value of embedment depth d and stabilising base projection from the wall b .

3.5 The results of limit-equilibrium analyses of stabilising base retaining walls based on Scheme 4.

The limiting horizontal effective stress and pore water pressure distributions acting on the stabilising base wall using the Scheme 4 approach are shown in Figures 3.5a and 3.5b respectively. In front of the wall, the horizontal effective stress distributions were taken from the underside of the stabilising base and the phreatic surface was assumed to be at formation level. The horizontal resistance provided by the stabilising base itself was ignored as this was not expected to contribute greatly to the stability of the wall (Chandler, 1995).

A rectangular bearing pressure distribution (consistent with a plastic collapse analysis) beneath the stabilising base was assumed in all of the analyses. If the soil behaved as a linear elastic medium, rigid body rotation of the wall would be expected to result in a trapezoidal pressure distribution on the underside of the stabilising base. The contact stress would increase with vertical displacement towards the free end of the stabilising base. In reality, however, the soil stiffness will tend to reduce the increasing strain and the stabilising base will bend to make the contact stress below the base more uniform. A typical analysis involved the following steps:

a Input data:

- Mobilised angle of shearing resistance ϕ'
- Wall friction δ
- Earth pressure coefficients K_a and K_p from Caquot and Kerisel (1948)
- Base friction on the underside of the stabilising base δ_b
- Retained height h
- Width of the stabilising base b
- Unit density of soil γ
- Pore water pressure regime, i.e. steady state linear seepage
- Surcharge on the retained side (if any)

b Unknowns:

- Depth of embedment d
- Depth below formation level to the pivot point Z_p

c The following quantities were calculated in terms of d and/or Z_p (see Figure 3.5):

- Pore water pressures in front of and behind the wall for steady state linear seepage
- Bearing pressures on the underside of the stabilising base σ'_f from Equation 3.1
- Restoring moment M due to bearing pressure on the underside of the stabilising base, i.e. $M = \sigma'_f b^2 / 2$
- Shear force on the underside of the stabilising base $T_b = \tau b = (\sigma'_f \tan \delta_b) \times b$

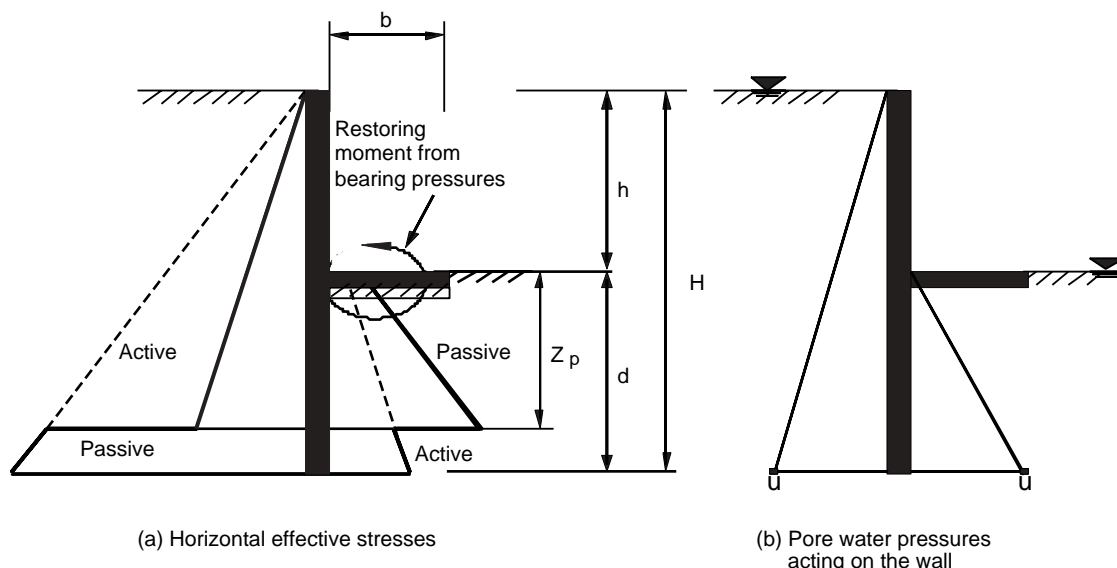


Figure 3.5 Forces acting on a stabilising base retaining wall after Scheme 4

Horizontal effective stresses due to soil self weight in front of and behind the wall

Horizontal effective stresses due to surcharge behind the wall (if any)

Horizontal effective stresses in front of the wall due to surcharge arising from the bearing pressure on the underside of the stabilising base

d Conditions of horizontal force and moment equilibrium:

Adjust Z_p and d until there is horizontal force equilibrium on both sides of the wall and moment equilibrium about the top of the wall

A spreadsheet version of the calculation was developed in order to reduce the time taken to carry out the analyses.

An investigation into the stress fields that can be developed below a stabilising base suggests that it may not be theoretically possible to develop full wall friction in front of the wall and zero base friction on the underside of the base, owing to a lack of space to achieve the required rotation in the principal stress directions. This means that the approach using Caquot and Kerisel's (1948) earth pressure coefficients lacks rigour, and may err on the unsafe side.

3.5.1 Stabilising base walls retaining speswhite kaolin clay

Two series of analyses based on the estimated actual conditions were undertaken. These assumed a prototype wall retaining 8m of saturated kaolin of unit weight 17.66kN/m^3 , a stabilising base projection from the wall of 4m, a full height groundwater level behind the wall and steady state linear seepage conditions. The first series of analyses investigated the depth of embedment required to prevent collapse assuming zero wall friction on both sides of the wall and varying angles of inclined stress on the stabilising base. The bearing pressure on the underside of the stabilising base was estimated on the basis of Equation 3.1. The second series of

analyses followed a similar approach but assumed full wall friction (with earth pressure coefficients taken from Caquot & Kerisel, 1948) on both sides of the wall. The results of the two analyses for different mobilised angles of soil friction ϕ' are presented in Figures A7 and A8 in Appendix A, and the results of the analyses for $\phi' = \phi'_{crit} = 22^\circ$ are summarised in Table 3.5.

Table 3.5 Results of limit-equilibrium analyses using Scheme 4 assuming 'estimated actual conditions' with $\phi' = 22^\circ$

	Zero wall friction		Full wall friction	
	Base friction $\delta/\phi' = 1.0$	Base friction $\delta/\phi' = 0$	Base friction $\delta/\phi' = 1.0$	Base friction $\delta/\phi' = 0$
Depth of embedment, d	28.84m (36.84m*)	12.27m (20.27m*)	19.60m (27.60m*)	8.59m (16.59m*)

* Figures in brackets represent the overall wall height, H .
(Retained height = 8.0m; Stabilising base width = 4m; Full height groundwater level;
Steady state linear seepage conditions;
Bearing pressure on the u/s of stabilising base determined in accordance with Equation 3.1)

In centrifuge model Test TRL 4, the wall of 4m embedment suffered large movements which culminated in a series of rupture surfaces being developed behind the wall (Section 2.7.1). This wall was clearly in a state of collapse: the results of the analyses in Table 3.5 all suggest that for a wall of 4m embedment this is certainly to be expected.

In centrifuge Test TRL 1, the wall of 8m embedment suffered large movements but was not in a state of outright collapse (Section 2.7.1). Shear box tests undertaken by Powrie (1986) suggested that the ultimate angle of friction between resin and kaolin was approximately $\delta = \phi'_{crit} = 22^\circ$. Bearing in mind the large relative movements of the soil

against the wall in the centrifuge model tests, it is reasonable to assume that full wall friction was mobilised everywhere with $\delta = \phi'_{crit}$.

The results of the analyses in Table 3.5 suggest that the wall of 8m embedment (TRL 1) would also be in a state of collapse, but only just so if full wall friction is assumed to be mobilised on both sides of the wall with zero friction on the underside of the stabilising base and bearing pressures on the underside of the stabilising base calculated in accordance with Equation 3.1. In this case, Figure A8 in Appendix A suggests that for a wall of 8m embedment, $\phi'_{mob} = 22.5^\circ$ would be needed to be mobilised everywhere for the wall to be in equilibrium. This is equivalent to a mobilisation factor $M = 0.98$ (assuming $\phi'_{peak} = \phi'_{crit} = 22^\circ$).

An assessment of the stability of the stabilising base retaining walls in centrifuge Tests TRL 1 and TRL 4 based on calculated pore water pressure distributions is overconservative. Also, the long term wall movements in Tests TRL 1 and TRL 4 were sufficiently large to warrant a back-analysis based on the deformed geometry. Further analyses were therefore undertaken to assess more accurately the stability of the two walls. Once again, the same soil friction angle was assumed to be uniformly mobilised on both sides of the wall and below the stabilising base and the bearing pressure on the underside of the stabilising base was calculated in accordance with Equation 3.1. Details of the altered geometries and measured pore water pressures adopted in the analyses are given in Table 3.6 and the results of the analyses are presented in Table 3.7.

Table 3.6 Deformed geometries and measured pore water pressure distributions assumed in the back-analysis of centrifuge Tests TRL1 and TRL4

	Deformed geometry (m)		Measured pore water pressure at toe of the wall, (kPa)	
	Retained height, h	Embedment depth, d	Behind the wall	In front of the wall
Test TRL 1	7.7	8	113.28	93.68
Test TRL 4	7.5	4	75.72	47.32

The results indicate that the wall/stabilising base in Test TRL 4 was in a state of collapse with a mobilisation factor $M = 0.91$ (assuming $\phi'_{peak} = \phi'_{crit} = 22^\circ$) and that the wall/stabilising base in Test TRL 1 was close to limiting equilibrium with a mobilisation factor $M = 1.05$.

3.5.2 Stabilising base walls retaining Leighton Buzzard Sand

The stability of the stabilising base walls retaining Leighton Buzzard Sand (i.e. centrifuge Tests TRL 2 and TRL 3) was assessed on the basis of measured pore water pressure distributions on the wall. The long term wall movements in both tests were sufficiently small for back-analysis using the original geometry. Hydrostatic conditions were assumed below a depth of 8m on both sides of the wall in accordance with Figures 2.23 and 2.24.

Unfortunately, data regarding the angle of friction

Table 3.7 Results of the back analyses of centrifuge Tests TRL 1 and TRL 4 using the Scheme 4 approach

	Mobilised shear strength, ϕ'_{mob} (degrees)	Pivot depth below formation level, Z_p (m)
Test TRL 1 (8m embedment)	21	6.69
Test TRL 4 (4m embedment)	23.9	3.16

(Unit weight $\gamma = 17.66\text{kN/m}^3$; Full height groundwater level;

Stabilising base width = 4m; Full wall friction on both sides of wall after Caquot & Kerisel, 1948; Zero friction on the underside of stabilising base;

Bearing pressure on the u/s of stabilising base determined in accordance with Equation 3.1).

between resin and 52/100 Leighton Buzzard Sand were not available. Analyses were therefore carried out for $\delta/\phi'_{mob} = 0$ and $\delta/\phi'_{mob} = 1$. The results of the analyses assuming zero base friction and bearing pressures on the underside of the stabilising base calculated in accordance with Equation 3.1 are given in Table 3.8.

Table 3.8 The results of the back-analyses of centrifuge Tests TRL 2 and TRL 3 using the Scheme 4 approach

	Wall friction $\delta/\phi'_{mob} = 0$		Wall friction $\delta/\phi'_{mob} = 1$	
	ϕ'_{mob} (degrees)	Pivot depth Z_p (m)	ϕ'_{mob} (degrees)	Pivot depth Z_p (m)
Test TRL 2 (8m embedment)	20	6.78	17.9	6.96
Test TRL 3 (4m embedment)	22	3.36	20.1	3.41

(Unit weight $\gamma = 19.7\text{kN/m}^3$; Retained height = 8m; Groundwater level at 8m below OGL;

Stabilising base width = 4m; Wall friction on both sides of wall after Caquot & Kerisel, 1948;

Zero friction on the underside of stabilising base;

Bearing pressure on the u/s of the stabilising base determined in accordance with Equation 3.1).

The results suggest that both the 8m (Test TRL 2) and 4m embedment (Test TRL 3) walls were remote from collapse with mobilisation factors corresponding to $M = 1.92$ and 1.73 respectively for $\delta/\phi'_{mob} = 0$ and $M = 2.17$ and 1.91 respectively for $\delta/\phi'_{mob} = 1$ (assuming $\phi'_{peak} = \phi'_{crit} = 35^\circ$).

3.6 The results of limit-equilibrium analyses of free cantilever walls

For comparative purposes, a series of analyses was carried out to investigate the depth of embedment at collapse of free cantilever walls retaining saturated kaolin clay and saturated Leighton Buzzard sand. The results of the analyses based on the 'estimated actual condition' described in Section 3.2, with a retained height of 8m, are presented in Figures A9 (kaolin clay) and A10 (Leighton Buzzard Sand) in Appendix A: a summary is given in Table 3.9.

Table 3.9 The results of limit-equilibrium analyses for a free cantilever wall assuming 'estimated actual conditions' (FOS = 1, i.e. at limiting equilibrium)

	<i>Estimated actual condition</i>	
	<i>Zero wall friction</i>	<i>Full wall friction</i>
Depth of embedment Speswhite kaolin clay $\phi' = 22^\circ$, $\gamma = 17.5\text{kN/m}^3$	32.52m (40.52m*)	22.02m (30.02m*)
Depth of embedment Leighton Buzzard Sand $\phi' = 35^\circ$, $\gamma = 19.7\text{kN/m}^3$	15.33m (23.33m*)	8.79m (16.79m*)

* Figures in brackets represent the overall wall height, *H*. (Retained height = 8.0m; Full height groundwater level; Steady state linear seepage conditions)

The analyses show that an unpropped cantilever wall without a stabilising base requires a significantly deeper embedment to prevent collapse than a stabilising base retaining wall. For the unpropped cantilever walls retaining speswhite kaolin clay, large depths of embedment are required to prevent collapse. This is consistent with the results of centrifuge model tests carried out by Powrie (1986).

3.7 A summary of the results of the limit-equilibrium analyses

Analyses in which the stabilising base is assumed to act as a rigid prop (i.e. Schemes 1 and 2) may be unsafe because it is unlikely that the base will be sufficiently rigid to act as the point of rotation: the end of the stabilising base reacts against soil and not another wall.

Analyses in which the stabilising base wall is assumed to act as a gravity wall (i.e. Scheme 3) may be overconservative - in particular for the walls retaining speswhite kaolin clay - and are probably not representative of the actual stresses acting on the structure.

The results of the centrifuge model tests presented in this report would tend to suggest that the method of analysis described by Scheme 4 is the most appropriate. Reasonably close agreement was apparent between the centrifuge model tests carried out in speswhite kaolin clay and limit-equilibrium analyses in which there was full wall friction on both sides of the wall, zero base friction on the underside of the stabilising base and bearing pressures on the underside of the stabilising base calculated in accordance with Equation 3.1. In these analyses the same soil friction angle was assumed to be uniformly mobilised everywhere around the structure.

However, an investigation into the stress fields that can be developed below a stabilising base suggests that it may not be theoretically possible to develop full wall friction in front of the wall and zero base friction on the underside of the base, owing to a lack of space to achieve the required rotation in the principal stress directions. This means that the approach using Caquot and Kerisel's (1948) earth pressure coefficients lacks rigour, and may be unduly

optimistic. The effectiveness of stabilising base retaining walls was therefore investigated further by means of a series of finite element analyses.

4 Finite element analyses

4.1 Scope and description

The effectiveness of stabilising base retaining walls has been further investigated by means of a series of finite element analyses. The analyses were carried out using the program SAGE CRISP, which features fully coupled consolidation. The analyses replicated as closely as possible the geometry, boundary conditions and sequences of construction imposed in the centrifuge model tests described in Section 2. Previous analyses of the actual centrifuge procedure (White, 1987; Bolton et al, 1989) have shown that the modelling procedure is reasonably realistic. Analyses were therefore carried out for an idealised 94g centrifuge model at prototype scale.

Figure 4.1 shows a typical two-dimensional finite element mesh which consists of 437 linear strain quadrilateral finite elements. The vertical boundaries of the mesh were pinned in the horizontal direction but free to move vertically, and the horizontal boundary at the base of the mesh was assumed to be pinned in both the vertical and horizontal directions. Conditions of plane strain were assumed throughout.

The wall and stabilising base were modelled as a 1m thick, non-consolidating, linear elastic material with a Young's Modulus (*E*) of 23.4MPa, giving a flexural rigidity similar to the centrifuge model walls ($EI=1.95 \times 10^6 \text{kNm}^2/\text{m}$). Poisson's ratio (ν) was taken as 0.15.

4.2 Soil parameters

Speswhite kaolin clay tests - Tests TRL 1 and TRL 4

In the back-analyses of the centrifuge model tests on stabilising base retaining walls in kaolin clay (i.e. Tests TRL1 and TRL 4), the soil was represented using consolidating elements and a model proposed by Schofield (1980). The Schofield model incorporates the Cam clay yield surface on the wet side of the critical state and the Hvorslev surface and a no-tension cut off on the dry side (Figure 4.2).

Both centrifuge tests were back-analysed with two different sets of soil parameters. The first analysis (Case 1) used soil parameters suggested by Richards (1995), who back-analysed a series of centrifuge model tests on multi-propped embedded retaining walls. The vertical and horizontal permeabilities of kaolin were taken as $0.66 \times 10^{-9} \text{m/s}$ and $1.8 \times 10^{-9} \text{m/s}$ respectively, and the Hvorslev slope *H* as 0.64. The second analysis (Case 2) used parameters similar to those used by Li (1990) who back-analysed a series of centrifuge model tests carried out by Powrie (1986) on singly-propped embedded retaining walls. In this case, the vertical and horizontal permeabilities were $4.68 \times 10^{-9} \text{m/s}$ and $6 \times 10^{-9} \text{m/s}$ respectively and the slope of the Hvorslev surface was taken as 0.59. The permeabilities used in the two analyses are within the range quoted by Al-Tabaa (1987). Details of the soil parameters are given in Table 4.1.

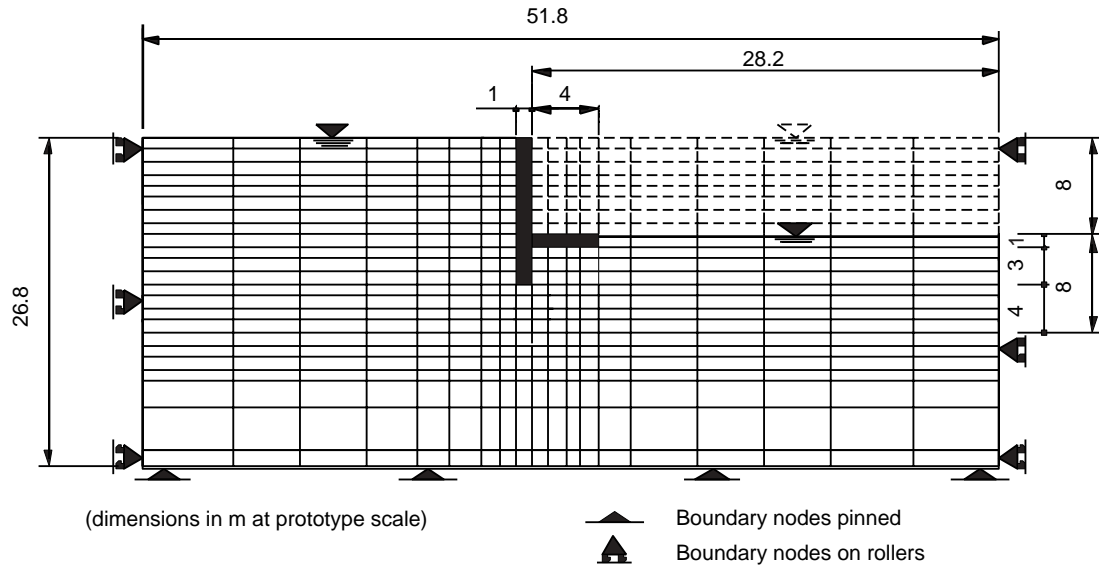


Figure 4.1 Finite element mesh and boundary conditions

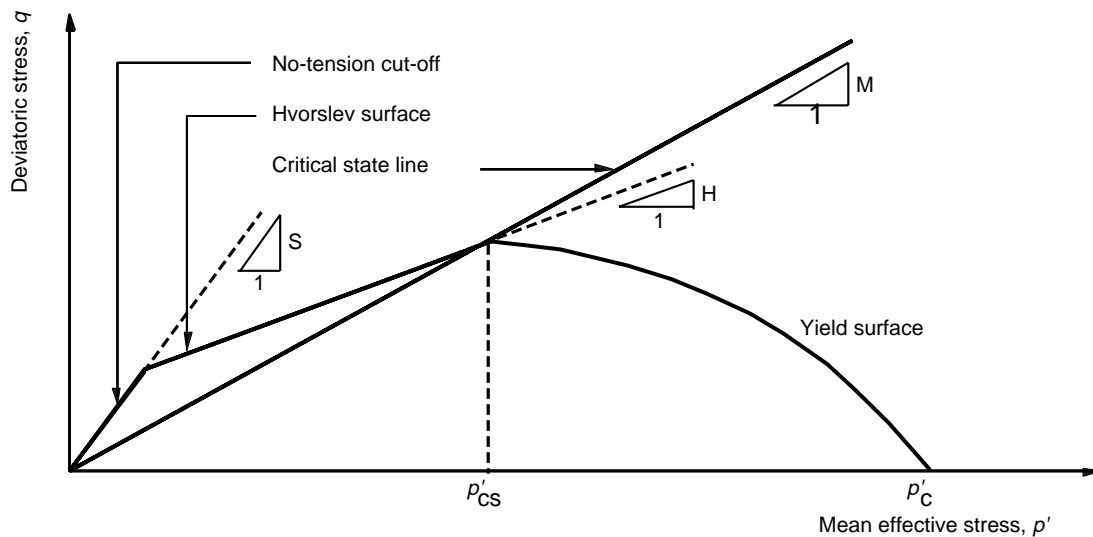


Figure 4.2 Schofield soil model

Table 4.1 Details of speswhite kaolin clay critical state soil parameters used in finite element analyses

Soil parameter	Value
Common parameters	
Slope of 1-dimensional compression line in v - $\ln p'$ space	$\lambda = 0.25$
Slope of unload/reload line in v - $\ln p'$ space	$k = 0.05$
Specific volume (and void ratio) on critical state line at $p'=1$ kpa in v - $\ln p'$ space	$\Gamma = 3.48$ ($e_0 = 2.48$)
Slope of critical state line in q : p' space	$M = 0.65$
Poisson's ratio	$\nu = 0.33$
Bulk unit weight of soil	$\gamma = 17.35 \text{ kN/m}^3$
Slope of no-tension cut-off in q : p' space	$S = 2$
Permeability in vertical and horizontal direction for tensile fracture region	$k_{x,y} = 10^{-7} \text{ m/s}$
Case 1 analysis (In addition to common parameters)	
Slope of Hvorslev surface in q : p' space	$H = 0.64$
Permeability in the vertical direction	$k_y = 0.66 \times 10^{-9} \text{ m/s}$
Permeability in the horizontal direction	$k_x = 1.8 \times 10^{-9} \text{ m/s}$
Case 2 analysis (In addition to common parameters)	
Slope of Hvorslev surface in q : p' space	$H = 0.59$
Permeability in the vertical direction	$k_y = 4.68 \times 10^{-9} \text{ m/s}$
Permeability in the horizontal direction	$k_x = 6 \times 10^{-9} \text{ m/s}$

The size of the initial yield surface is determined by the value of p'_c in Figure 4.2. From the Cam clay yield surface equation with σ'_{vmax} of 1250kPa and K_{onc} of 0.625, p'_c is equal to 2021.7kPa.

Leighton Buzzard Sand tests - Tests TRL 2 and TRL 3

In the back-analyses of the centrifuge model tests on stabilising base retaining walls in sand (i.e. Tests TRL2 and TRL 3), the soil was represented using consolidating elements and an elastic-perfectly plastic model with a Mohr-Coulomb failure envelope having a critical state angle of shearing resistance $\phi'_{crit} = 35^\circ$ (Stroud, 1971).

According to British Standard BS1377 Part 2 (BSI, 1991), 52/100 Leighton Buzzard Sand may be classified on the basis of its particle size distribution as a uniform fine/medium sand with representative particle sizes D_{10} and D_{50} of 0.15mm and 0.212mm respectively. From this, the permeability of the sand was estimated to be 2.25×10^{-4} m/s using Hazen's (1892) empirical formula for clean filter sands

$$(4.1)$$

Poisson's ratio was taken as $\nu' = 0.3$ based on Equations 4.2 and 4.3

$$(4.2)$$

$$(4.3)$$

A summary of the soil parameters is given in **Table 4.2**.

Table 4.2 Details of the Leighton Buzzard Sand soil parameters used in the finite element analyses

Soil parameter	Value
Angle of soil friction	$\phi' (= \phi'_{crit}) = 35^\circ$
Cohesion intercept	$c' = 0$
Poisson's ratio	$\nu' = 0.3$
Bulk unit weight of soil	$\gamma = 19.7\text{kN/m}^3$
Permeability	$k = 2.25 \times 10^{-4}$ m/s

4.3 In situ stress state and soil stiffness profile

Speswhite kaolin clay tests - Tests TRL 1 and TRL 4

In common with the centrifuge model tests, the stress history of the kaolin sample was assumed to comprise one dimensional compression to a maximum vertical effective stress of 1250kPa followed by unloading to a vertical effective stress of 80kPa. The initial in situ lateral effective stresses were computed using Equation 4.4 (Mayne and Kulhawy, 1982) up to the passive limit $K_p = 2.198$ for $\phi'_{crit} = 22^\circ$.

$$(4.4)$$

The water table was set at original ground level. The boundary conditions imposed by the zinc chloride solution

in the flexible PVC bag were represented approximately by reducing the pre-excavation lateral earth pressure coefficient to unity in the soil above formation level, below which the pre-excavation lateral earth pressure coefficients returned to their initial in situ values. The resulting stiffness profile, which is shown in Figure 4.3, was computed using Equations 4.5 and 4.6:

$$(4.5)$$

where

$$(4.6)$$

Leighton Buzzard Sand tests - Tests TRL 2 and TRL 3

The initial in situ lateral effective stresses were computed using Jaky's (1944) expression for K_{onc} (Equation 4.2) with $\phi'_{crit} = 35^\circ$. The boundary conditions imposed by the zinc chloride solution in the flexible PVC bag were represented in a similar way to that described previously i.e. the pre-excavation lateral earth pressure coefficient was increased to unity in the soil above formation level below which point they remained at their initial in situ values.

Unfortunately, stress-strain data were not available for 52/100 Leighton Buzzard Sand. A range of normalised shear moduli G/p' of 75 to 200, however, was taken as typical of medium-dense granular materials over a shear strain increment of approximately 0.2% (Bellotti et al, 1989). The analyses started with the wall and stabilising base already in place and assumed a groundwater level at 8m below original ground level. The resulting stiffness profiles are shown in Figure 4.4. Preliminary analyses, in which attempts were made to model a reducing groundwater level behind the wall as evidenced in the centrifuge tests, developed numerical problems.

4.4 Construction sequence

Speswhite kaolin clay tests - Tests TRL 1 and TRL 4

The sequence of each analysis, starting with the wall and stabilising base already in place and assuming a groundwater level initially at original ground level, was as follows:

- Simulate bulk excavation by removing elements from in front of the wall in 8 1m layers over a period of 3 days, with the pore water pressures being re-set to zero at the current excavated surface.
- Consolidate in the long term with time intervals of 1, 2, 4, 7, 10, 20, 40 and 70 months to model the long term behaviour of the wall.

Each analysis was carried out using a total of 950 increments.

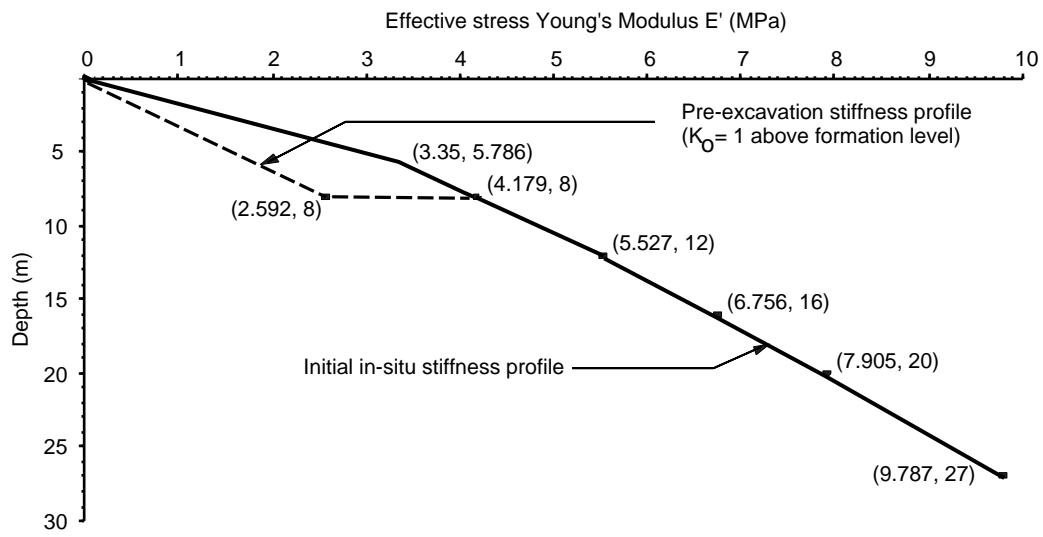


Figure 4.3 Stiffness variation with depth for speswhite kaolin clay

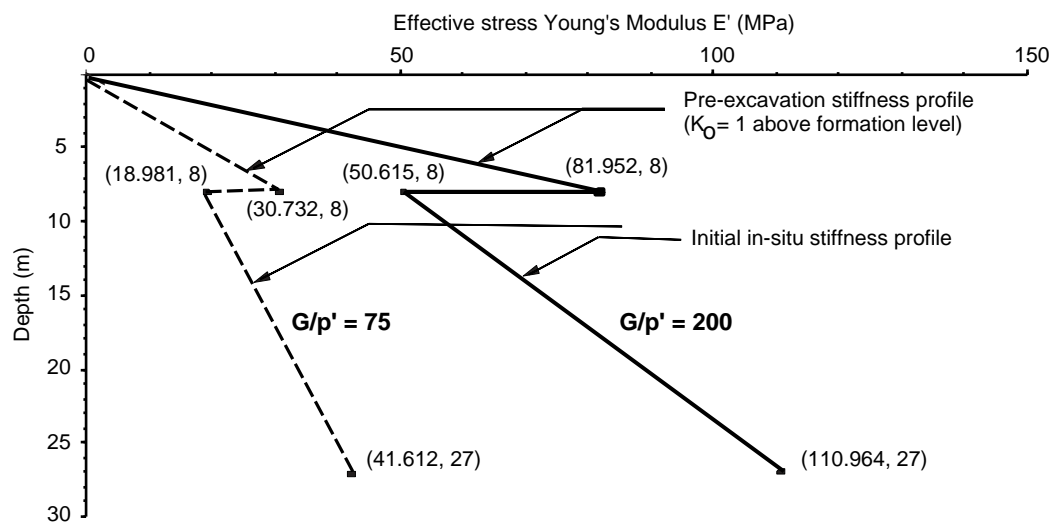


Figure 4.4 Stiffness variation with depth for Leighton Buzzard Sand

Leighton Buzzard Sand tests - Tests TRL 2 and TRL 3

The sequence of each analysis, again starting with the wall and stabilising base already in place but this time with the groundwater level at 8m below original ground level, was as follows:

- a Simulate bulk excavation by removing elements from in front of the wall in 8 x 1m layers over a period of 3 days.
- b Consolidate in the long term with time intervals of 1, 2, 4, 8 and 18 months to model the long term behaviour of the wall.

Each analysis was carried out using a total of 350 increments.

4.5 Results of finite element analyses

4.5.1 Test TRL 1 (8m embedment wall in speswhite kaolin clay)

Wall and soil movements

Measured and computed movements of the crest of the wall into the excavation, shown as a function of time, are compared in Figure 4.5. The crest movements into the excavation were reasonably well predicted during excavation and the effect of the increased soil permeability in the Case 2 analysis only become apparent after approximately 1 year. This would suggest that the excavation process was a substantially undrained event in the analyses.

Up to 6.5 years following excavation, the crest movements were under-predicted by the finite element analyses. One reason for this is that the computed pore water pressures on both sides of the wall were less than those measured in the centrifuge. This is discussed in more detail later. Another possible reason is that the adoption of a single value of κ throughout the depth of the clay could have lead to an over-stiff response in the short to medium term. Research carried out by Al-Tabaa (1987) on specimens of speswhite kaolin clay suggested that there is an approximately linear relation between the slope of the swelling/recompression line κ , and overconsolidation ratio OCR, in that κ increases with OCR. The Schofield model takes no account of this and instead assumes that κ is constant, i.e. the unload/reload line is represented as a straight line in $v - \ln p'$ space.

After approximately 6.5 years, the Case 2 finite element analysis became unstable. The rate of crest movement increased dramatically suggesting that the wall was in a state of collapse. After 13 years the crest of the wall had moved approximately 1.2m - a factor of approximately 2 greater than that measured in the centrifuge. In comparison, the Case 1 analysis remained stable after 13 years but the rate of crest movement was still increasing. The pore water pressures on the wall were significantly under-predicted by the Case 1 analysis (discussed later). It seems likely that the wall in the Case 1 analysis would also have reached a state of collapse once full pore water pressure dissipation had occurred, i.e. if this analysis were run longer.

Measured and computed soil settlement profiles behind the wall after 13 years are shown in Figure 4.6. The profile computed in the Case 2 analysis gives better agreement, although the effects of shear close to the wall appear to have been under-estimated in both analyses.

Pore water pressures

Measured and computed pore water pressure distributions immediately after excavation and after approximately 13 years are compared in Figures 4.7 and 4.8 respectively.

During excavation (Figure 4.7), the pore water pressure distributions computed for Cases 1 and 2 were similar, which tends to confirm that the excavation process was indeed undrained in the analyses. The unloading response, in terms of pore water pressure reduction, to the removal of overburden was generally over-predicted by the finite element analyses. This may be due to the way in which excavation was modelled in the finite element analyses. In the centrifuge, the lateral unloading effect due to simulated excavation was gradual as the zinc chloride solution was drained from the flexible PVC bag. In the finite element analyses, however, the excavation procedure involved the instantaneous removal of a series of 1m layers of soil. This apart, the following trends were apparent in both the centrifuge and the finite element analyses during excavation:

- Behind the wall, pore water pressures fell in all cases on excavation, with the lateral unloading effect most pronounced closest to the wall (i.e. compare Figures 4.7a and 4.7b);
- In front of the wall beyond the stabilising base (i.e. 24m in front), the pore water pressures fell considerably due to the removal of the overburden (Figure 4.7b);
- In front of the wall below the stabilising base (i.e. 2.16m in front), the effect of overburden removal was less than it was beyond the base (i.e. compare Figures 4.7a and 4.7b). Excavation in both the centrifuge and finite element analyses was simulated with the stabilising base already in place. Rotation of the wall into the excavation resulted in the development of significant bearing pressures beneath the base during excavation, partly compensating for the effects of vertical unloading beneath the stabilising base.

Following excavation, similar trends were also apparent in the centrifuge and the finite element analyses. These were:

- Behind the wall, the pore water pressures furthest away from the wall (i.e. 12.8m) continued to fall to their long term equilibrium values whereas the pore water pressures immediately behind (i.e. 2.16m) and within the depth of the wall tended to rise to their long term equilibrium values as the clay in this region swelled and softened;
- In front of the wall (i.e. 24m) beyond the stabilising base, the pore water pressures rose as the clay in this region swelled.

The pore water pressure distributions after approximately 13 years (Figures 4.8a and 4.8b) suggest that by increasing the permeability and hence the consolidation characteristics of the kaolin (i.e. Case 2 analysis), close agreement was obtained with the pore water pressure distributions measured in the centrifuge.

Bending moments in the wall and stabilising base

Measured and computed bending moments in the wall immediately after excavation and after 13 years are shown in Figures 4.9a and 4.9b respectively.

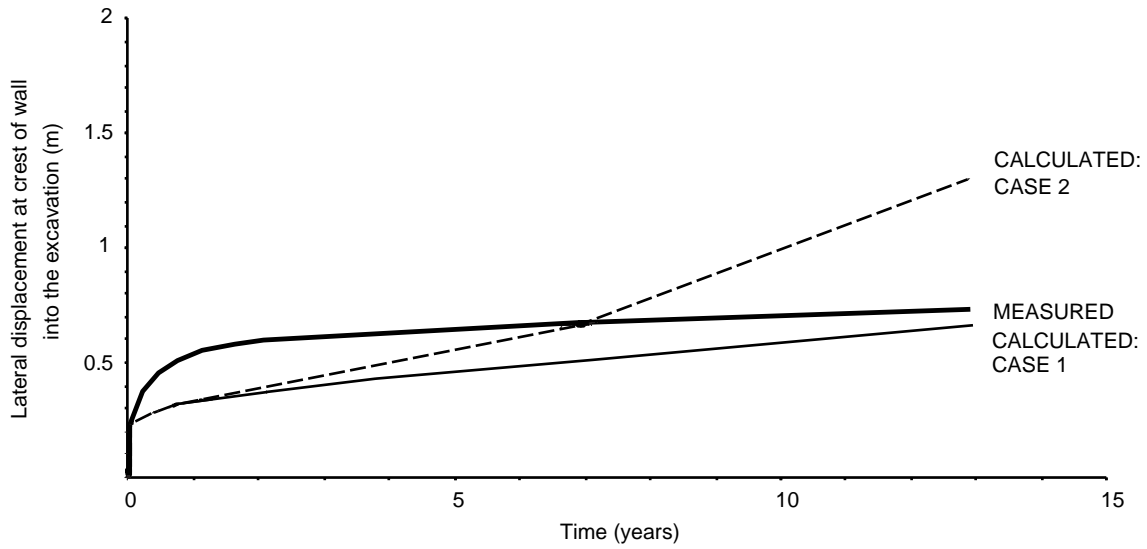


Figure 4.5 Calculated and measured crest movements into the excavation vs time, Test TRL 1

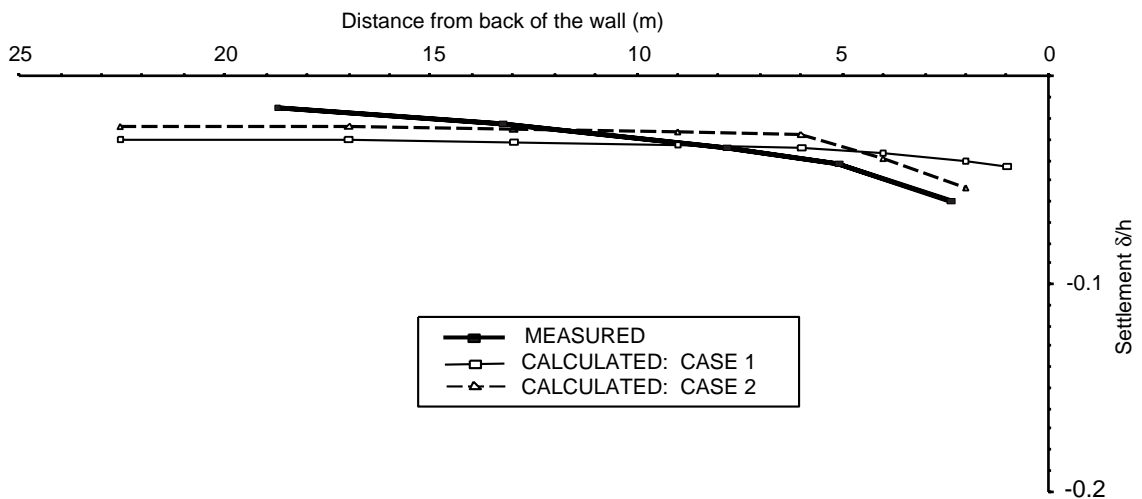


Figure 4.6 Calculated and measured soil settlement profiles behind the wall after 13 years, Test TRL 1
(normalised with respect to the retained height)

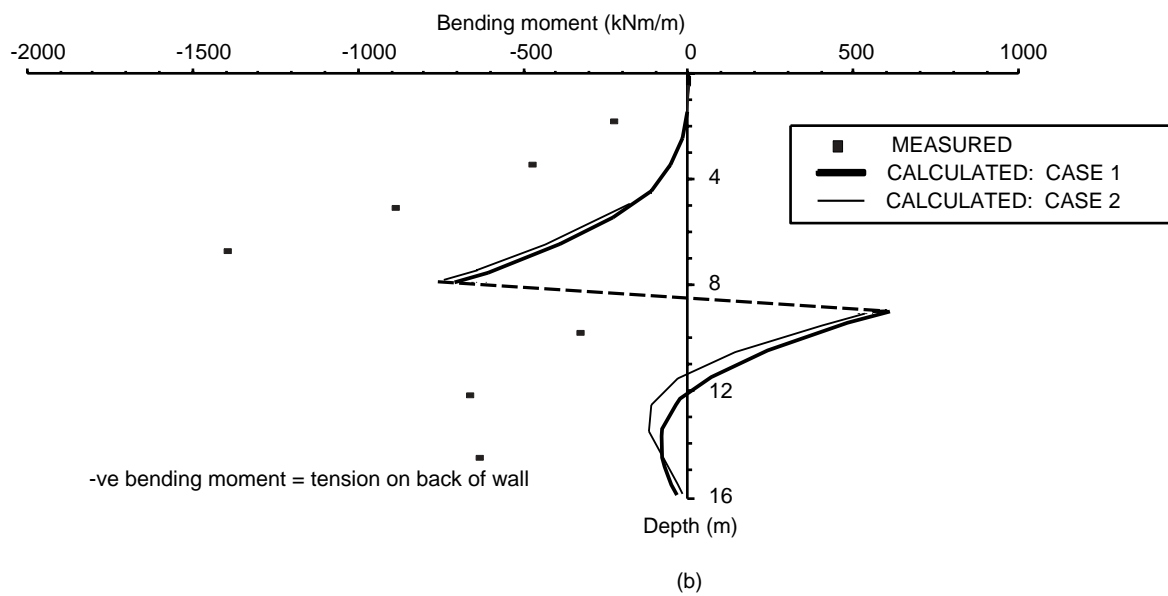
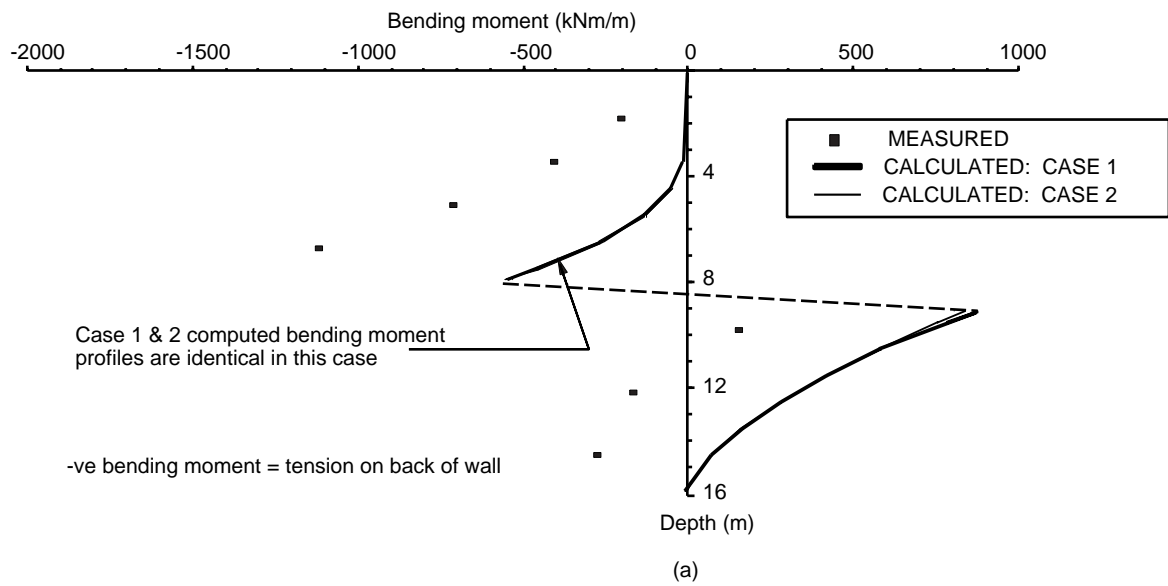


Figure 4.9 Calculated and measured bending moment profiles in the wall, Test TRL 1
a immediately after excavation
b after 13 years

With the stabilising base already in place, the restoring moment imparted by the base as the wall rotates into the excavation is evident in both the finite element analyses and in the centrifuge (Figure 4.9a). Immediately after excavation, the bending moments in the wall computed in the Case 1 and Case 2 finite element analyses were identical. In terms of magnitude, however, they were significantly less than those measured in the centrifuge. Although the magnitude of the maximum bending moment measured in the wall in Figure 4.9 is implausibly high, the magnitude of the measured and computed restoring moments at formation level is broadly consistent.

Bending moments in the wall computed in the finite element analyses tended to increase (i.e. become more negative) in the long term. This is consistent with the trend measured in the centrifuge and is probably due to an increase in pore water pressures immediately behind the wall.

Computed bending moments in the stabilising base and vertical effective stresses on the underside of base after 13 years are shown in Figures 4.10 and 4.11 respectively. Unfortunately, these can not be corroborated with data from the centrifuge test as no data were forthcoming from the strain gauges on the stabilising base in this test. The computed bending moment profiles in the two analyses were similar with a common maximum restoring moment of approximately 1300kNm/m (Figure 4.10). The computed vertical effective stress distributions on the underside of the stabilising base were also similar (Figure 4.11). At the extreme edge of the stabilising base (i.e. 4m away from the wall), large bearing pressures of up to 300kPa were computed in both analyses.

Lateral stresses on the wall

Horizontal stress distributions at the end of the Case 1 and Case 2 analyses (i.e. 13 years) are presented in Figures 4.12 and 4.13 respectively. Also shown are the pre-excavation horizontal effective stress profiles computed on the basis of Equation 4.4.

The horizontal effective stress distributions computed in the Case 1 analysis (Figure 4.12) are consistent with the mode of deformation of the wall i.e. rigid body rotation into the excavation about some point near the toe of the wall. Behind the wall, the soil was generally in an active state except for the region of soil close to the toe of the wall. In front of the wall, the horizontal effective stresses were marginally greater than the corresponding pre-excavation horizontal effective stresses. However, the soil in this region was remote from passive failure because the vertical effective stresses remained high following excavation as a result of the stabilising base being already in place during simulated excavation.

The horizontal effective stress distribution behind the wall computed in the Case 2 analysis tends to confirm that this wall was in a state of collapse (Figure 4.13). Up to a depth of 9m, very low horizontal effective stresses were computed and failure occurred by tensile fracture. By reducing the slope of the Hvorslev surface from 0.64 to 0.59, the extent of the no-tension cut-off failure envelope was increased significantly in the Case 2 analysis compared with the Case 1 analysis.

The pore water pressure distributions computed in the Case 2 analysis were greater than in the Case 1 analysis reflecting the increased rate of consolidation in this analysis.

4.5.2 Test TRL 4 (4m embedment wall in speswhite kaolin clay)

Wall and soil movements

Measured and computed movements of the crest of the wall into the excavation, shown as a function of time, are compared in Figure 4.14. During excavation, the computed crest movements into the excavation were reasonably well predicted by both analyses. In the long term, the crest movements computed in the Case 1 analysis were significantly less than those measured in the centrifuge for the reasons given in Section 4.5.1. The Case 2 analysis, however, was in reasonably good agreement until the analysis became unstable after approximately 3.7 years.

A comparison of the soil settlement profiles behind the wall in Figure 4.15 suggests that the Case 2 analysis gives better agreement. It is clear, however, that both analyses were unable to replicate the rupture behaviour evident in the centrifuge test. The modelling of ruptures using a finite element continuum model is generally acknowledged to be difficult (White, 1987; Li, 1990).

Pore water pressures

Measured and computed pore water pressure distributions immediately after excavation are compared in Figures 4.16. Once again, the unloading response in terms of pore water pressure reduction to the removal of overburden was generally over-predicted by the finite element analyses. Also, the same broad trends evident in Test TRL 1 (Section 4.5.1) both during and immediately following excavation were apparent in this test.

In the long term, the pore water pressure distributions were under-predicted by the Case 1 finite element analysis (Figure 4.17). In the Case 2 analysis, however, close agreement was obtained (Figure 4.18) with the measured pore water pressures. It is therefore not surprising that the crest movements into the excavation were under-predicted by the Case 1 analysis in the long term.

Bending moments in the wall and stabilising base

Measured and computed bending moments in the wall immediately after excavation are shown in Figure 4.19. The restoring moment imparted by the base as the wall rotates into the excavation is evident in both the finite element analyses and in the centrifuge. The bending moment profiles given by the Case 1 and Case 2 finite element analyses immediately following excavation - which were again identical in shape and magnitude - are in reasonable agreement with the bending moments measured in the centrifuge.

At the end of both the Case 1 (i.e. 7 years) and Case 2 (i.e. 3.7 years) analyses, the bending moments computed in the wall above formation level were less than those computed immediately following excavation. This can be seen in Figures 4.20 and 4.21 respectively and is not consistent with the bending moments measured in the centrifuge.

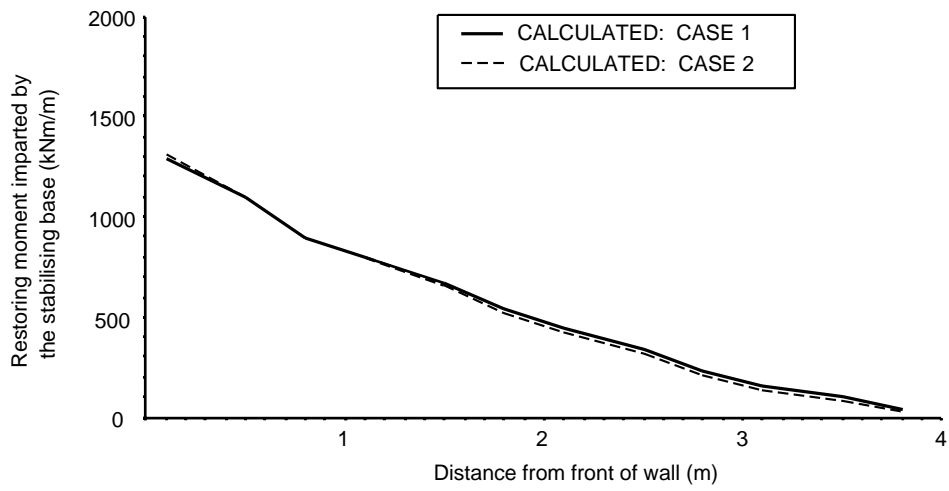


Figure 4.10 Calculated bending moments in the stabilising base after 13 years, Test TRL 1

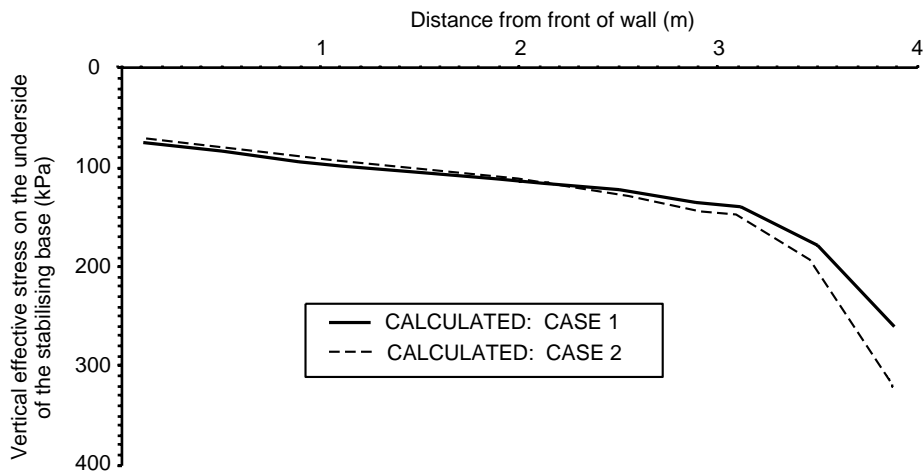


Figure 4.11 Calculated vertical effective stresses on the underside of the stabilising base after 13 years, Test TRL 1

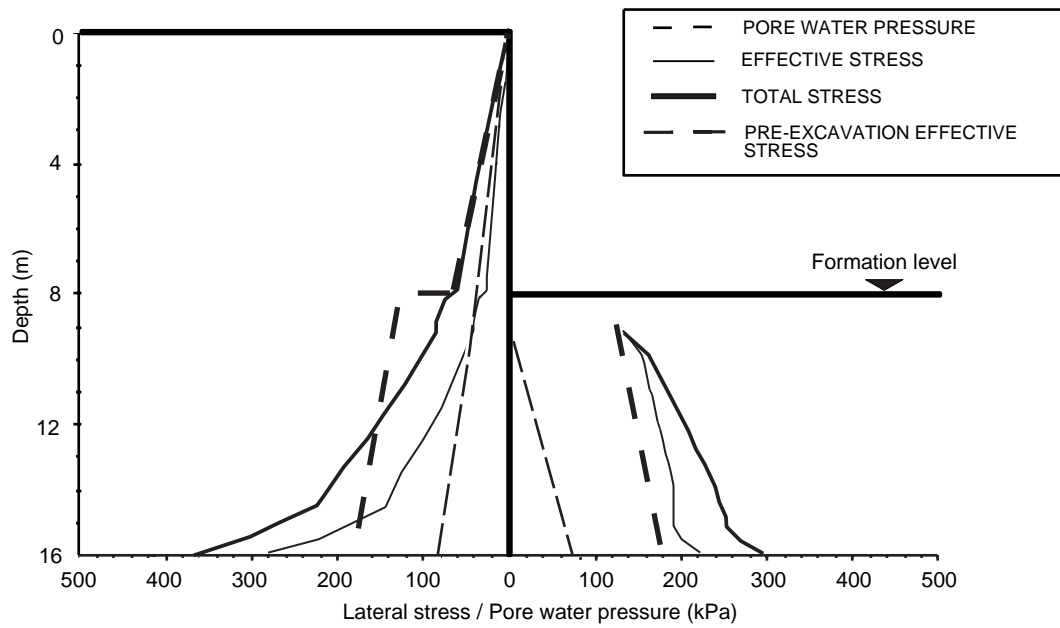


Figure 4.12 Lateral stresses and pore water pressure distributions acting on the wall after 13 years, Case 1 analysis - Test TRL 1

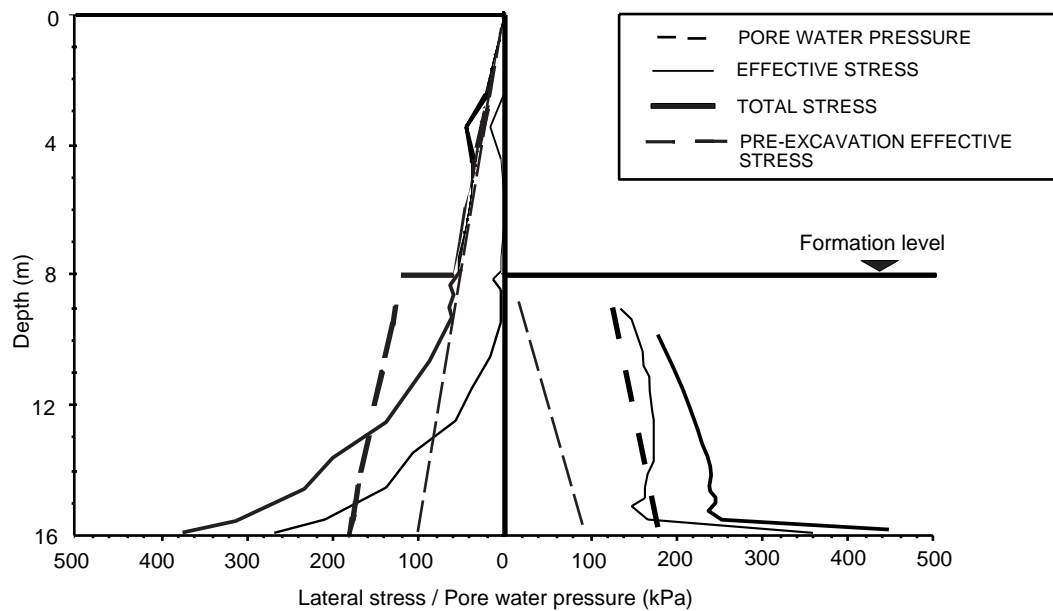


Figure 4.13 Lateral stresses and pore water pressure distributions acting on the wall after 13 years, Case 2 analysis - Test TRL 1

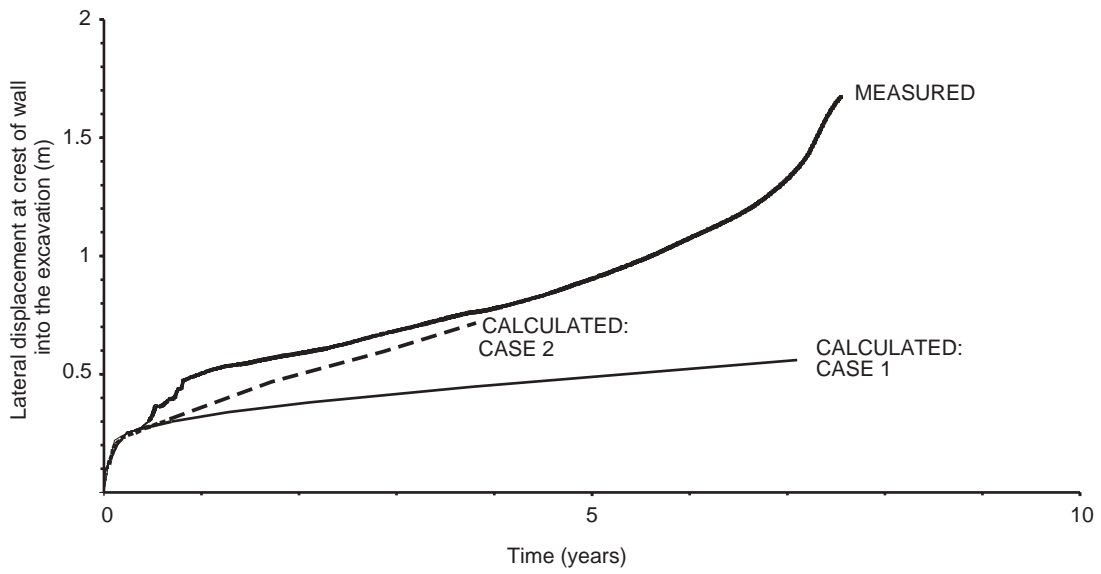


Figure 4.14 Calculated and measured crest movements into the excavation vs time, Test TRL 4

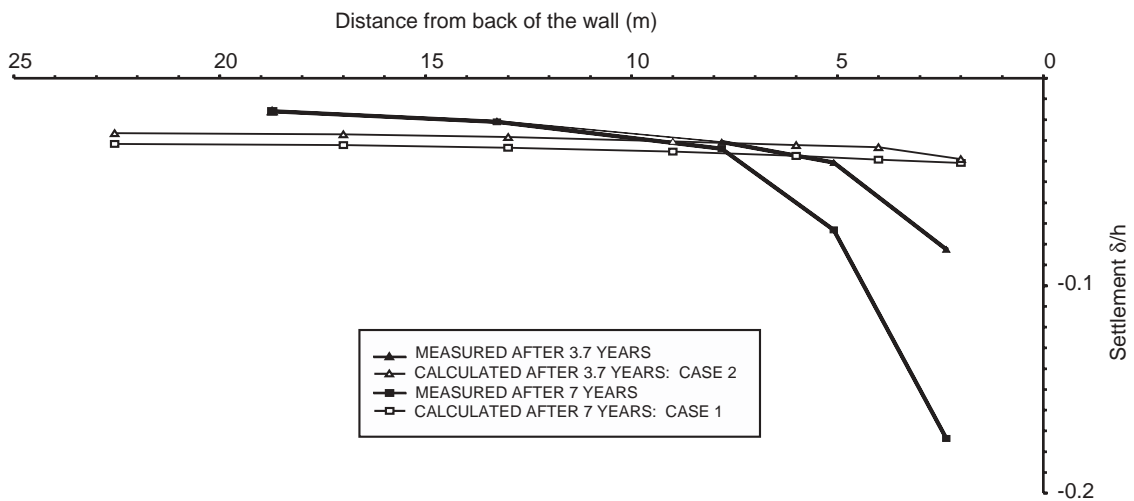
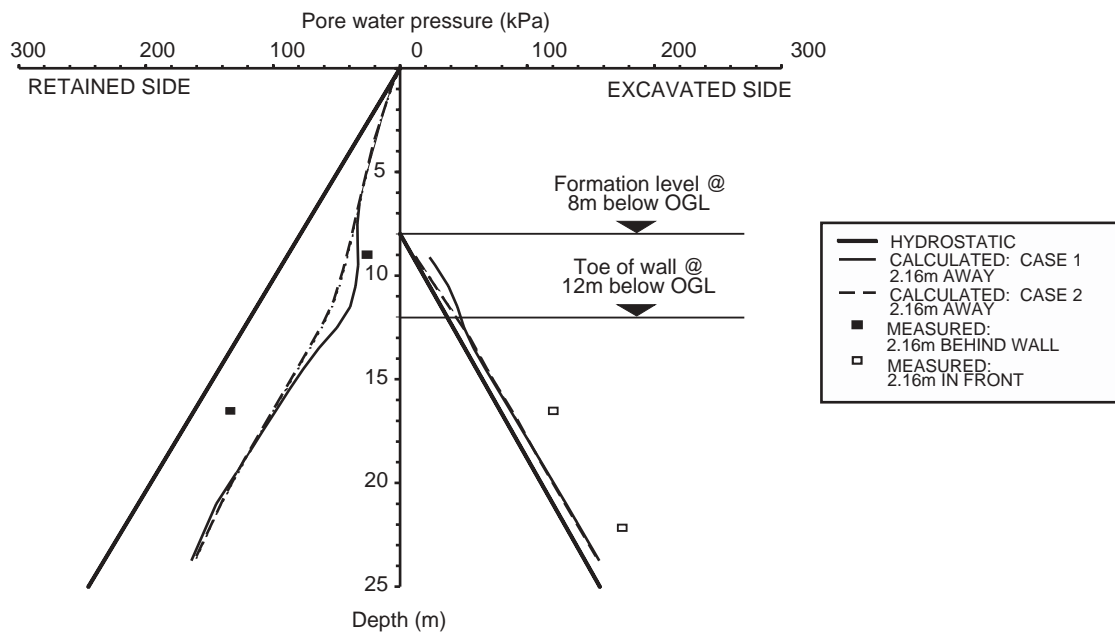
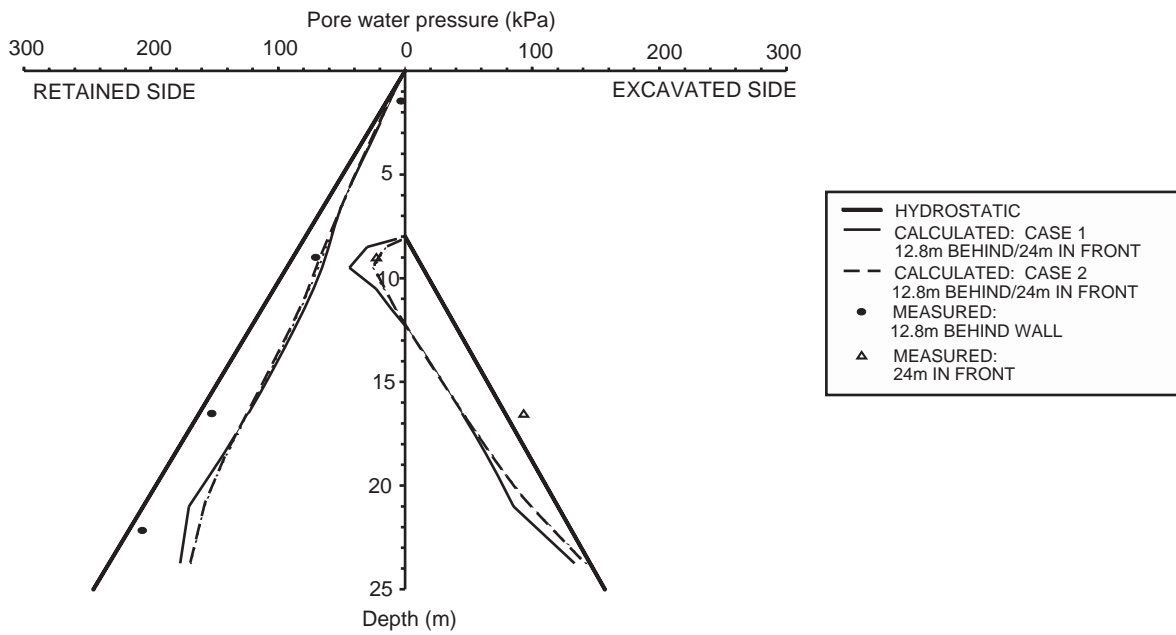


Figure 4.15 Calculated and measured soil settlement profiles behind the wall, Test TRL 4
(Normalised with respect to the retained height)



(a)



(b)

Figure 4.16 Calculated and measured pore water pressure profiles immediately after excavation, Test TRL 4
a close to the wall
b away from the wall

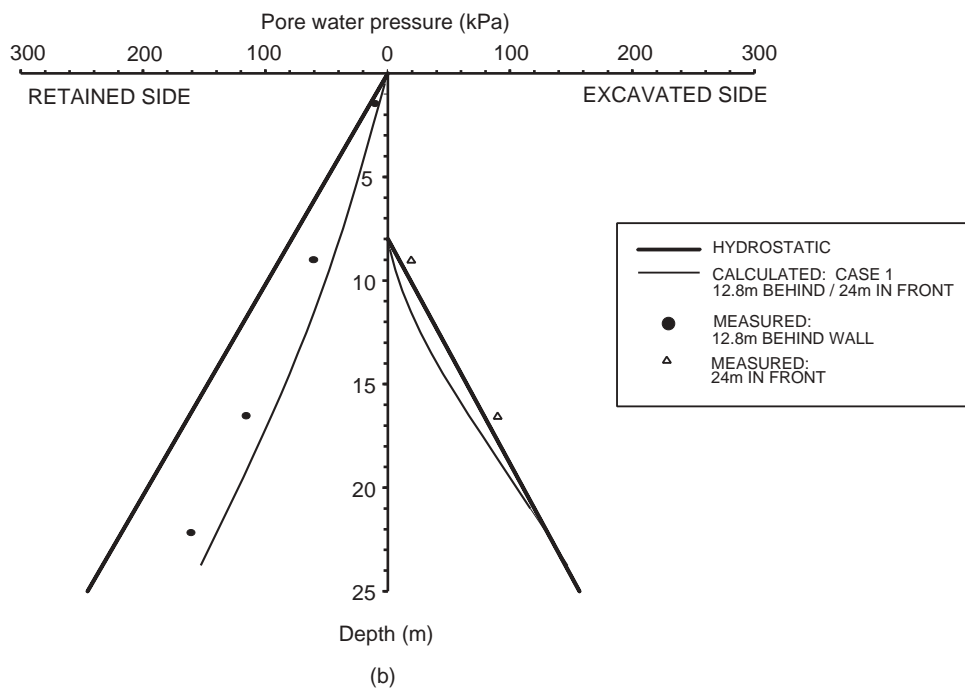
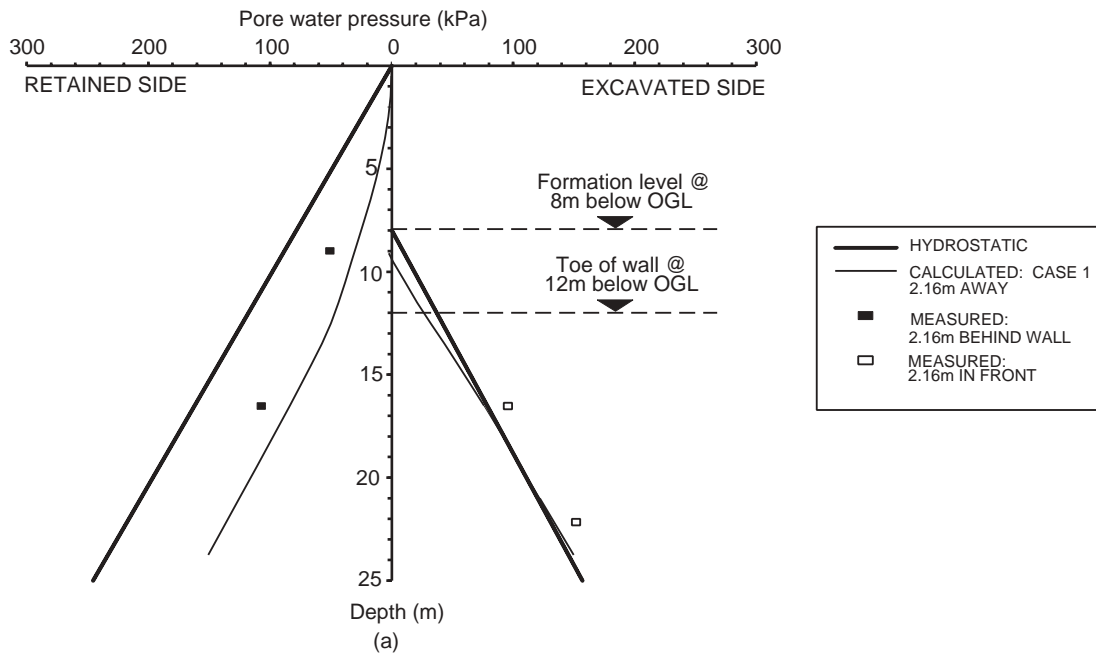


Figure 4.17 Calculated (Case 1 analysis) and measured pore water pressure profiles at the end of Test TRL 4 (7 years)
a close to the wall
b away from the wall

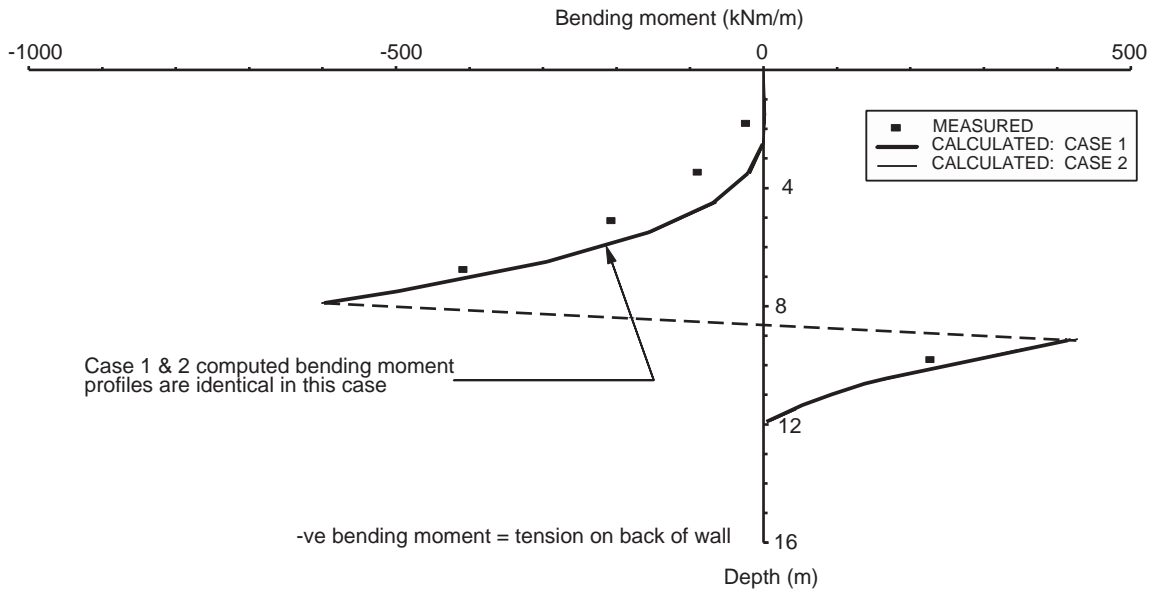


Figure 4.19 Calculated and measured bending moment profiles in the wall immediately after excavation, Test TRL 4

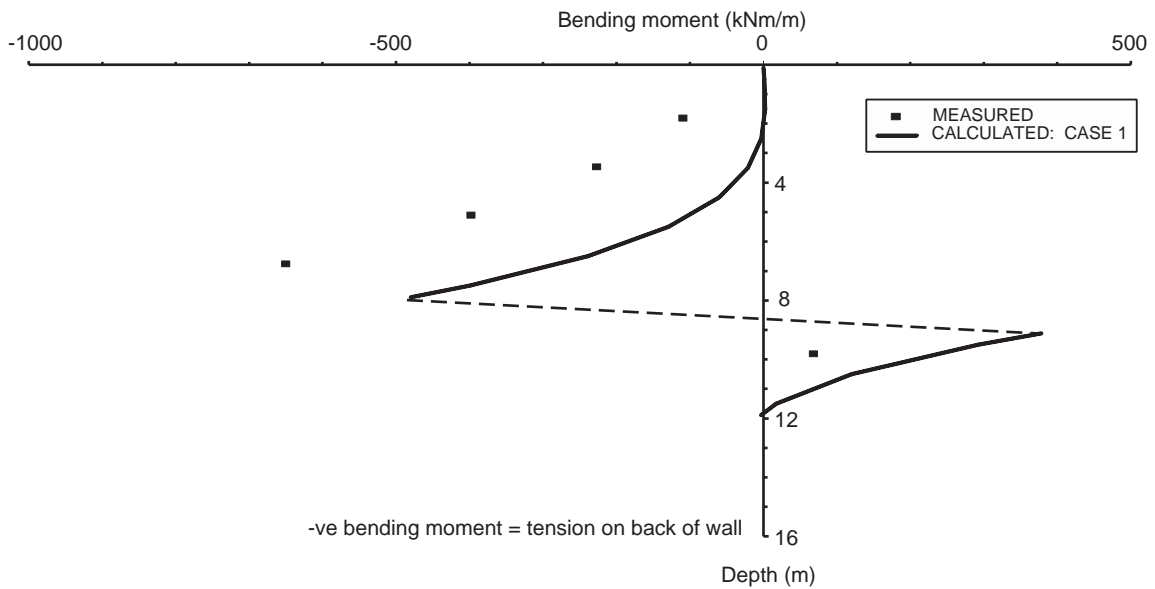


Figure 4.20 Calculated (Case 1 analysis) and measured bending moment profiles in the wall after 7 years, Test TRL 4

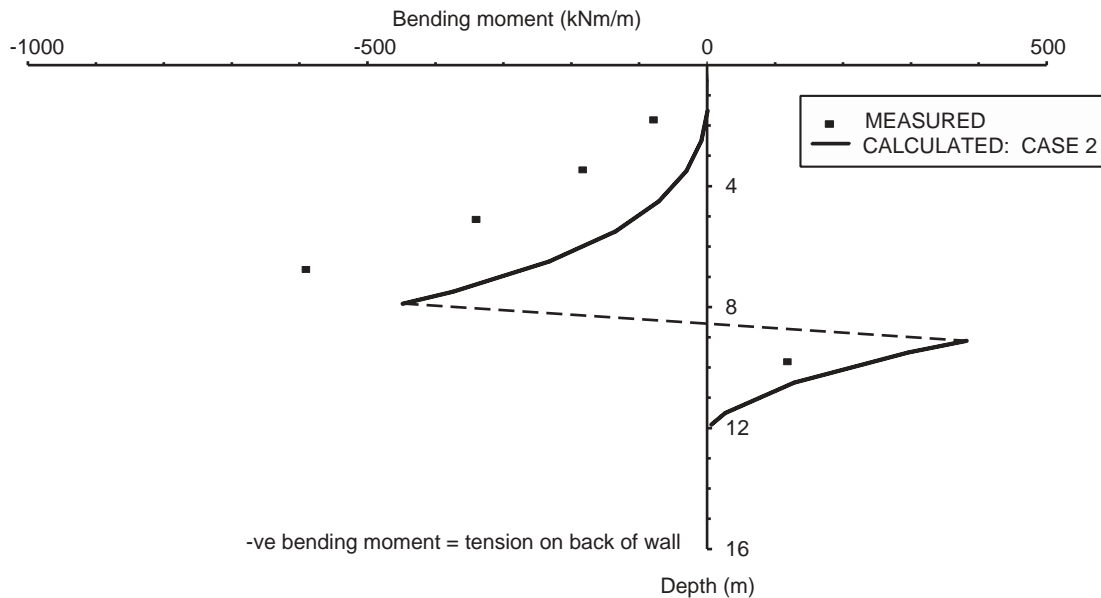


Figure 4.21 Calculated (Case 2 analysis) and measured bending moment profiles in the wall after 3.7 years, Test TRL 4

The bending moments in the stabilising base computed at the end of the Case 1 and Case 2 analyses are shown in Figures 4.22 and 4.23 respectively. A range of possible measured bending moments has also been superimposed onto these figures (see Section 2.7.1). These have been calculated on the basis of the smallest and largest calibration factors found during wall calibration. The computed bending moment profiles in the two analyses are generally in reasonable agreement with the measured profiles determined on the basis of the smallest calibration factors.

The computed vertical effective stress distributions on the underside of the stabilising base at the end of the Case 1 (i.e. 7 years) and Case 2 (i.e. 3.7 years) analyses are shown in Figure 4.24. The stress distributions are generally smaller in magnitude than the lower estimate of measured bearing pressure of 130kPa (assuming a rectangular pressure distribution) given in Table 2.2.

Lateral stresses on the wall

Horizontal stress distributions at the end of the Case 1 (i.e. 7 years) and Case 2 (i.e. 3.7 years) analyses are presented in Figures 4.25 and 4.26 respectively.

The horizontal effective stress distribution behind the wall computed in the Case 1 analysis (Figure 4.25) shows a significant reduction below the pre-excavation horizontal effective stresses. This is consistent with the mode of deformation of the wall. In the Case 2 analysis, however, the horizontal effective stress distribution behind the wall suggests that this wall was in a state of collapse (Figure 4.26). Very low horizontal effective stresses were computed to a depth of 8m and failure occurred by tensile fracture.

In front of the wall, the horizontal effective stress distributions at the end of both analyses suggest that there was a significant increase - particularly towards the toe of the wall - above with the pre-excavation horizontal effective stresses. The soil in this region, however, was remote from collapse.

The pore water pressure distributions computed in the Case 2 analysis were greater than the Case 1 analysis, once again reflecting the increased consolidation coefficient in this analysis.

4.5.3 Test TRL 2 (8m embedment wall in 52/100 Leighton Buzzard Sand)

Wall movements

Measured and computed movements of the crest of the wall into the excavation are shown as a function of time in Figure 4.27.

The sensitivity of the crest movements into the excavation to the stiffness of the sand is clearly evident. As mentioned in Section 4.4, the analyses were unable to replicate the falling phreatic surface behind the wall that occurred in the centrifuge test and instead commenced with a phreatic surface at formation level on both sides of the wall. The high permeability of the sand resulted in the wall reaching a state of equilibrium shortly after excavation in both analyses. The analysis assuming a normalised shear modulus G/p' of 75 gave the better correlation in terms of magnitude. Both analyses, however, under-predicted the crest movements actually measured in the centrifuge. This is probably due to the inability of the analyses to replicate the exact conditions imposed during excavation in the centrifuge. The analysis assuming G/p' of 75 should therefore be treated with caution.

Bending moments in the wall and stabilising base

Figure 4.28 compares the measured and computed bending moments in the wall after 2.54 years. The restoring moment imparted by the stabilising base is evident in both the computed and measured bending moment profiles. Above formation level, the computed bending moments are similar in shape to, but significantly smaller than, those measured in the centrifuge. At formation level, however, the magnitudes of computed and measured restoring

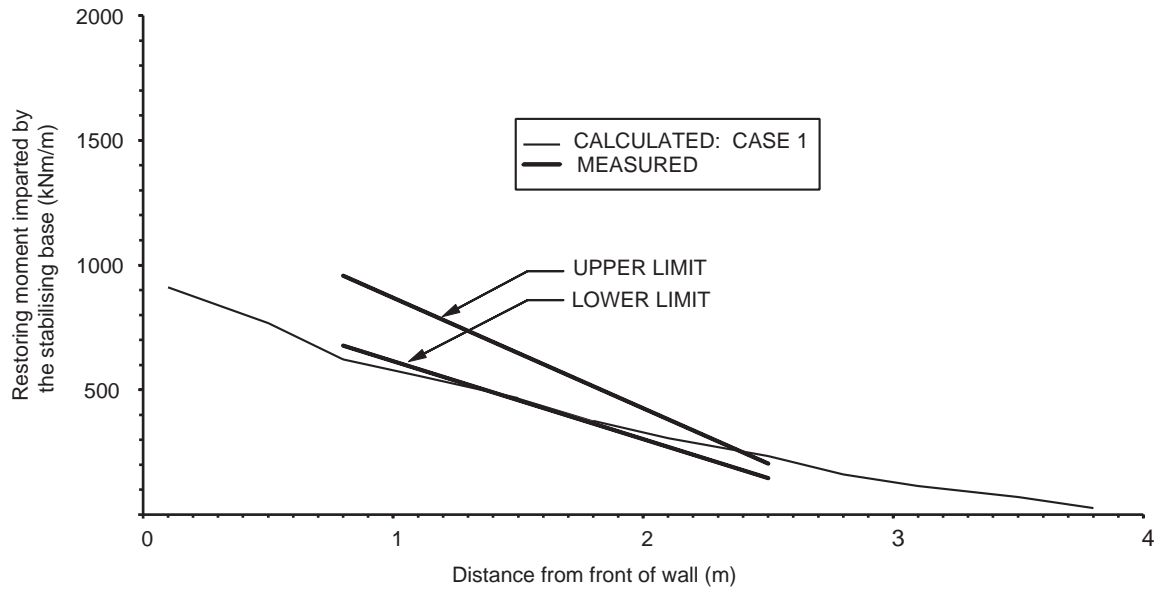


Figure 4.22 Calculated (Case 1 analysis) and measured bending moments in the stabilising base after 7 years, Test TRL 4

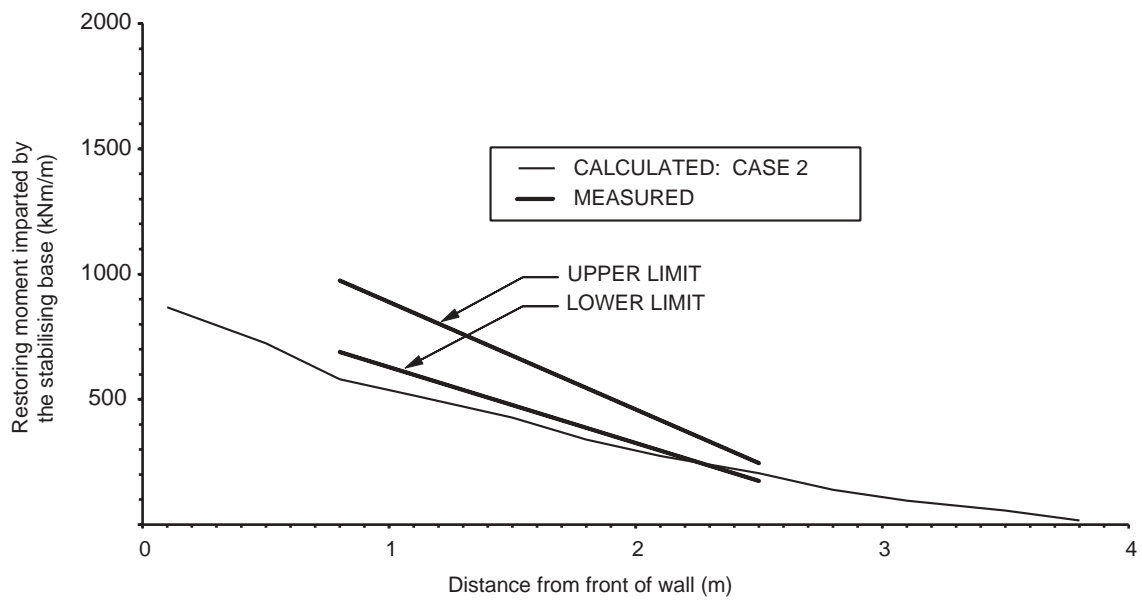


Figure 4.23 Calculated (Case 2 analysis) and measured bending moments in the stabilising base after 3.7 years, Test TRL 4

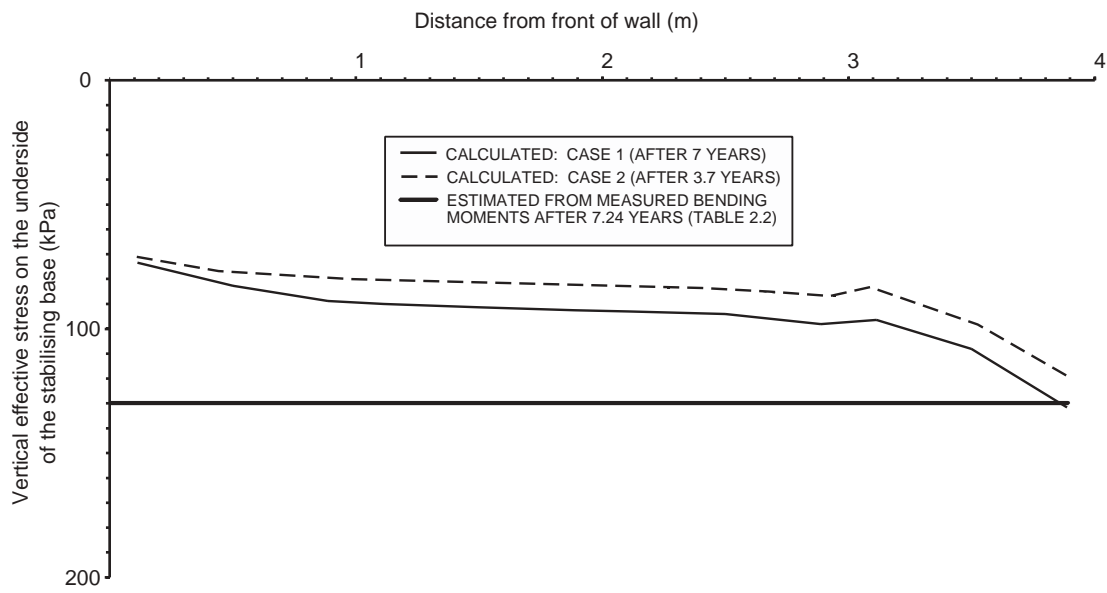


Figure 4.24 Calculated vertical effective stresses on the underside of the stabilising base at the end of the analyses, Test TRL 4

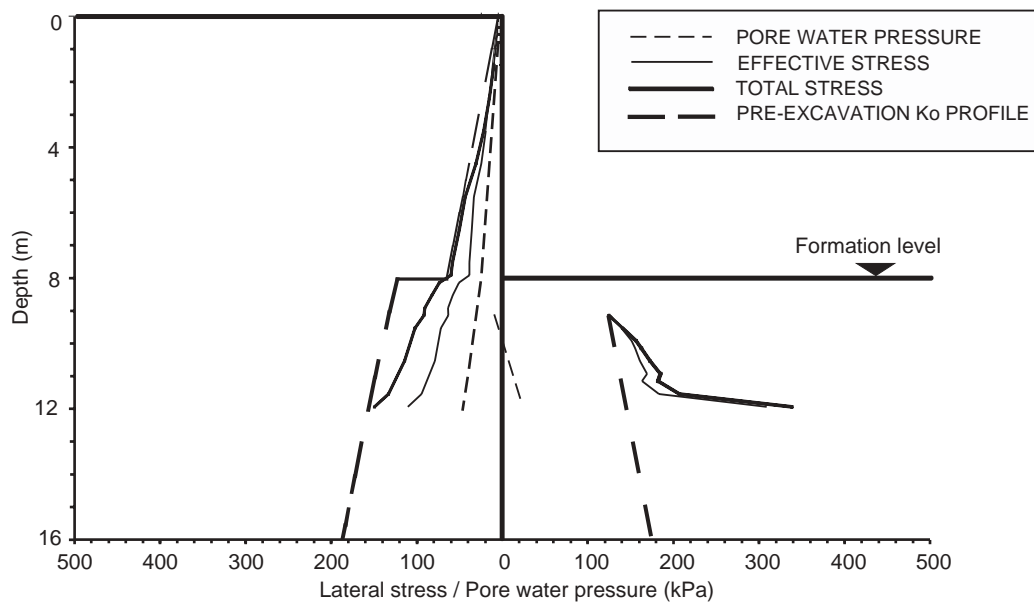


Figure 4.25 Lateral stresses and pore water pressure distributions acting on the wall after 7 years, Case 1 analysis - Test TRL 4

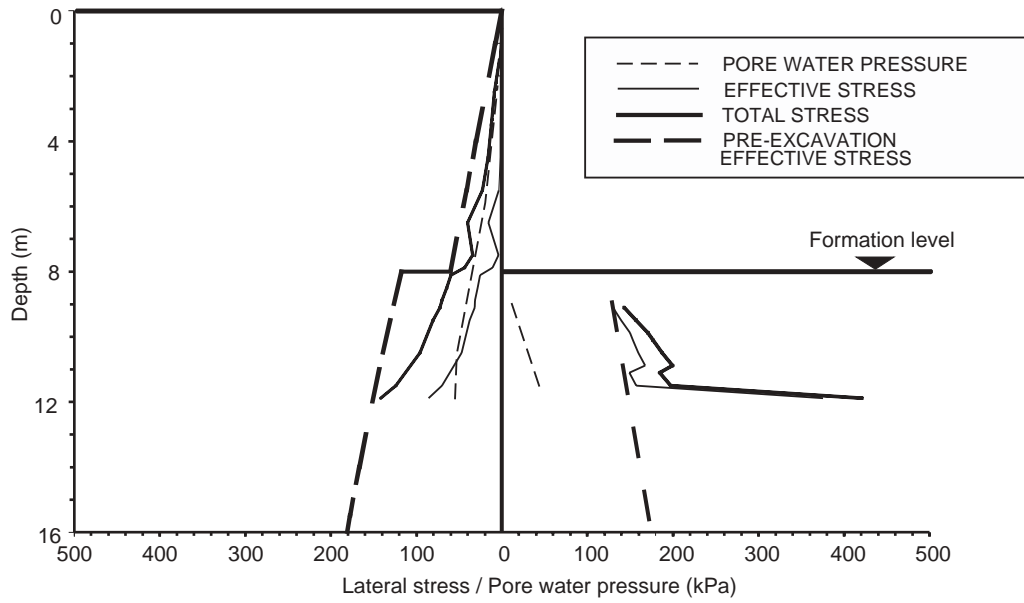


Figure 4.26 Lateral stresses and pore water pressure distributions acting on the wall after 3.7 years, Case 2 analyses - Test TRL 4

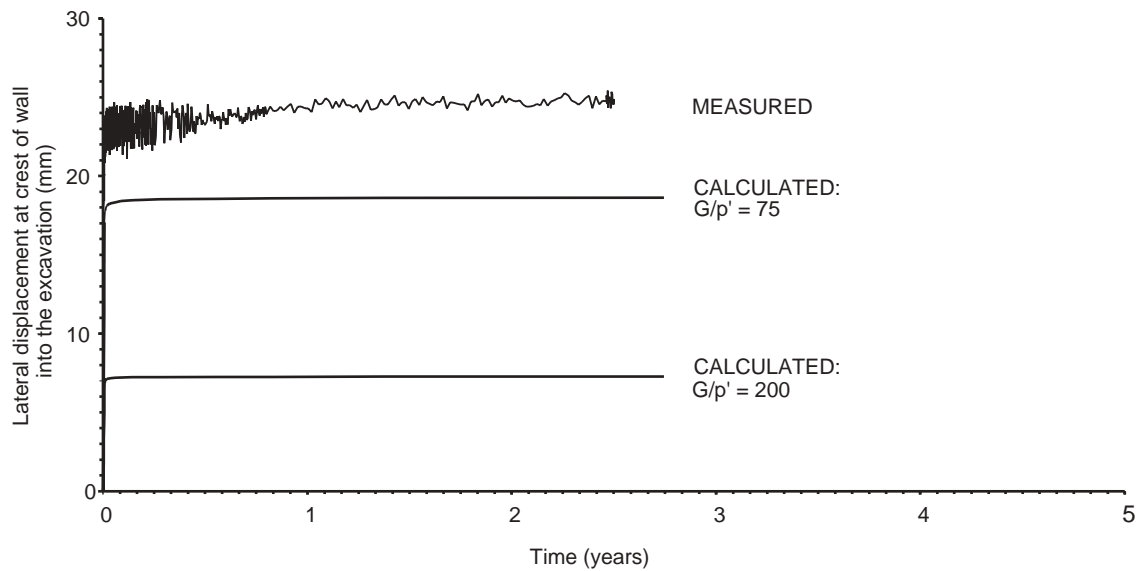


Figure 4.27 Calculated and measured crest movements into the excavation vs time, Test TRL 2

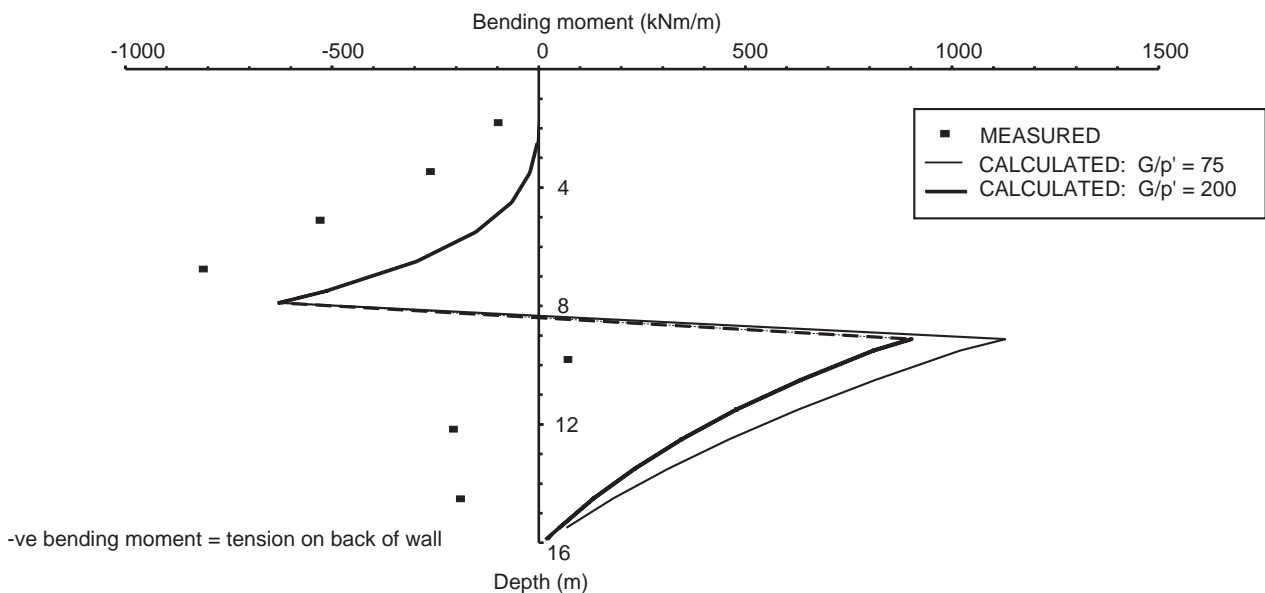


Figure 4.28 Calculated and measured bending moment profiles in the wall after 2.54 years, Test TRL 2

moments in the wall were broadly consistent. Whilst the shape of the computed and measured bending moment profiles appears logical, it was concluded that not too much reliance should be placed on the magnitude of the maximum measured bending moments in the wall.

The computed bending moments in the stabilising base at the end of the analyses are shown in Figure 4.29. A range of possible measured bending moments has been superimposed onto this figure (see Section 2.7.2). The computed bending moment profiles in the two analyses are generally in reasonable agreement with the measured profiles calculated on the basis of the smallest calibration factors found during wall calibration. Computed bending moments in the stabilising base were larger for the analysis with G/p' of 75, because the larger wall movements (and rotations) in this case led to slightly higher bearing pressures being developed on the underside of the stabilising base than in the analysis with G/p' of 200 (Figure 4.30). As a result of the greater restoring moment imparted by the stabilising base, the bending moments in the wall below formation level were also larger.

The vertical effective stress distributions below the stabilising base in Figure 4.30 are generally rectangular in shape and compare reasonably well with the lower estimate of measured bearing pressure of 188 kPa (assuming a rectangular pressure distribution) given in Table 2.3.

Lateral stresses on the wall

The computed horizontal stress distributions after 2.54 years for the analyses assuming G/p' of 75 and 200 are presented in Figures 4.31 and 4.32 respectively.

Behind the wall, the soil was at or very close to mobilising its full strength (i.e. $\phi'_{\text{mob}} = \phi'_{\text{crit}} = 35^\circ$) throughout the depth of the wall in both analyses. Above formation level, the effective stress and total stress profiles behind the wall are identical in both analyses. This is because this region of soil was modelled with having zero pore water

pressures throughout the analyses. The effective stress profiles behind the wall also suggest that there was a significant reduction in the pre-excavation effective stresses throughout the depth of the wall and that this soil had indeed reached the active state. This is not surprising as normally consolidated soils generally require small movements to reach the active state. In front of the wall, the soil was remote from mobilising its full strength in both analyses. This was because the vertical effective stresses in front of the wall remained high following excavation as a result of the stabilising base already being in place during simulated excavation.

The pore water pressure distributions at the end of the analyses on both sides of the wall are identical to those at the start of the analyses i.e. they increase hydrostatically with depth below formation level.

4.5.4 Test TRL 3 (4m embedment wall in 52/100 Leighton Buzzard Sand)

Wall movements

Figure 4.33 compares the measured and computed wall movements at the crest of the wall and shows that the measured crest movements fall between those computed in the two analyses. It is interesting to note that the computed crest movements into the excavation given in Figure 4.33 were less than those computed for the deeper embedment wall (Test TRL 2) given in Figure 4.27. This trend was also apparent in the centrifuge tests and is discussed in more detail later.

Bending moments in the wall and stabilising base

Measured and computed bending moments in the wall after 2.54 years are shown in Figure 4.34. The computed bending moment profiles were generally similar in shape, but smaller in magnitude than those measured in the centrifuge.

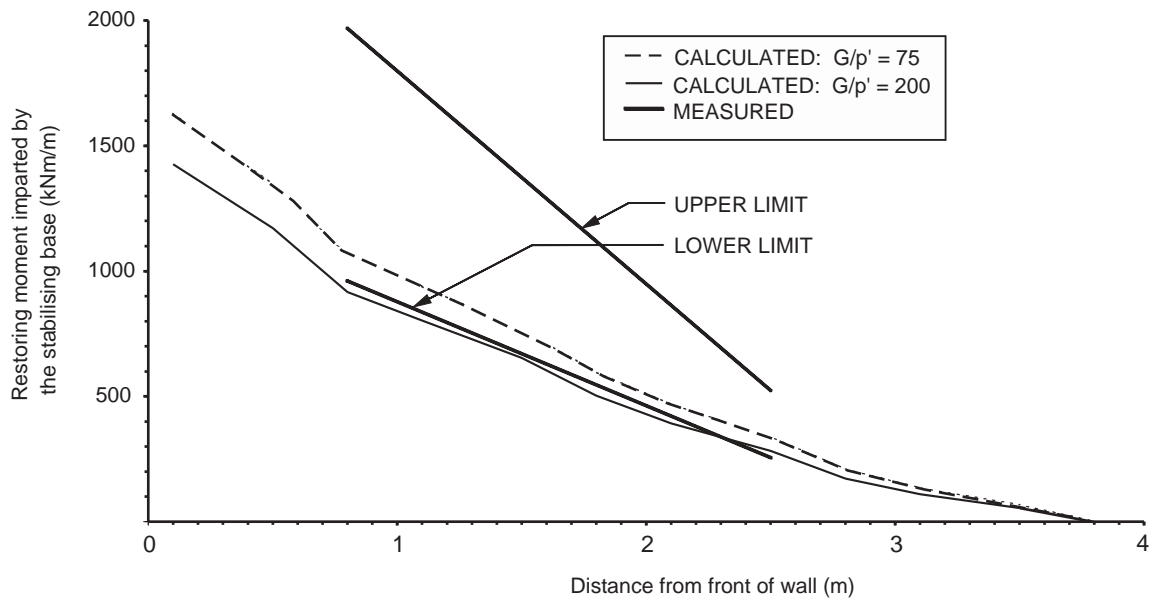


Figure 4.29 Calculated and measured bending moments in the stabilising base after 2.54 years, Test TRL 2

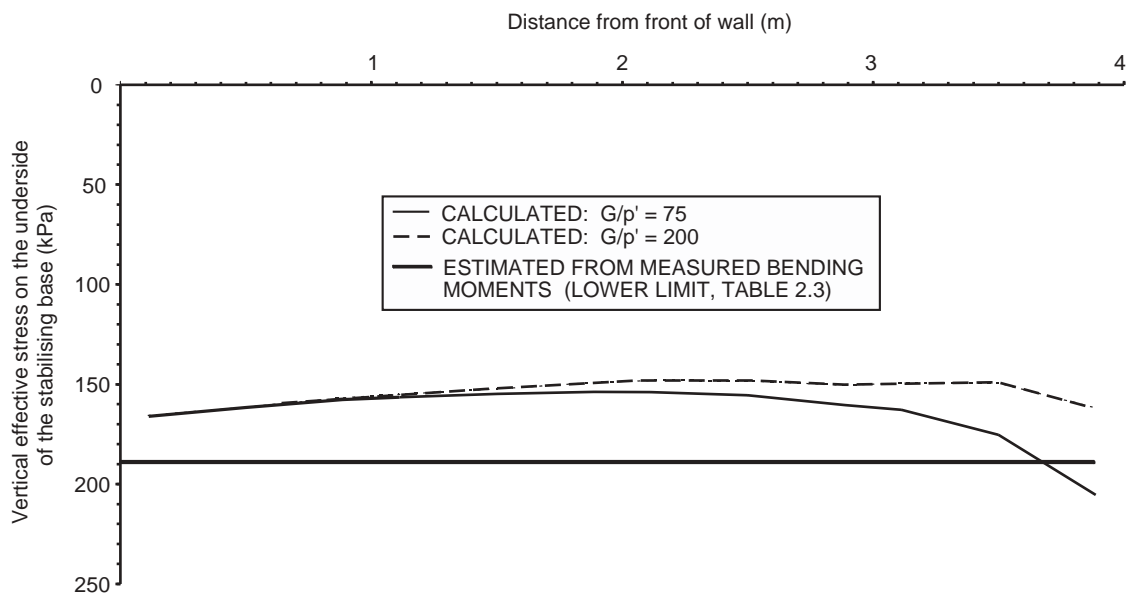


Figure 4.30 Calculated vertical effective stresses on the underside of the stabilising base after 2.54 years, Test TRL 2

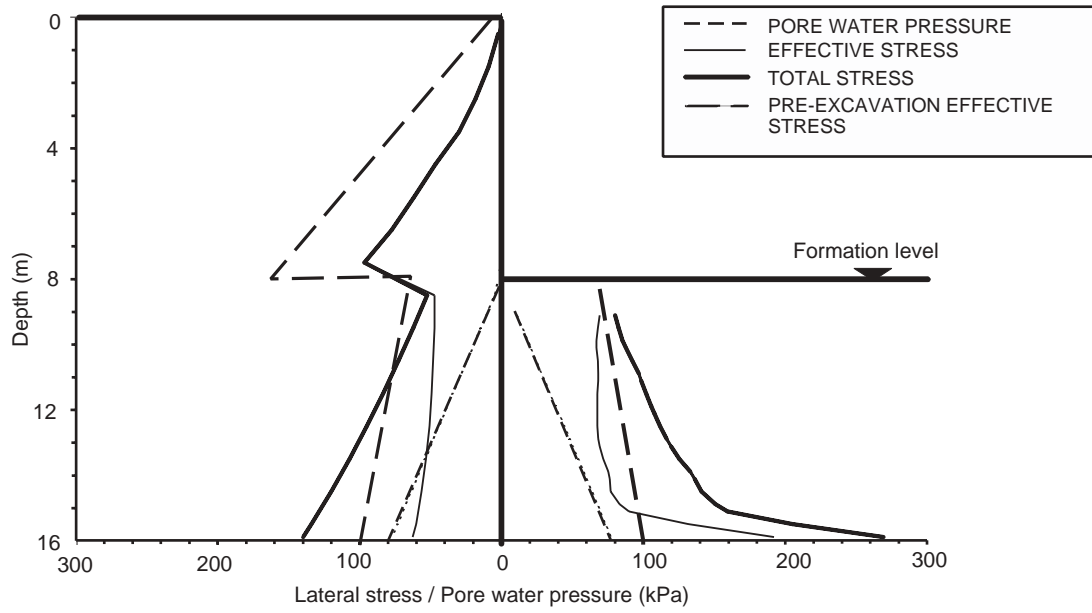


Figure 4.31 Lateral stresses and pore water pressure distributions acting on the wall after 2.54 years, $G/p'=75$ - Test TRL 2

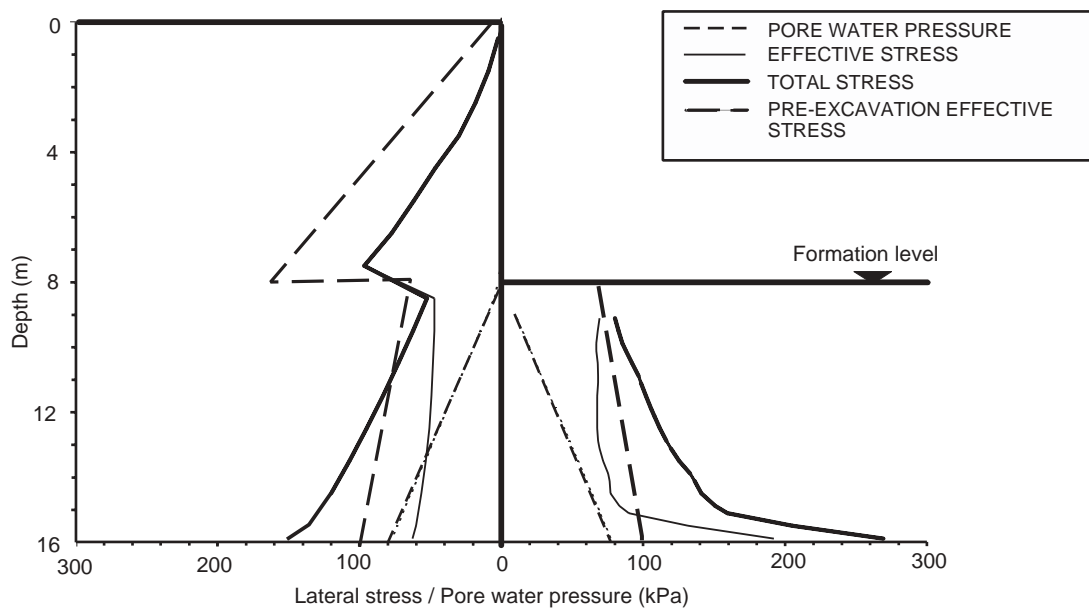


Figure 4.32 Lateral stresses and pore water pressure distributions acting on the wall after 2.54 years, $G/p' = 200$ - Test TRL 2

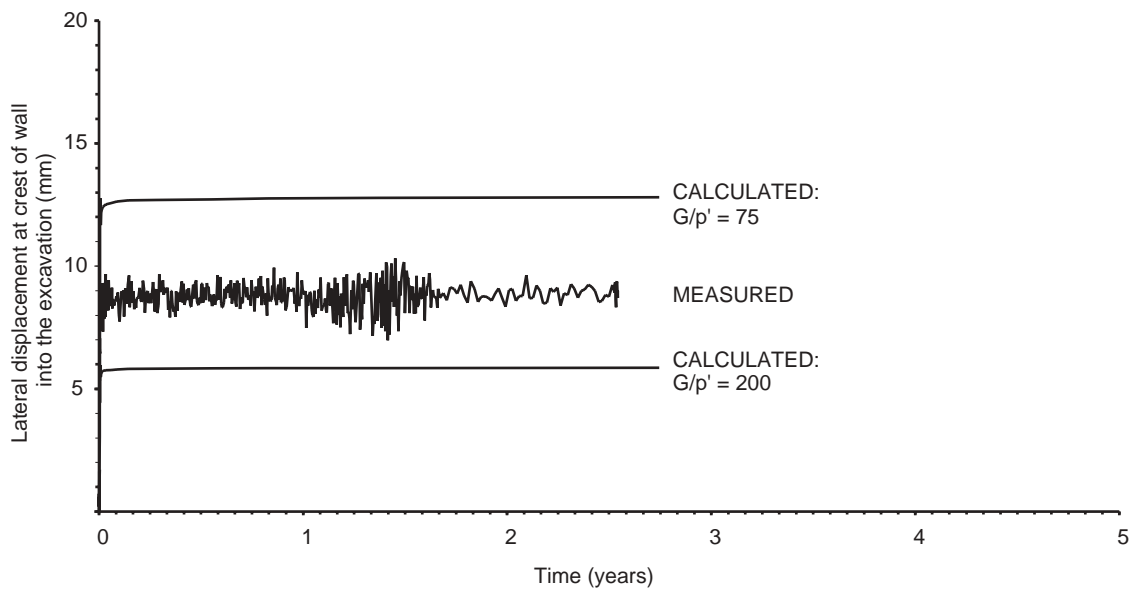


Figure 4.33 Calculated and measured crest movements into the excavation vs time, Test TRL 3

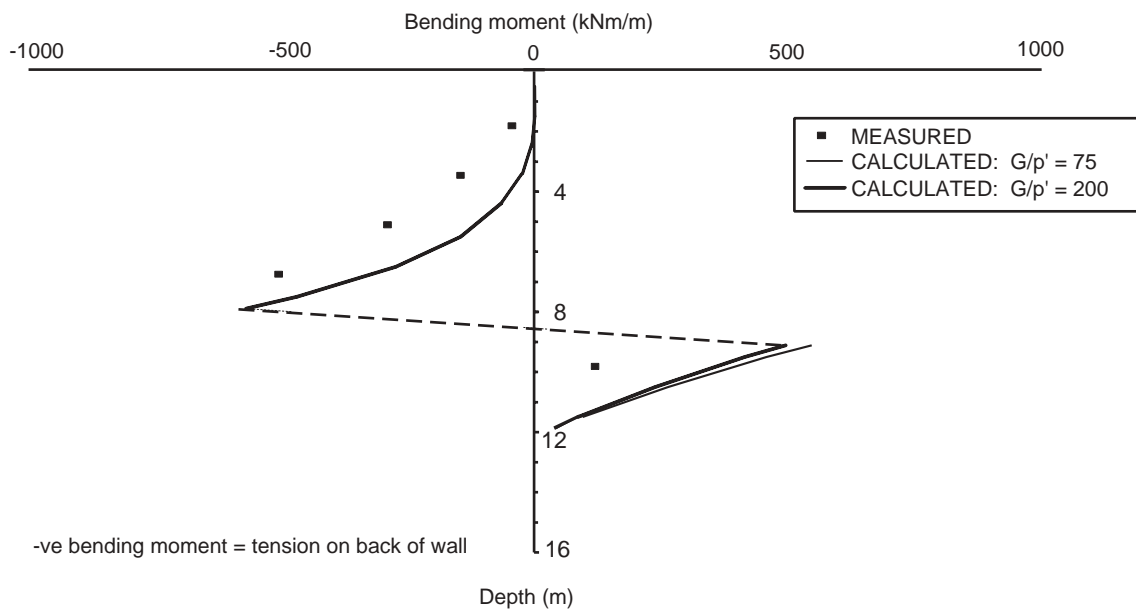


Figure 4.34 Calculated and measured bending moment profiles in the wall after 2.54 years, Test TRL 3

Figure 4.35 compares the measured and computed bending moments in the stabilising base after 2.54 years. It can be seen that there is close agreement between the computed bending moment profile with G/p' of 200 and the measured profile calculated on the basis of the smallest calibration factors found during wall calibration.

Computed vertical effective stresses on the underside of the stabilising base after 2.54 years are shown in Figure 4.36. The larger bearing pressures computed in the analysis with G/p' of 75 reflect the larger wall movements in this analysis, and the computed bending moments in the stabilising base were correspondingly increased (Figure 4.35).

The shapes of the computed bearing pressure distributions in Figure 4.36 are interesting. The profiles suggest that the bearing pressures are decreasing away from the wall along the stabilising base. The reason for this can be seen in the deformed mesh after 2.54 years given in Figure 4.37. The mode of deformation of the wall comprised forwards translation towards the excavation together with backwards rotation. Consequently, the stabilising base rotated backwards and the bearing pressures on the underside of the stabilising base were greatest close to the wall. This is in contrast to the mode of deformation computed in Test TRL 2 which generally comprised forwards translation of the wall (Figure 4.38).

Unfortunately, the image processing facility was not suitable for the sand tests and these modes of deformation could therefore not be validated in the centrifuge tests.

In terms of magnitude, the computed bearing pressures on the underside of the stabilising base in Test TRL 3 compare reasonably well with the lower estimate of measured bearing pressure of 119-140 kPa (assuming a rectangular pressure distribution) given in Table 2.4.

Lateral stresses on the wall

The computed horizontal stress distributions after 2.54 years for the analyses assuming G/p' of 75 and G/p' of 200 are presented in Figures 4.39 and 4.40 respectively. The lateral stress and pore water pressure distributions are generally similar in terms of shape and magnitude.

Behind the wall, the soil was at or very close to mobilising its full active strength (i.e. $\phi'_{\text{mob}} = \phi'_{\text{crit}} = 35^\circ$) throughout the depth of the wall in both analyses. This can be seen in the effective stress profiles behind the wall in Figures 4.39 and 4.40. In front of the wall, the soil was remote from collapse in both analyses for the reasons given in Section 4.5.3.

The pore water pressure distributions at the end of the analyses on both sides of the wall are identical to those at the start of the analyses i.e. they increase hydrostatically with depth below formation level.

4.6 A summary of the results of the finite element analyses

A comparison of crest movements into the excavation, bending moments in the stabilising base and pore water pressures in front of and behind the wall suggests that the principal aspects of behaviour of the stabilising base retaining walls in the centrifuge model tests were modelled in a reasonably realistic manner. Whilst the shape of the computed and measured bending moment profiles in the

wall were also similar, it was considered that not too much reliance should be placed on the magnitude of the maximum measured bending moments.

In the back-analyses of the centrifuge model tests in kaolin clay (i.e. Tests TRL 1 and TRL 4), better overall correlation was apparent in the Case 2 analyses, i.e. analyses in which both the permeability of the kaolin and its potential to mobilise greater strength was increased. However, collapse was predicted in the back-analyses of both centrifuge tests using the Case 2 parameters but was not apparent in centrifuge Test TRL 1. The limit-equilibrium back-analyses presented in Section 3.5.1 suggest that the wall/stabilising base arrangement of Test TRL 1 was just stable on the basis of measured pore water pressures and deformed geometry. A separate calculation (not included in this report) based on the original geometry suggested that this wall was at limiting equilibrium. Small external effects such as friction at the wall/strongbox and/or clay/strongbox interface could have been significant enough to have maintained the structure just at equilibrium in the centrifuge thereby preventing the onset of collapse.

In the back-analyses of the centrifuge model tests in sand (i.e. Tests TRL 2 and TRL 3), it was not possible to model the exact conditions imposed in the centrifuge tests during simulated excavation. A series of idealised analyses was therefore carried out and the principal aspects of behaviour were reasonably well modelled. Measured crest movements and stabilising base bending moments generally fell between those computed in the analyses with normalised shear moduli G/p' between 75 and 200. The analyses also showed that crest movements were smaller in the 4m embedment wall compared with the 8m embedment wall. This trend, which was also apparent in the centrifuge tests, was attributed to a difference in displacement mechanisms. The main mode of deformation for the 8m embedment wall was forward translation towards the excavation. In the case of the 4m embedment wall, however, forward translation towards the excavation was accompanied by backward rotation of the wall.

5 Summary and implications for design

A series of centrifuge model tests, finite element analyses and limit-equilibrium analyses has been carried out to investigate the effectiveness of stabilising base retaining walls.

Common retained heights corresponding to 8m at prototype scale and stabilising base projections from the wall of 4m were adopted in all of the centrifuge model tests. Depths of wall embedment corresponding to 4m and 8m at prototype scale were investigated in both 52/100 Leighton Buzzard Sand and overconsolidated speswhite kaolin clay.

The findings of the research can be summarised as follows:

- In the centrifuge tests carried out in kaolin clay, both the 4m and 8m embedment wall were of sufficient depth to prevent a short-term undrained collapse. In the long term, however, the 4m embedment wall was in a state of collapse whereas the 8m embedment wall apparently stabilised.

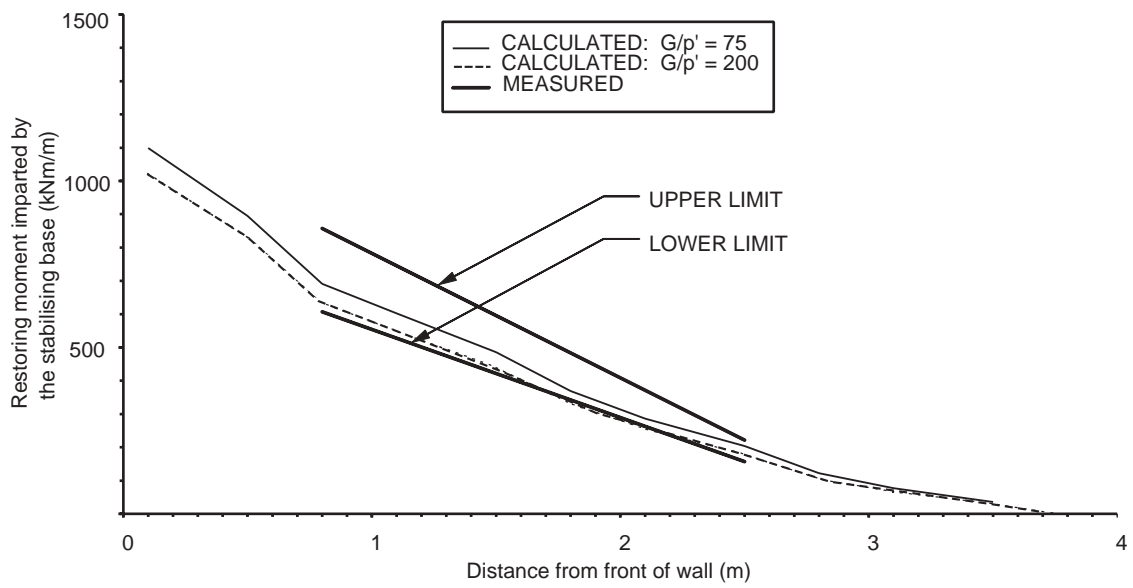


Figure 4.35 Calculated and measured bending moments in the stabilising base after 2.54 years, Test TRL 3

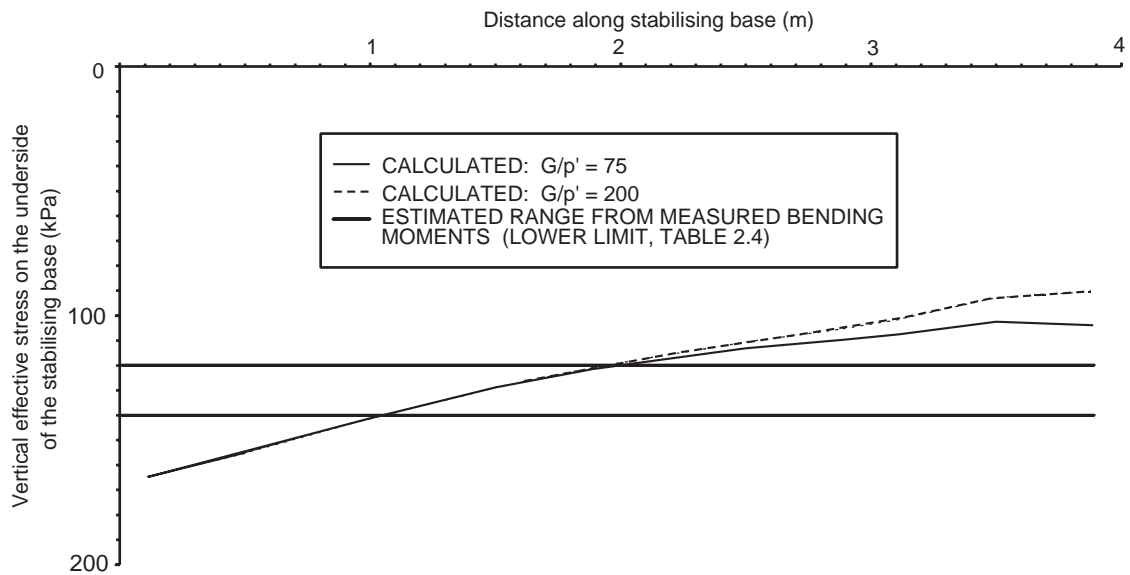


Figure 4.36 Calculated vertical effective stresses on the underside of the stabilising base after 2.54 years, Test TRL 3

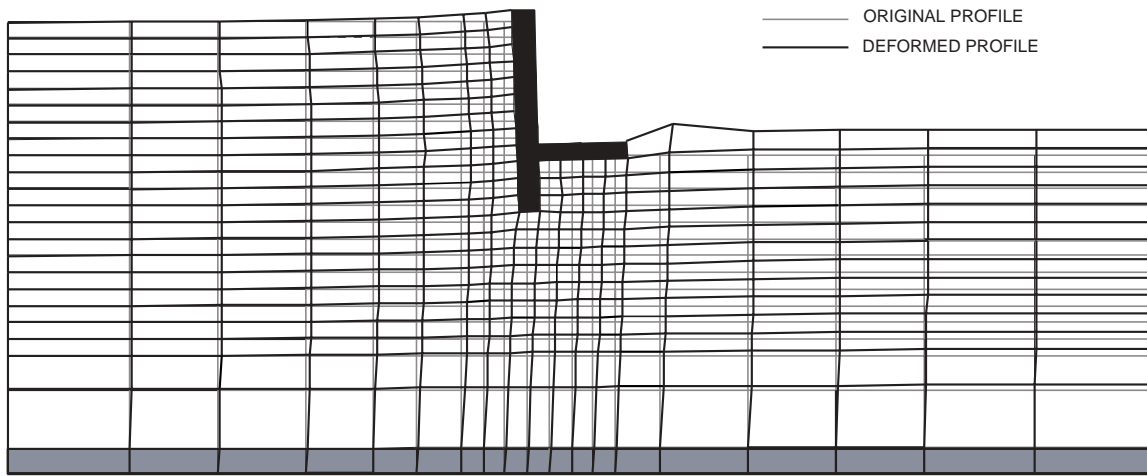


Figure 4.37 Deformed mesh after 2.54 years, $G/p' = 200$ - Test TRL 3
(movements magnified by a factor of 50)

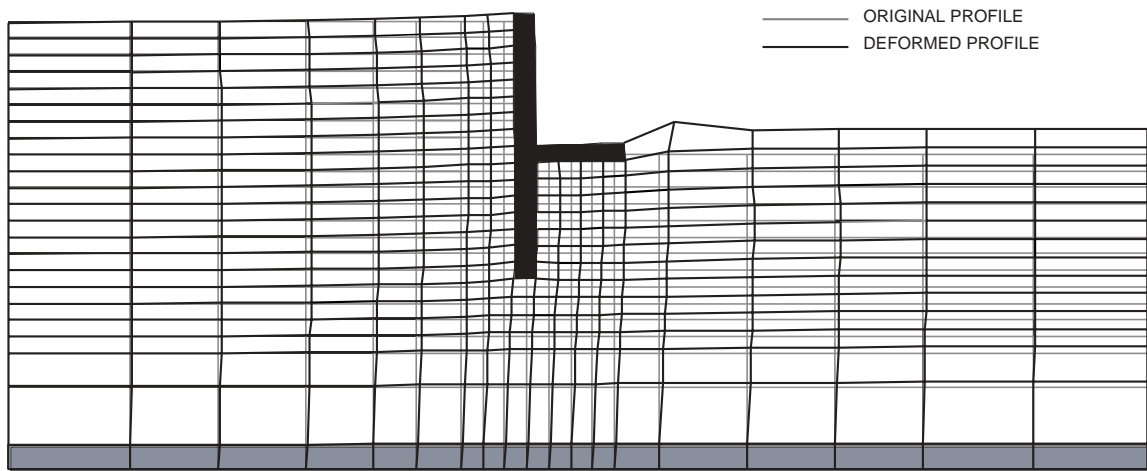


Figure 4.38 Deformed mesh after 2.54 years, $G/p' = 200$ - Test TRL2
(movements magnified by a factor of 50)

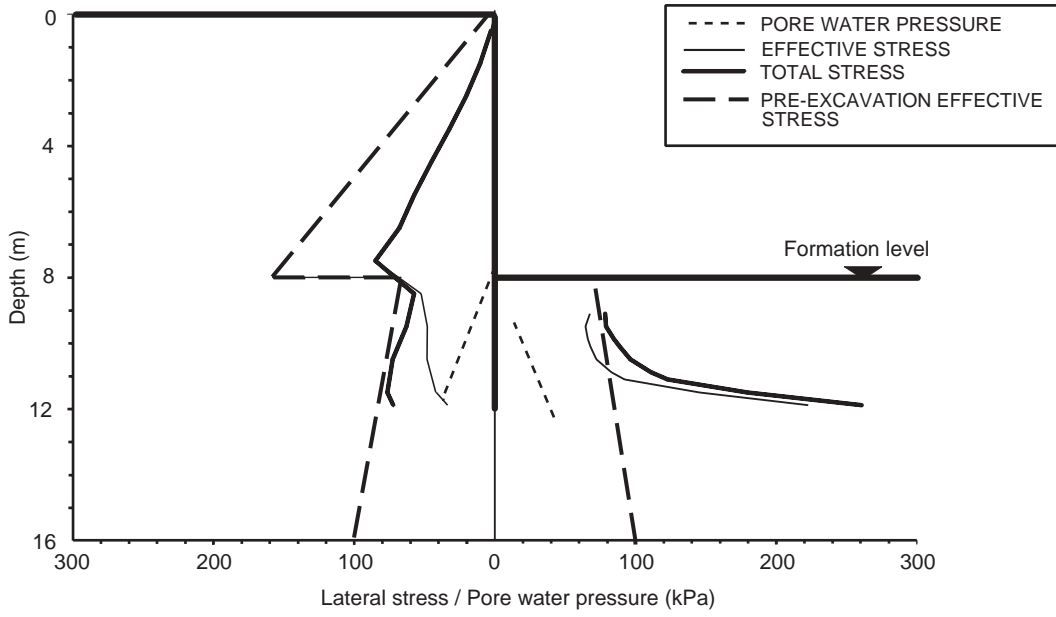


Figure 4.39 Lateral stresses and pore water pressure distributions acting on the wall after 2.54 years, $G/p' = 75$ - Test TRL 3

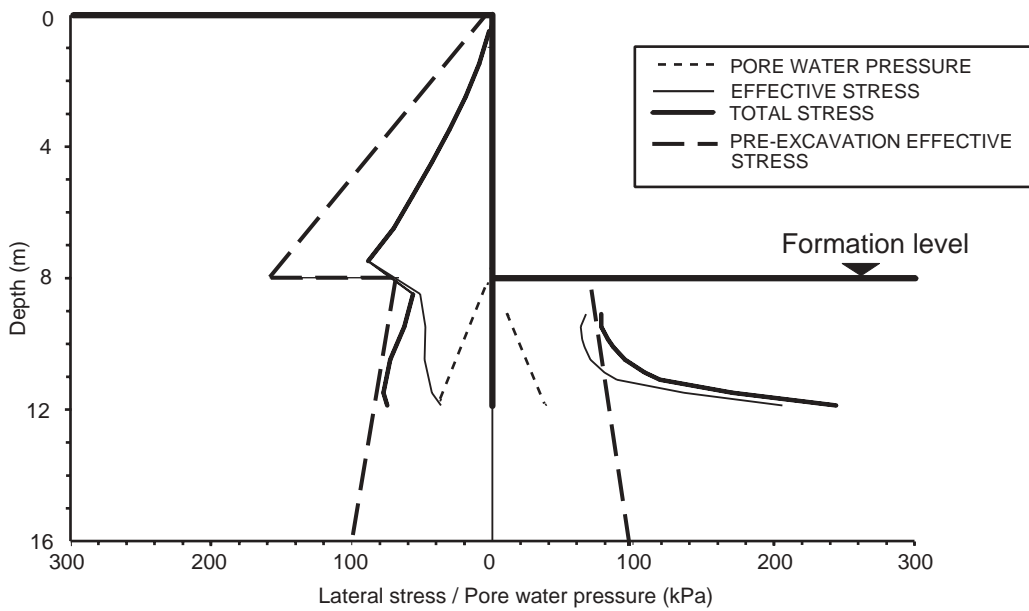


Figure 4.40 Lateral stresses and pore water pressure distributions acting on the wall after 2.54 years, $G/p' = 200$ - Test TRL 3

In the centrifuge tests carried out in sand, wall movements were much smaller, reflecting the significantly greater stiffness and possibly strength of the sand compared with the kaolin clay. Wall movements at the crest of the wall, however, were at all times larger for the wall of 8m embedment than for the wall of 4m embedment.

- The finite element analyses of the centrifuge tests carried out in kaolin clay confirmed that the 4m embedment wall was unstable in the long term. They also confirmed that the 8m embedment wall would have been unstable on the basis of the undeformed geometry (i.e. the original retained height). Comparison of the bending moments in the stabilising base and the pore water pressures in front of and behind the wall suggested that the principal aspects of behaviour were modelled in a reasonably realistic manner.

The finite element analyses of the centrifuge tests carried out in sand confirmed that both the 4m and 8m embedment wall were stable. Different modes of movement were evident in the analyses which may explain the reason for the smaller crest movements measured in the 4m embedment wall. The 4m embedment wall suffered forwards translation together with backwards rotation whereas the 8m embedment wall translated forwards without significant rotation.

- Limit-equilibrium analyses in which the stabilising base is assumed to act as a rigid prop are probably unsafe because it is unlikely that the base will be able to provide sufficient lateral force to act as the point of rotation: the end of the stabilising base reacts against soil and not another wall.
- The limit-equilibrium back-analyses of the stabilising base retaining walls in the centrifuge tests were carried out in two ways:
 - a Scheme 3, assuming a collapse mechanism analogous to that for a mass gravity wall. The wall and the soil below the stabilising base and above the toe of the wall are assumed to act as a rigid block. Collapse will occur when there is limiting equilibrium with active conditions behind the block, passive conditions in front of the block and bearing pressures (calculated on the basis of Equation 3.1) on the underside of the block.
 - b Scheme 4, assuming a collapse mechanism analogous to that for an unpropped cantilever wall. Rigid body rotational failure is assumed to occur about an axis lying in the plane of the wall at some point between formation level and the toe (i.e. fixed earth support conditions). The bearing pressure on the underside of the stabilising base imparts a restoring moment to the retaining wall and also acts as a surcharge on the soil in front of the wall (the stress distribution on the underside of the stabilising base has been assumed to be rectangular in shape: see Section 3.5).

According to the Scheme 3 approach - and assuming the same soil friction angle mobilised everywhere on the

structure, full wall friction on both sides of the soil/wall block, zero friction on the base of the soil/wall block, a full height groundwater level and steady state seepage conditions - the analyses of stabilising base walls in kaolin clay indicated a minimum depth of embedment for stability (i.e. F.O.S of 1) of 9.8m and a base projection from the wall of 14.5m. Given that the 8m embedment wall with a 4m stabilising base projection in the centrifuge test was marginally stable, this calculation would appear to be overconservative. Making similar design assumptions, the back-analyses of the stabilising base walls in sand indicated a minimum depth of embedment for stability of 3m and a base projection from the wall of 5.9m.

According to the Scheme 4 approach - and assuming the same soil friction angle mobilised everywhere on the structure, full wall friction on both sides of the wall, zero friction on the underside of the stabilising base, measured pore water pressures and the deformed geometry - the analyses of stabilising base walls in kaolin clay confirmed that the 4m embedment wall was in a state of collapse with a strength mobilisation factor M of 0.91 and that the 8m embedment wall was close to limiting equilibrium with a mobilisation factor M of 1.05. Both the 4m and 8m embedment walls in sand were stable according to this calculation.

However, an investigation into the stress fields that can be developed below a stabilising base suggests that it may not be theoretically possible to develop full wall friction in front of the wall and zero base friction on the underside of the base owing to a lack of space to achieve the required rotation in the principal stress directions. This means that the Scheme 4 approach using Caquot and Kerisel's (1948) earth pressure coefficients lacks rigour, and may err on the unsafe side.

With this in mind, the following recommendations are given for the design of a stabilising base retaining wall:

- Adopt the Scheme 4 limit-equilibrium approach summarised in (b) above in conjunction with the recommendations for design given in BS 8002 (BSI, 1994: Clause 3.2.5). These are:

- 1 the adoption of a (reduced) mobilised soil strength ϕ'_{mob} taken as the lesser of
 - (a) the representative peak strength of the soil ϕ'_{peak} divided by a soil mobilisation factor M of 1.2
- (5.1)

or

- (b) the critical state strength of the soil ϕ'_{crit}
- 2 the application of a surcharge of 10kPa to the retained surface; and
 - 3 the over-excavation (by 10% of the retained height or 0.5m whichever is greater) of the soil in front of the wall.

It is also recommended that the following design assumptions are incorporated.

- 1 In the absence of suitable data from shear box tests, wall friction δ on both sides of the wall should be limited to 75% of the mobilised soil strength ϕ'_{mob} (BS 8002, 1994: Clause 3.2.6).
- 2 Calculate the bearing capacity factor N_q (Equation 3.2) assuming that the load inclination angle on the underside of the stabilising base $\delta_b = 0$.
- 3 Using conventional foundation design theory, the ultimate bearing pressure (σ'_f) (calculated for example using Equation 3.1 and enhancement factors given in Table 3.1) on the underside of the stabilising base should be reduced to an allowable bearing pressure (σ'_a) taken as the lesser of

- (a) the ultimate bearing capacity divided by a factor of safety F (typically 2.5 - 3.0: BS 8004, 1986) with
- $$\phi' = \phi'_{\text{peak}}$$

(5.2)

or

- (b) the ultimate bearing capacity divided by a factor of safety $F = 1.0$ with $\phi' = \phi'_{\text{mob}}$.

- 4 The long term pore water pressure distributions on either side of the wall may be estimated on the basis of the linear seepage model.

The conditions for design and the resulting stress distributions are indicated in Figure 5.1.

- In view of the assumptions made and the theoretical shortcomings of the approach, the proposed limit-equilibrium calculation (which could be used for preliminary sizing purposes) should be accompanied by a detailed analysis (e.g. finite element analysis) to take proper account of construction sequence and the complex soil/structure interactions involved.

The width of the stabilising base will also affect the stability and serviceability of the retaining wall. In the research described in this report, the ratio of stabilising base width to retained height was 0.5 which is consistent with the recommended optimum value suggested by Powrie & Chandler (1998).

The centrifuge model tests and finite element analyses described in this report have given an insight into the behaviour of stabilising base retaining walls. There is, however, a need for further monitoring of this class of retaining wall in the field.

6 Acknowledgements

The work was carried out in the Department of Civil and Environmental Engineering at the University of Southampton, under contract to the Transport Research Laboratory on behalf of the Highways Agency. The TRL Project Manager was Dr D R Carder and the HA Project Managers were Dr D I Bush and Mr N Finegan.

Model preparation and fabrication of the centrifuge

strongbox components were carried out at the Southampton University workshops. The centrifuge model tests were carried out using the Acutronic Series 661 geotechnical centrifuge at the London Geotechnical Centrifuge Centre. The image processing facility used in the centrifuge model tests was set up and supervised by Dr J Chen and Mr N Woodhouse of City University. The authors are grateful to Messrs H P Skinner and D Taylor for technical advice and assistance.

7 References

- Al-Tabaa A (1987).** *On the permeability and stress-strain response of speswhite kaolin.* PhD dissertation, University of Cambridge.
- Batten M (1998).** *Measurements of prop loads in two large braced excavations.* PhD dissertation, University of Southampton.
- Bellotti R, Ghionna V, Jamiolkowski M, Robertson P K and Peterson R W (1989).** *Interpretation of moduli from self boring pressuremeter tests in sands.* Géotechnique, Vol. 3, No. 2, 269-292.
- Bolton MD, Britto A M, Powrie W and White T P (1989).** *Finite element analysis of a centrifuge model of a retaining wall embedded in a heavily overconsolidated clay soil.* Computers and Geotechnics, Vol 7, 289-318.
- Bolton M D and Powrie W (1987).** *The collapse of diaphragm walls retaining clay.* Géotechnique, Vol. 37, No. 3, 335-353.
- Bowles J E (1988).** *Foundation analysis and design.* 4th edition, McGraw-Hill, New York.
- Brinch Hansen J (1970).** *A revised and extended formula for bearing capacity.* Danish Geotechnical Institute Bulletin No. 28, DGI, Copenhagen.
- BSI (1986).** *BS 8004: Code of practice for foundations.* British Standards Institution, London.
- BSI (1991).** *BS 1377: Methods of test for soils for civil engineering purposes, Part 2: Classification tests.* British Standards Institution, London.
- BSI (1994).** *BS 8002: Code of practice for earth retaining structures.* British Standards Institution, London.
- Burland J B and Kalra J C (1986).** *Queen Elizabeth II Conference Centre: geotechnical aspects.* Proceedings of the Institution of Civil Engineers, Part 1, Vol 80, 1479-1504.
- Caquot A and Kerisel J (1948).** *Tables for the calculation of passive pressures, active pressures and bearing capacity of foundations.* Gauthier-Villars, Paris.

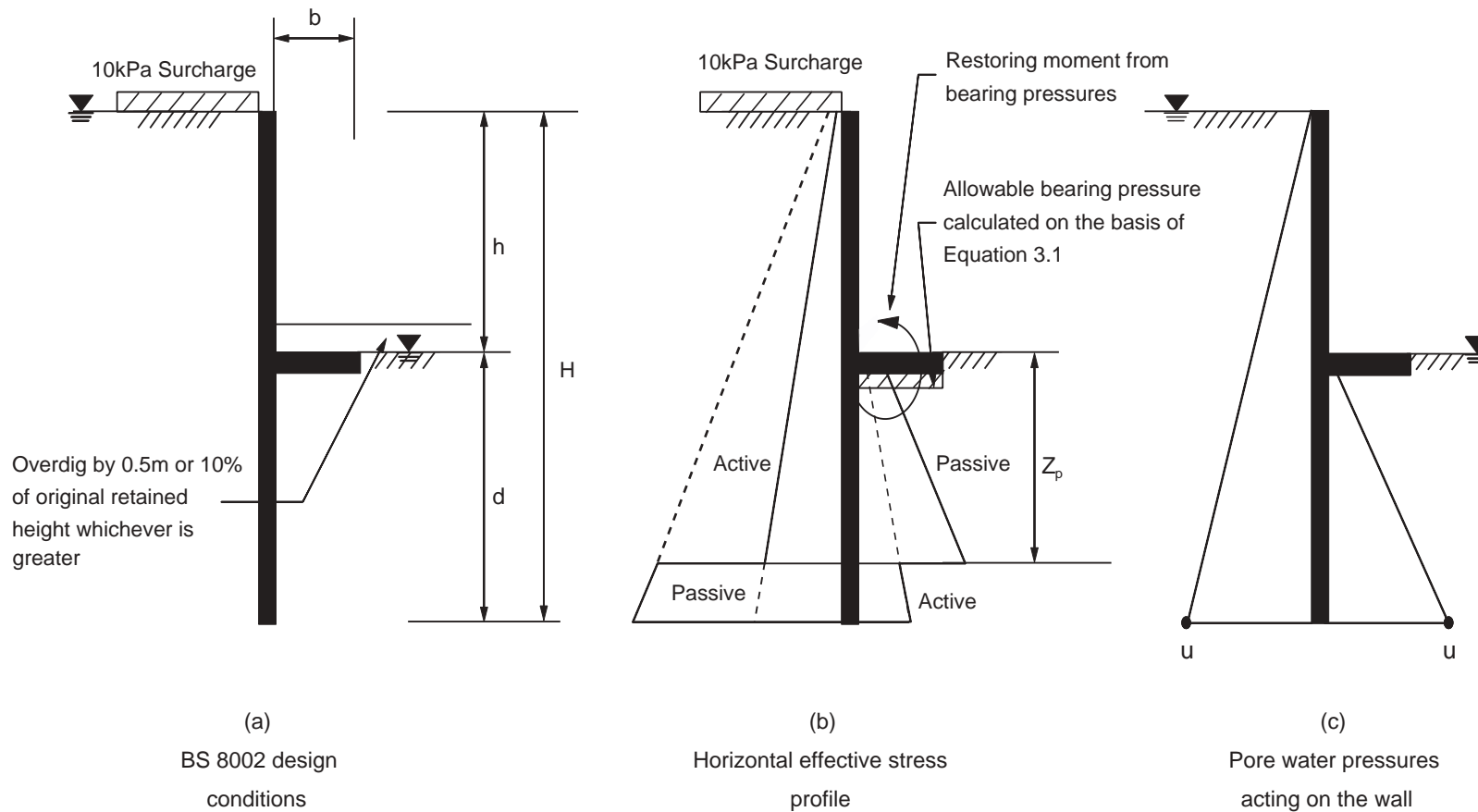


Figure 5.1 Recommended design conditions and idealised stress distributions to be used in the limit-equilibrium analysis of a stabilising base retaining wall

- Carder DR, Watson G V R, Chandler R J and Powrie W (1999).** *Long term performance of an embedded retaining wall with a stabilising base.* Proceedings of the Institution of Civil Engineers, Geotechnical Engineering (in press).
- Chandler R J (1995).** *Field studies, analysis and numerical modelling of retaining walls propped at formation level.* PhD dissertation, QMW, University of London.
- Chen J, Robson S, Cooper M A R and Taylor R N (1996).** *An evaluation of three different image capture methods for measurement and analysis of deformation within a geotechnical centrifuge.* International Archives of Photogrammetry and Remote Sensing, Vol. XXXI, Part B5, 70-75.
- Daly M P D (1999).** *Earth berms as temporary supports for embedded retaining walls.* PhD dissertation, QMW, University of London (in preparation).
- Hazen A (1892).** *Physical properties of sands and gravels with reference to their use in filtration.* Report of the Massachusetts State Board of Health.
- Jaky J (1944).** *The coefficient of earth pressure at rest.* Journal of the Union of Hungarian Engineers and Architects, 355-358.
- Konig D, Jessberger H L, Bolton M, Phillips R, Bagge G, Renzi R and Garnier J (1994).** *Pore pressure measurement during centrifuge tests: Experience of five laboratories.* Centrifuge 94, edited by Leung, Lee & Tan, 101-108.
- Li E S F (1990).** *On the analysis of singly-propped diaphragm walls.* PhD dissertation, King's College, University of London.
- Mayne P W and Kulhawy F H (1982).** *K_o -OCR relationships in soil.* Proc. ASCE, J. Geotechnical Engineering Division, Vol 103, No GT6, 851-872.
- Meyerhof G G (1963).** *Some recent research on the bearing capacity of foundations.* Canadian Geotechnical Journal, Vol 1, No 1, 16-26.
- Padfield C J and Mair R J (1984).** *Design of retaining walls embedded in stiff clay.* Report 104, Construction Industry Research & Information Association, London.
- Page J R T (1996).** *Changes in lateral stress during slurry trench wall installation.* PhD dissertation, QMW, University of London.
- Powrie W (1985).** *Discussion on the 5th Geotechnique symposium in print.* The performance of propped and cantilevered rigid walls. Géotechnique, Vol. 35, No 4, 546-548.
- Powrie W (1986).** *The behaviour of diaphragm walls in clay.* PhD dissertation, University of Cambridge.
- Powrie W (1997).** *Soil mechanics: Concepts and applications.* E & F N Spon, London.
- Powrie W and Chandler R J (1998).** *The influence of a stabilising platform on the performance of an embedded retaining wall: A finite element study.* Géotechnique, Vol. 48, No 3, 403-409.
- Powrie W and Kantartzi C (1996).** *Ground response during diaphragm wall installation in clay: Centrifuge model tests.* Géotechnique, Vol. 46, No 3, 1-15.
- Powrie W and Li, E S F (1991).** *Finite element analyses of in situ retaining walls propped at formation level.* Géotechnique, Vol. 41, No. 4, 499-514.
- Richards D J (1995).** *Centrifuge and numerical modelling of twin-propped retaining walls.* PhD dissertation, QMW, University of London.
- Schofield A N (1980).** *Cambridge geotechnical centrifuge operations.* Géotechnique, Vol. 20, No. 2, 129-170.
- Stroud M A (1971).** *The behaviour of sand at low stress levels in the simple shear apparatus.* PhD dissertation, University of Cambridge.
- Symons I F (1983).** *Assessing the stability of a propped in situ retaining wall in overconsolidated clay.* Proceedings of the Institution of Civil Engineers, Part 2, No 75, 617-633
- Symons I F and Carder D R (1993).** *Stress changes in stiff clay caused by the installation of embedded retaining walls.* Retaining Structures, ed. C R I Clayton, 227-236. London: Thomas Telford (ICE).
- Tedd P, Chard B M, Charles J A and Symons I F (1984).** *Behaviour of a propped embedded retaining wall in stiff clay at Bell Common tunnel.* Géotechnique, Vol. 34, No. 4, 513-532.
- White T P (1987).** *Finite element calculations involving the yielding of dilatant soils.* MPhil dissertation, University of Cambridge.

Appendix A

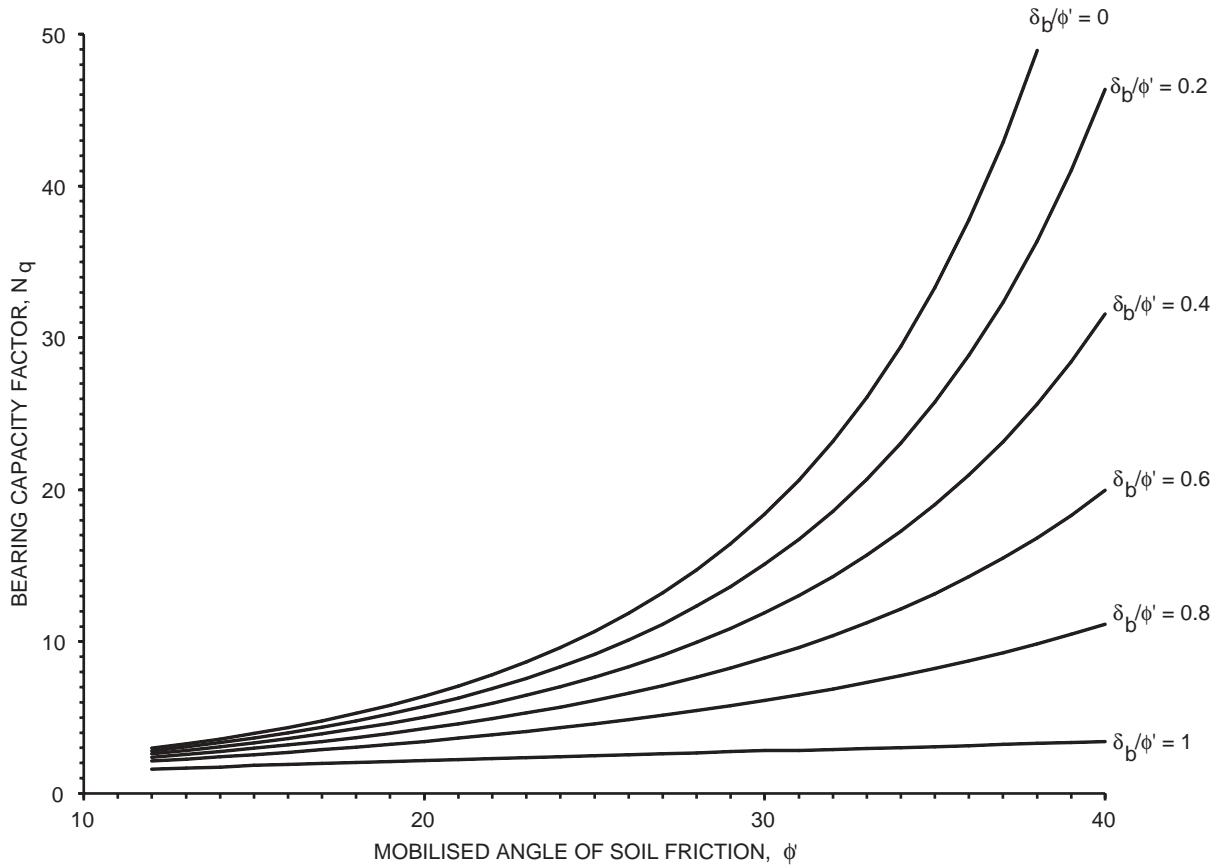


Figure A1 Bearing capacity factors N_q for inclined loads, according to Equation 3.2

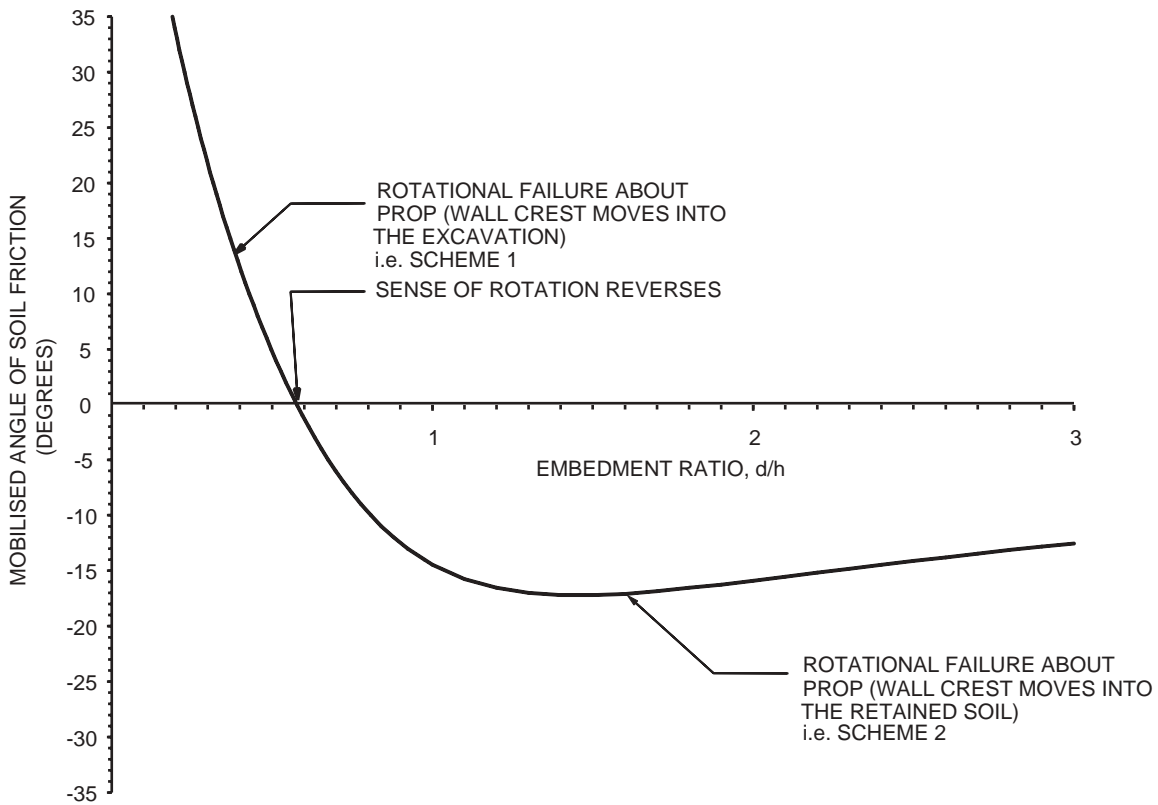


Figure A2 Mobilised soil strength as a function of embedment ratio for a smooth wall rigidly propped at formation level retaining 8m of kaolin clay of unit weight $\gamma=17.5\text{kN/m}^3$

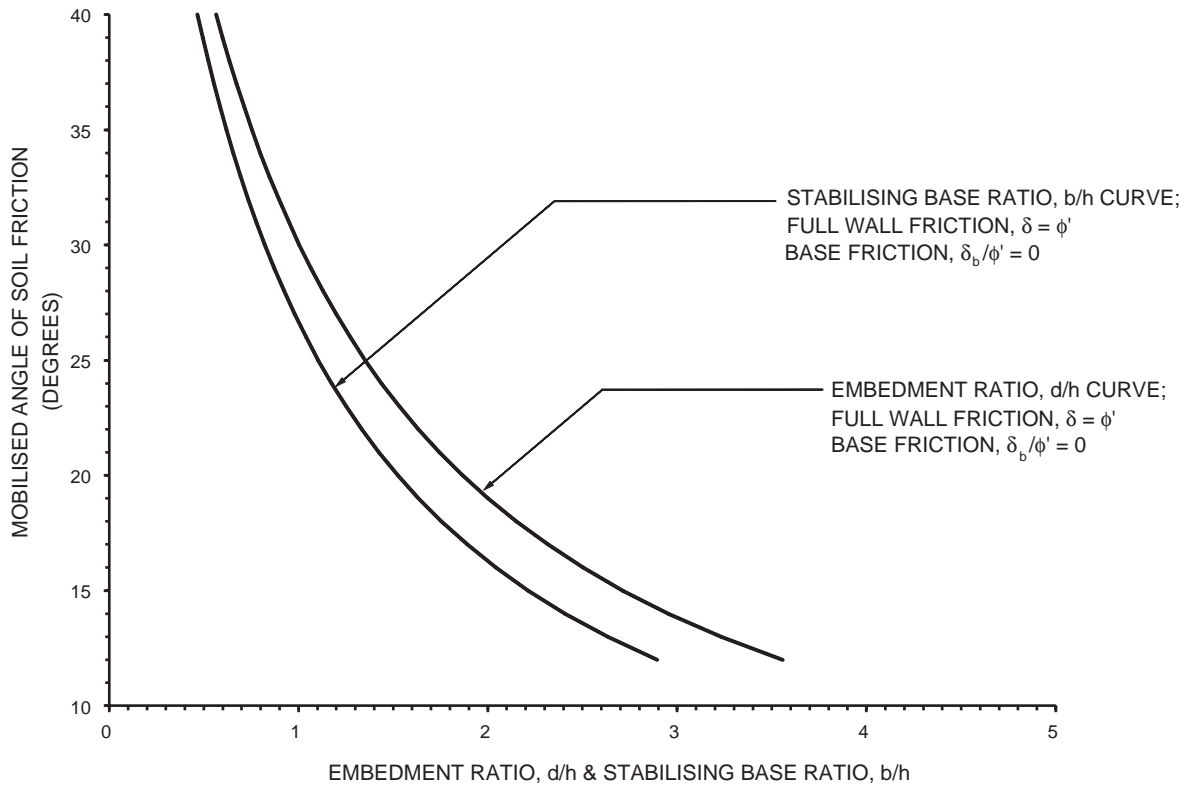


Figure A3 Scheme 3 - Estimated actual conditions; Mobilised soil strength as a function of embedment ratio and stabilising base ratio for a wall/soil block retaining 8 m of saturated kaolin clay of unit weight $\gamma=17.5\text{kN/m}^3$ assuming full wall friction and zero base friction

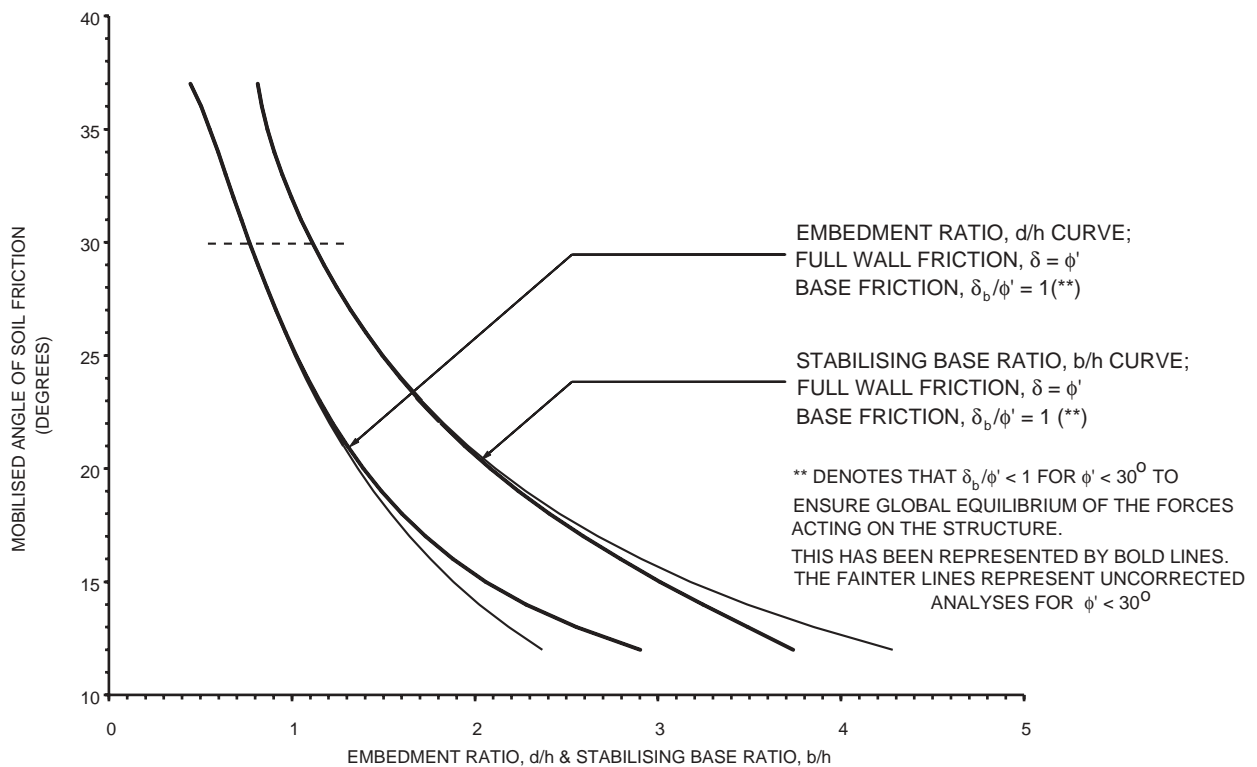


Figure A4 Scheme 3 - Estimated actual conditions; Mobilised soil strength as a function of embedment ratio and stabilising base ratio for a wall/soil block retaining 8m of saturated kaolin clay of unit weight $\gamma=17.5\text{kN/m}^3$ assuming full wall friction and full base friction (**)

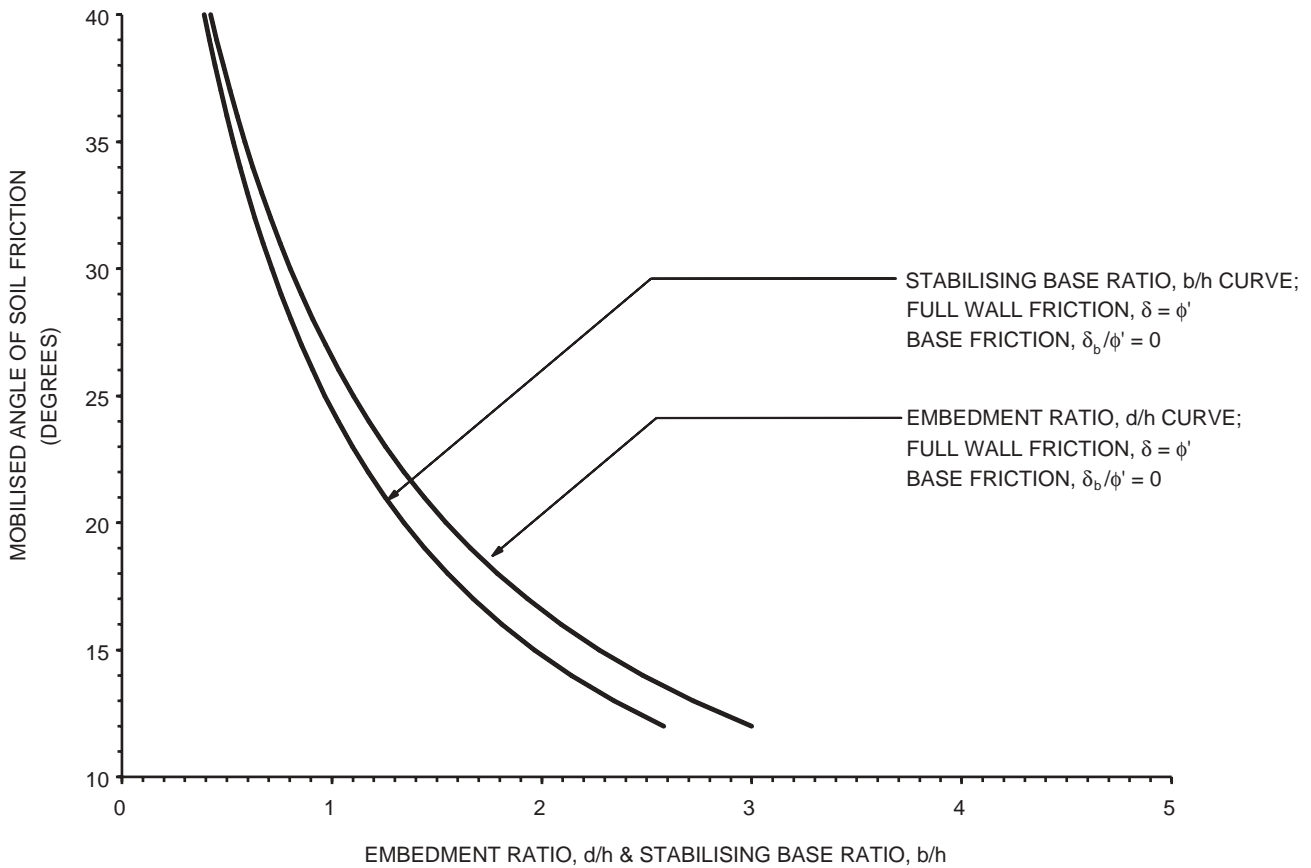


Figure A5 Scheme 3 - Estimated actual conditions; Mobilised soil strength as a function of embedment ratio and stabilising base ratio for a wall/soil block retaining 8m of saturated sand of unit weight $\gamma=20\text{kN/m}^3$ assuming full wall friction and zero base friction

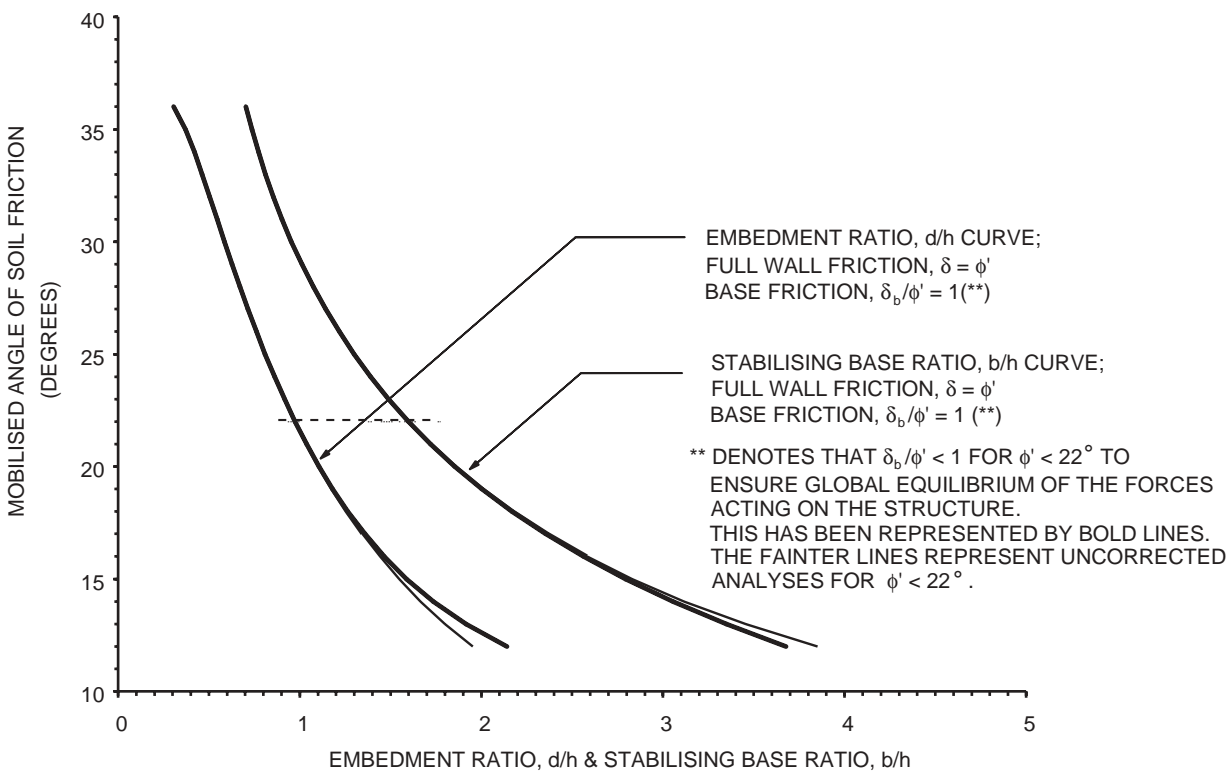


Figure A6 Scheme 3 - Estimated actual conditions; Mobilised soil strength as a function of embedment ratio and stabilising base ratio for a wall/soil block retaining 8m of saturated sand of unit weight $\gamma=20\text{kN/m}^3$ assuming full wall friction and full base friction (**)

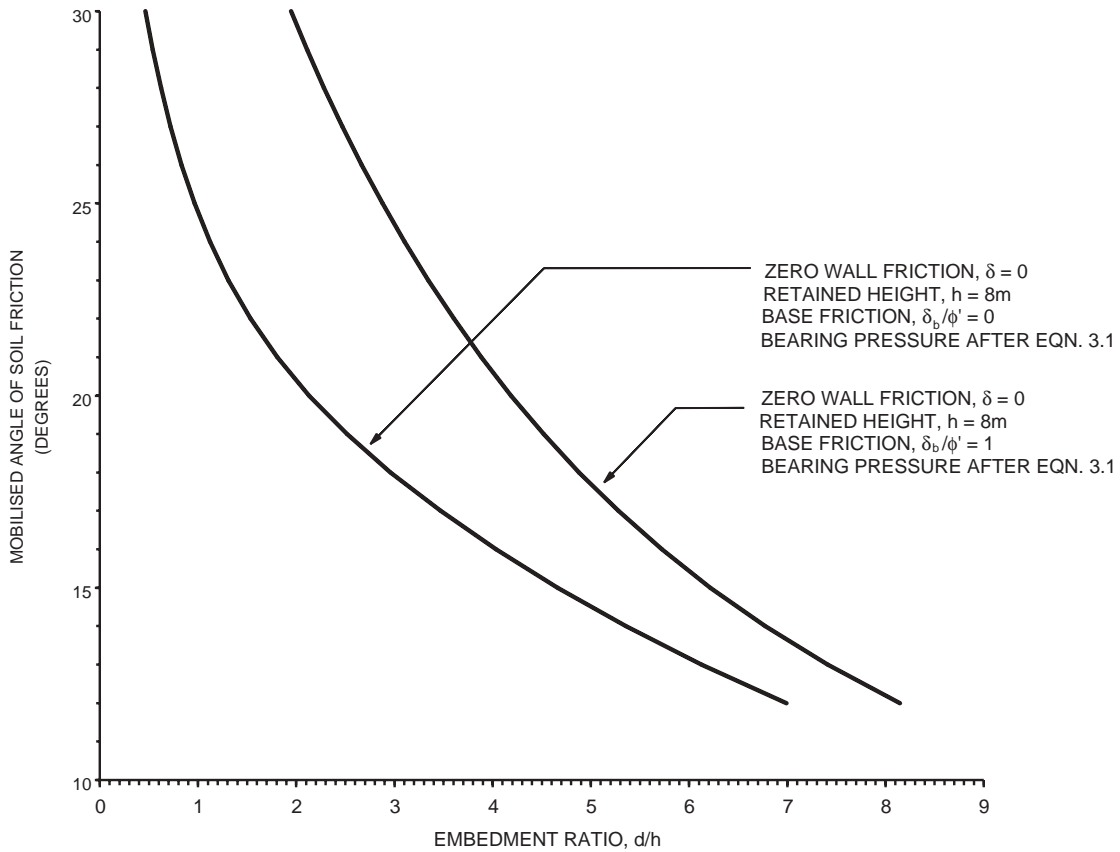


Figure A7 Scheme 4 - Estimated actual conditions; Mobilised soil strength as a function of embedment ratio for a smooth retaining wall with integral stabilising base retaining 8m of kaolin clay of unit weight $\gamma=17.66\text{kN/m}^3$; Stabilising base projection from wall = 4m

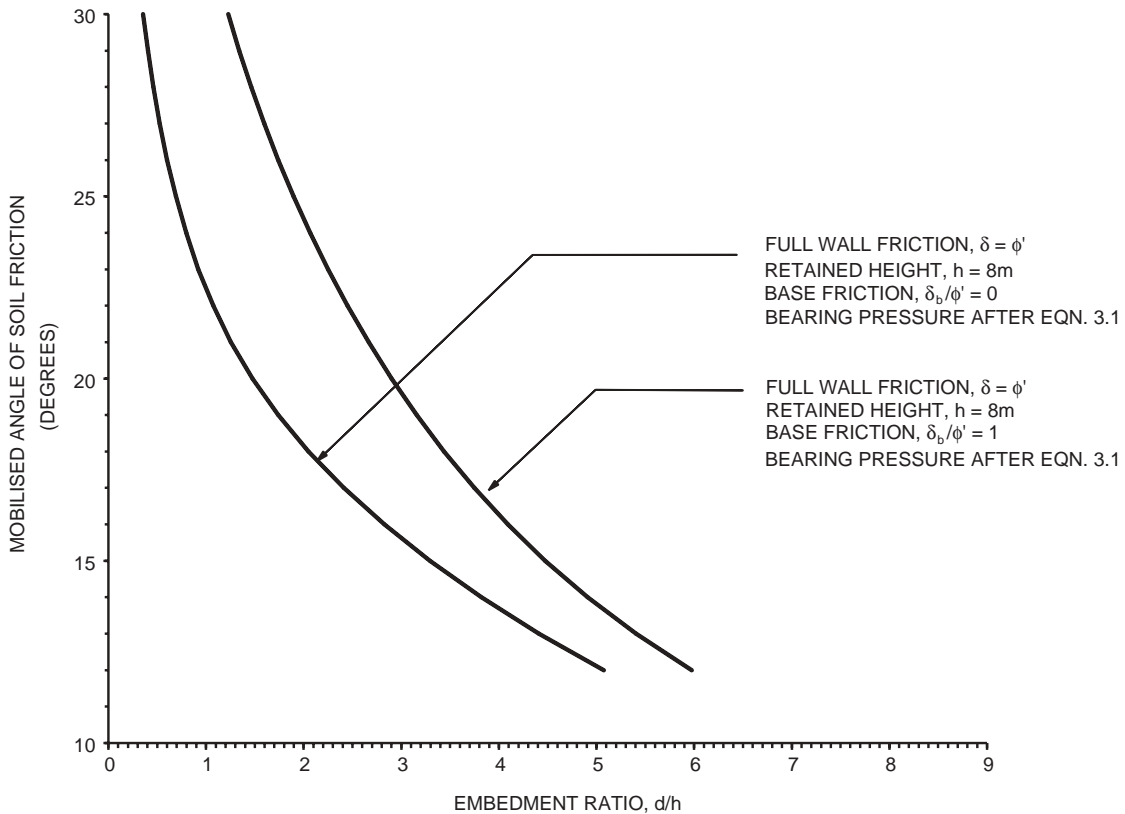


Figure A8 Scheme 4 - Estimated actual conditions; Mobilised soil strength as a function of embedment ratio for a rough retaining wall with integral stabilising base retaining 8m of saturated kaolin clay of unit weight $\gamma=17.66\text{kN/m}^3$; Stabilising base projection from wall = 4m

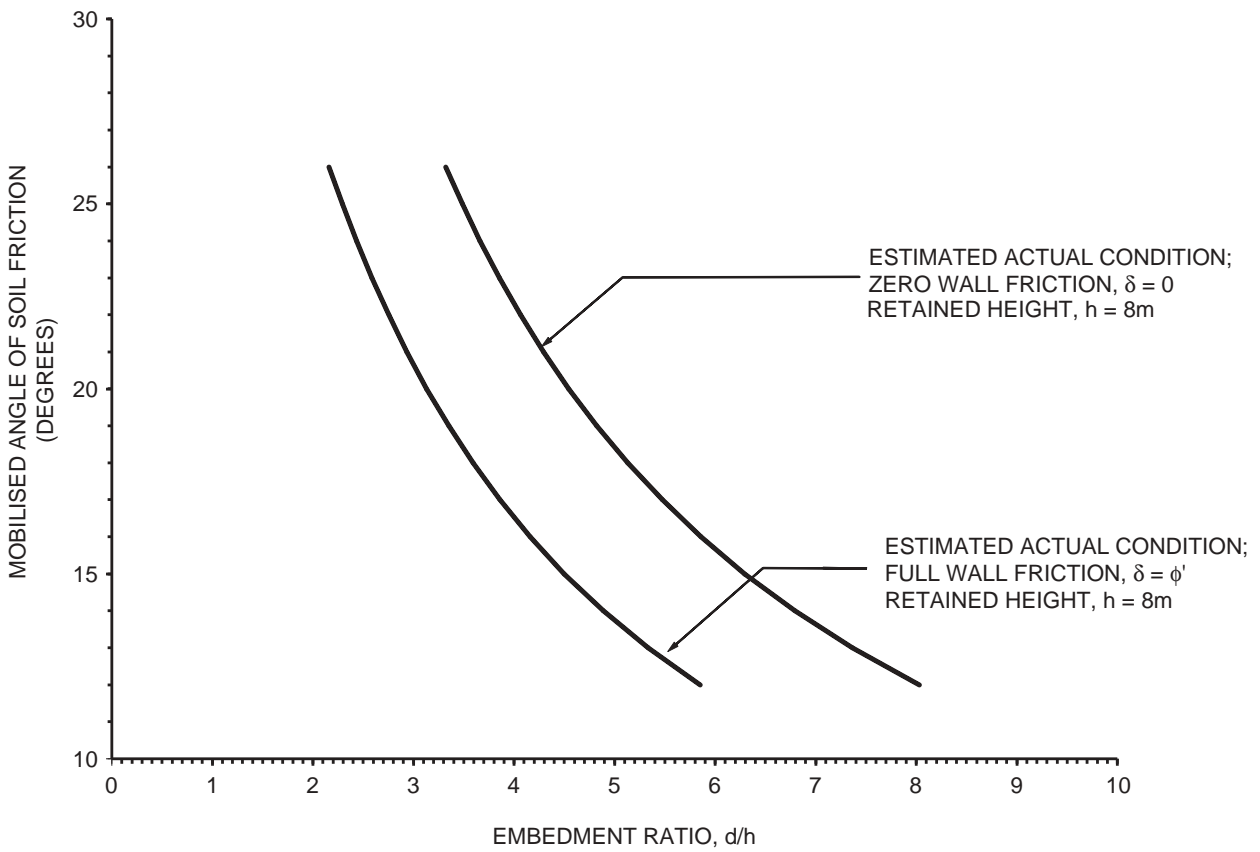


Figure A9 Mobilised soil strength as a function of embedment ratio for a free cantilever wall retaining saturated kaolin clay of unit weight $\gamma=17.5\text{kN/m}^3$

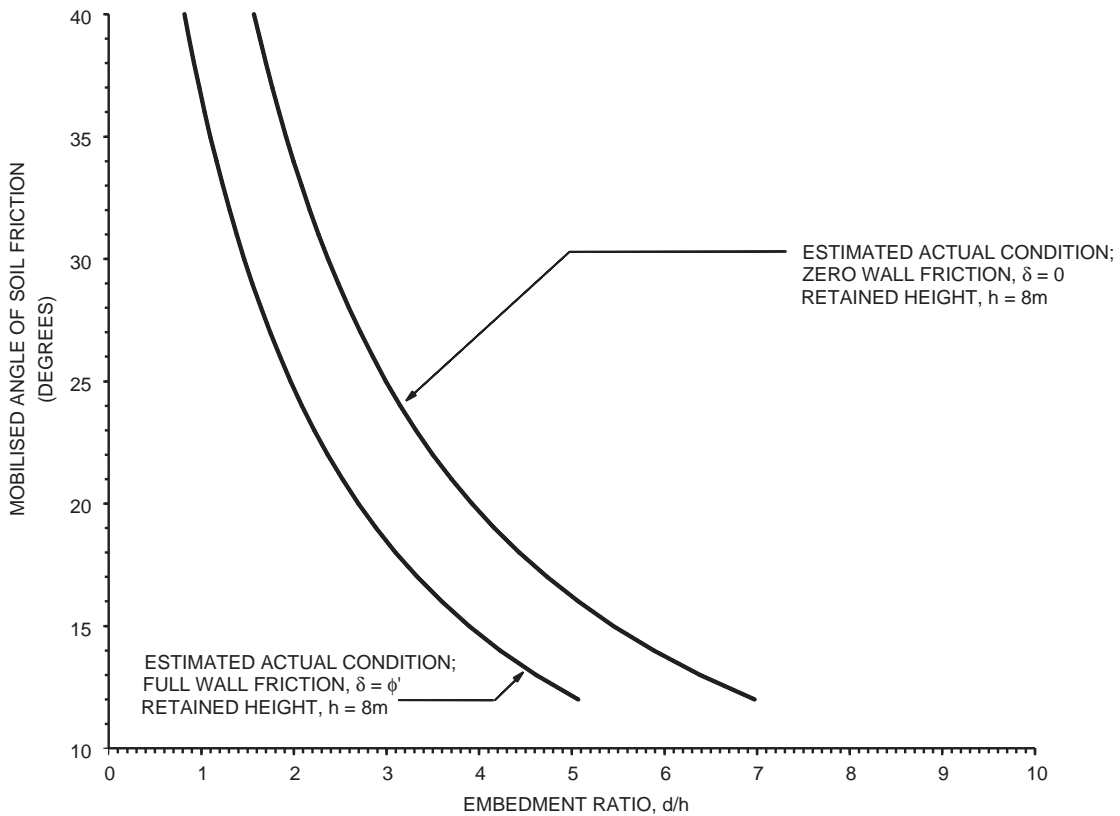


Figure A10 Mobilised soil strength as a function of embedment ratio for a free cantilever wall retaining saturated sand of unit weight $\gamma=19.7\text{kN/m}^3$

Abstract

A series of centrifuge model tests and complementary finite element analyses have been carried out to investigate the behaviour of stabilising base retaining walls of two different embedment depths in two different types of soil. In this report, the results of the centrifuge model tests and the finite element analyses are presented. They are then used to assess the applicability of various possible limit-equilibrium type calculations for this class of retaining wall. Finally, the implications for design are discussed and an outline design procedure is proposed.

Related publications

TRL381 *The long term performance of embedded retaining walls* by D R Carder and P Darley. 1998 (price £35 code H)

TRL172 *Ground movements caused by different embedded retaining wall construction techniques* by D R Carder. 1995 (price £25 code E)

TRL128 *Doubly-propped embedded retaining walls in clay* by D J Richards and W Powrie. 1995 (price £35 code H)

Prices current at May 1999

For further details of these and all other TRL publications, telephone Publication Sales on 01344 770783 or 770784, or visit TRL on the Internet at <http://www.trl.co.uk>.